

# **Function and Inhibition of Protein-only Ribonuclease P**

by

Nancy Wu

A dissertation submitted in partial fulfillment  
of the requirements for the degree of  
Doctor of Philosophy  
(Chemical Biology)  
in the University of Michigan  
2017

Doctoral Committee:

Professor Carol A. Fierke, Chair  
Professor Anna K. Mapp  
Associate Professor Patrick J. O'Brien  
Professor Nils G. Walter

Nancy Wu

[nancywu@umich.edu](mailto:nancywu@umich.edu)

ORCID iD: 0000-0001-8901-6030

© Nancy Wu 2017

## **DEDICATION**

To my parents, who love and support me and give me the freedom to explore new things. Your dedication to our family and your work ethic inspire and encourage me to pursue higher education that has resulted in this work.

And to my future students and all the young girls who enjoy learning.

## ACKNOWLEDGEMENTS

The work presented in this thesis would not have been accomplished without many people who have contributed to the work and those who have made an impact in my life. I would like to thank my mentors over the years. First, I want to thank my thesis advisor, Carol Fierke, who has been a wonderful mentor. Thank you for your guidance and for giving me the freedom to explore my interests without getting too far off track. You have helped me to become a better scientist. I thank my thesis committee members, whose helpful advice has guided this work. I also want to thank my high school chemistry teacher, Paul Matsumoto. Your dedication to your students inspired me to study chemistry and value education.

I also want to thank the past and present members of the Fierke Lab. Not everyone can say they enjoy what they do, but I can. And a large reason is because of the people I worked with. I want to especially acknowledge the RNase P subgroup: Xin Liu, Mike Howard, and Yu Chen were my mentors in the lab when I started and I am very thankful for your guidance. I am very thankful for the time spent discussing data, RNA, kinetics, and mechanisms. Xin's expertise in assay development and enzyme mechanisms was very valuable for Chapters 2 and 3. Also, Bradley Klemm and Kipchumba Kaitany were always available for helpful discussions. I am also thankful for the members of the Fierke lab who have helped me with their valuable advice and assistance with experiments. It

has been an enjoyable 5 years working alongside you all. I thank Xin Liu, Benjamin Jennings, Eric Sullivan, Kelsey Diffley, Katherine Leng, and Kip Kaitany for helpful comments and suggestions on this thesis. I thank Markos Koutmos, Agnes Karasik, and Aranganathan Shanmuganathan for a wonderful collaboration. I also want to acknowledge Martha Larsen and the Center for Chemical Genomics at the University of Michigan. The work done there was critical for Chapter 3.

I am grateful to my parents for their love and support. Thank you for all of the sacrifices you have made for our family. Thank you for supporting my pursuit of education and encouraging me to do my best. To my brother, Robert my successes are yours as well. Thank you for supporting me.

I also thank the many friends I have had the pleasure to meet here in Ann Arbor. You have helped me to see the joys of living in the Midwest. Thank you also to all my friends and family who support me from afar. You have all contributed to shaping me into the person I am today.

## TABLE OF CONTENTS

<b>DEDICATION.....</b>	<b>ii</b>
<b>ACKNOWLEDGEMENTS .....</b>	<b>iii</b>
<b>LIST OF FIGURES .....</b>	<b>x</b>
<b>LIST OF TABLES.....</b>	<b>xii</b>
<b>LIST OF SCHEMES .....</b>	<b>xiii</b>
<b>ABSTRACT .....</b>	<b>xiv</b>
<b>CHAPTER 1: Introduction .....</b>	<b>1</b>
<b>OVERVIEW .....</b>	<b>1</b>
<b>RIBONUCLEOPROTEIN (RNP) RNASE P .....</b>	<b>2</b>
Structural studies of RNP RNase P .....	6
<b>PROTEIN-ONLY RNASE P (PRORP).....</b>	<b>8</b>
Single-subunit PRORP.....	9
Multi-subunit PRORP .....	10
Structural studies of PRORP.....	13
<b>CATALYTIC MECHANISM OF RNASE P .....</b>	<b>16</b>
Catalytic mechanism of RNP RNase P .....	16
Catalytic mechanism of PRORP .....	17
<b>MITOCHONDRIAL tRNA PROCESSING .....</b>	<b>19</b>

Structural characteristics of mammalian mt-tRNAs.....	20
Mitochondrial tRNA in disease.....	22
CONCLUSIONS AND SIGNIFICANCE .....	23
OBJECTIVE.....	24
REFERENCES .....	26

<b>CHAPTER 2: Methyltransferase subcomplex of human mitochondrial RNase P activates the metallonuclease subunit by enhancing catalytic efficiency and pre-tRNA affinity .....</b>	<b>34</b>
ABSTRACT.....	34
BACKGROUND .....	35
RESULTS .....	38
MRPP1/2 enhances catalysis by MRPP3 .....	38
Pre-tRNA substrate enhances formation of mtRNase P holo-complex ...	42
Evidence of synergistic binding between MRPP subunits and pre-tRNA	43
MRPP1/2/3 complex ratio .....	44
The MRPP1/2 subcomplex does not enhance the apparent MRPP3 metal affinity.....	48
DISCUSSION .....	49
Kinetic model for mitochondrial RNase P catalysis.....	49
MRPP1/2 may play a structural role in mitochondrial RNase P activity ...	54
Pre-tRNA stabilizes the MRPP1/2/3 complex .....	54
CONCLUSION.....	55

METHODS.....	56
Pre-tRNA preparation.....	56
Purification of recombinant human mitochondrial RNase P subunits .....	57
Multiple-turnover (MTO) cleavage measurements.....	60
Magnetic capture assay .....	60
Fluorescence anisotropy (FA) binding assay .....	61
Single-turnover (STO) experiments .....	62
Derivation of rate law equations according to Scheme 2-2.....	62
Derivation of rate law equations according to Scheme 2-3.....	64
Magnesium dependence.....	65
Analytical ultracentrifugation .....	66
REFERENCES .....	67

### **CHAPTER 3: Inhibition of protein-only RNase P with Gambogic acid and**

<b>Juglone .....</b>	<b>70</b>
ABSTRACT.....	70
BACKGROUND .....	71
RESULTS .....	74
A high throughput FP assay for PRORP1 activity.....	74
Gambogic acid and juglone are more potent against PRORP compared to RNP RNase P .....	76
Gambogic acid is an uncompetitive inhibitor of PRORP1 activity .....	78
Juglone is a time-dependent inhibitor of PRORP1 activity .....	80
Crystallographic studies reveal a PRORP1-juglone complex .....	82



DISCUSSION .....	84
Gambogic acid binds to the enzyme-substrate complex .....	85
Juglone covalently modifies cysteine thiols in PRORP1 .....	86
CONCLUSIONS AND FUTURE DIRECTIONS .....	90
METHODS.....	92
Materials.....	92
Protein preparation.....	92
Pre-tRNA preparation.....	94
Fluorescence polarization (FP) assay.....	95
FP data analysis.....	96
High-throughput screening.....	96
Gel-based activity assay .....	97
Dose-response and determination of mode of inhibition.....	98
Human mitochondrial RNase P (MRPP1/2/3) activity assay.....	99
<i>B. subtilis</i> RNase P activity .....	100
Crystallization, Data processing and Refinement .....	100
APPENDIX A .....	102
REFERENCES .....	109
<b>CHAPTER 4: Conclusions and Future Directions.....</b>	<b>113</b>
OVERVIEW .....	113
CONCLUSIONS .....	114
Kinetic model for RNase P catalysis .....	114
The role of MRPP1/2 in human mitochondrial RNase P .....	115

MRPP1/2/3-pre-tRNA complex .....	115
Inhibition of plant PRORP1 and human MRPP1/2/3.....	116
Gambogic acid .....	116
Juglone.....	117
FUTURE DIRECTIONS .....	118
Mechanism of MRPP1/2/3 catalysis.....	119
Structure of PRORP1-pretRNA and MRPP1/2/3/pre-tRNA complexes .	120
Inhibition of PRORP1 with gambogic acid and juglone.....	121
Function of MRPP1/2/3 <i>in vivo</i> .....	122
tRNA methylation .....	122
REFERENCES .....	124

## LIST OF FIGURES

Figure 1-1 Precursor tRNA hydrolysis is catalyzed by RNase P .....	4
Figure 1-2 Secondary and tertiary structures of canonical tRNA.....	6
Figure 1-3 Secondary structure of RNase P RNA from <i>T. maritima</i> .....	7
Figure 1-4 Structure of <i>T. maritima</i> RNase P in complex with tRNA and 5'-leader .....	8
Figure 1-5 Crystal structure of <i>A. thaliana</i> PRORP1.....	10
Figure 1-6 Crystal structures of human mitochondrial RNase P proteins (MRPP) .....	14
Figure 1-7 Proposed chemical mechanism of pre-tRNA hydrolysis catalyzed by RNP RNase P and PRORP .....	18
Figure 1-8 Human mitochondrial tRNA structures. ....	20
Figure 2-1 Steady-state activity of human mitochondrial RNase P. ....	40
Figure 2-2 MRPP1/2/3/pre-tRNA complex forms in the presence of pre-tRNA. .	41
Figure 2-3 Binding affinity of mitochondrial RNase P proteins to Fl-pre-tRNA. .	43
Figure 2-4 The MRPP1/2 subunit ratio determined by analytical ultracentrifugation. ....	45
Figure 2-5 Single-turnover activity of mtRNase P.....	47
Figure 2-6 Magnesium dependence on the steady-state activity of mtRNase P.	48
Figure 3-1 Fluorescence polarization (FP) assay to measure RNase P activity.	75

Figure 3-2 A robust high throughput FP assay for identifying inhibitors of PRORP1 .....	77
Figure 3-3 Gambogic acid and juglone are inhibitors against protein-only RNase P in plant and human mitochondria .....	78
Figure 3-4 Gambogic acid is an uncompetitive inhibitor of PRORP1 .....	80
Figure 3-5 Juglone is a time-dependent inhibitor of PRORP1 .....	82
Figure 3-6 Crystal structure of PRORP1 in complex with juglone after overnight incubation.....	84

## LIST OF TABLES

Table 2-1 Steady-state kinetic parameters as a function of MRPP1/2 concentration as described in Figure 2-1 .....	41
Table 2-2 Dissociation constants ( $K_D$ ) of FI-pre-tRNA for mtRNase P proteins ..	43
Table 2-3 Thermodynamic constants listed in Scheme 2-3 .....	53
Table 3-1 The $IC_{50}$ values and Hill coefficients (n) for the inhibition of PRORP1, MRPP1/2/3, and <i>B. subtilis</i> RNase P with gambogic acid and juglone. ....	79
Table A-1 Compounds identified from a high throughput screen with more than 40% PRORP1 inhibition.....	102
Table A-2 X-Ray Crystallography Data Collection and Refinement Statistics ..	108

## LIST OF SCHEMES

Scheme 1-1 A minimal kinetic mechanism of bacterial RNase P .....	17
Scheme 2-1 Current kinetic model for human mitochondrial RNase P catalysis	49
Scheme 2-2 Random Binding Model .....	50
Scheme 2-3 New kinetic model for human mitochondrial RNase P catalysis ....	51
Scheme 3-1 Proposed model of inactivation by a slow-binding inhibitor .....	87
Scheme 3-2 Michael addition reaction mechanism of cysteine thiol with juglone at C-2 .....	87
Scheme 3-3 Radical addition reaction mechanism of cysteine thiol with juglone at C-3 .....	87

## ABSTRACT

Ribonuclease P (RNase P) is metal-dependent endonuclease responsible for the removal of extraneous 5'-ends in precursor tRNA (pre-tRNA). RNase P is essential and present in all domains of life. In many organisms, RNase P is a ribonucleoprotein (RNP) complex with a catalytic RNA subunit and accessory proteins. Our view of RNase P expanded with the identification of protein-only RNase P (PRORP) found in plants and human mitochondria. In plants, PRORP endonuclease activity functions as a single-subunit enzyme. In contrast, human mitochondrial RNase P (mtRNase P) is composed of three protein subunits: mitochondrial RNase P protein (MRPP) 1, 2 and 3. MRPP3, which is homologous to plant PRORP, contains the active site that catalyzes pre-tRNA hydrolysis. However, MRPP3 requires a tRNA methyltransferase (MRPP1) and a dehydrogenase/reductase (MRPP2) for catalysis.

To investigate the mechanism of pre-tRNA cleavage catalyzed by human mitochondrial RNase P, we describe a model for pre-tRNA hydrolysis that highlights the importance of the MRPP1/2 subcomplex on recognition and processing of mitochondrial tRNA transcripts. Our data suggests that pre-tRNA stabilizes the interactions between MRPP3 and MRPP1/2. We propose that binding of MRPP1/2 to pre-tRNA alters the pre-tRNA structure, yielding a pre-tRNA structure that is recognized by MRPP3 at a higher affinity and is efficiently

cleaved. Furthermore, the identification of inhibitors against PRORP1 from a high throughput screen provides lead compounds to probe PRORP activity. We have identified an uncompetitive and a time-dependent inhibitor of PRORP1, revealing several cysteine residues that may be involved in the inactivation of PRORP1. Both compounds inhibit *A. thaliana* PRORP1 and human MRPP1/2/3. Taken together, this work provides a mechanistic approach for investigating the function of PRORP in the human mitochondria and multi-subunit RNA-protein complexes and a framework for studying mitochondrial disease states that arise from dysfunctional RNA processing.



# CHAPTER 1

## Introduction<sup>1, 2</sup>

### OVERVIEW

The central dogma of molecular biology involves the transcription and translation of genetic information from nucleic acids to expressed proteins. Transfer ribonucleic acid (tRNA) is an essential adapter molecule in translation critical for relating the 4-letter genetic code to amino acids. All tRNAs are synthesized as inactive precursor molecules (pre-tRNA) that undergo a number of post-transcriptional maturation steps including but not limited to the removal of extra 5' and 3' nucleotides, addition of a 3'-CCA sequence, and base modifications (1,2). One of the initial steps essential for tRNA maturation is the cleavage of extra 5'-ends catalyzed by ribonuclease P (RNase P). This is a metal-dependent hydrolysis reaction at a specific phosphodiester bond, resulting in tRNA with a 5'-phosphate and a cleaved 5' leader byproduct with a 3'-hydroxyl (Figure 1-1) (3). To gain a better understanding of the function of RNase P, I will discuss previous research describing the different types of RNase P enzymes and earlier work investigating their catalytic mechanism and biological relevance.

---

<sup>1</sup> Reproduced, in part, from Klemm, BP; Wu, N; Chen, Y; Liu, X; Kaitany, KJ; Howard, MJ; Fierke, CA. The Diversity of Ribonuclease P: Protein and RNA Catalysts with Analogous Biological Functions. *Biomolecules* 2016, 6(2):E27.

<sup>2</sup> Original text written by Bradley P. Klemm, Nancy Wu, Yu Chen, Xin Liu and Kipchumba J. Kaitany. The text was updated by Nancy Wu and revised for this thesis.

RNase P is present in nearly all species of life. The exception is *Nanoarchaeum equitans*, which does not encode pre-tRNAs with extra nucleotides at the 5' end (4). There are two types of RNase P enzymes: ribonucleoprotein (RNP) RNase P and protein-only RNase P (PRORP). Altman and colleagues discovered that the catalytic activity of RNase P in *E. coli* originates from its RNA subunit (P RNA) and thus RNase P was termed a ribozyme (5). Sidney Altman shared the 1989 Nobel Prize in Chemistry with Thomas Cech for the discovery of catalytic RNA. The discovery of PRORP in human mitochondria in 2008 shifted the field from a view of RNase P as ribozymes to a broader view where some enzymes are composed of only protein (6). RNP RNase P is found in all domains of life, whereas PRORP is found strictly in Eukarya. RNP RNase P and PRORP have completely different subunit compositions, yet catalyze the same reaction and produce identical products. This makes them an exciting system to study the underlying catalytic principles. The goal of this work is to better understand the function of human mitochondrial PRORP. Many of the investigations into the mechanism and role of catalytic metal ions in PRORP are compared to previous work done with RNP RNase P. Thus, a summary of the work describing RNP RNase P will be followed by a description of our knowledge of PRORP.

## **RIBONUCLEOPROTEIN (RNP) RNASE P**

RNP RNase P is composed of a single conserved catalytic RNA subunit that is associated with a varying number of protein subunits. The number of protein subunits in RNase P increases across domains of life as the organism complexity increases. Bacteria have one small protein (P protein), Archaea have 4-5 proteins, and Eukarya have 9-10 proteins (1,7,8). The RNA component of RNase P is sufficient to catalyze tRNA maturation in the absence of proteins *in vitro* under high metal and salt conditions (5,9,10). However, the associated proteins are essential *in vivo* and important for substrate specificity and metal ion binding (11-14). Unlike self-cleaving ribozymes, RNP RNase P catalyzes multiple turnovers.

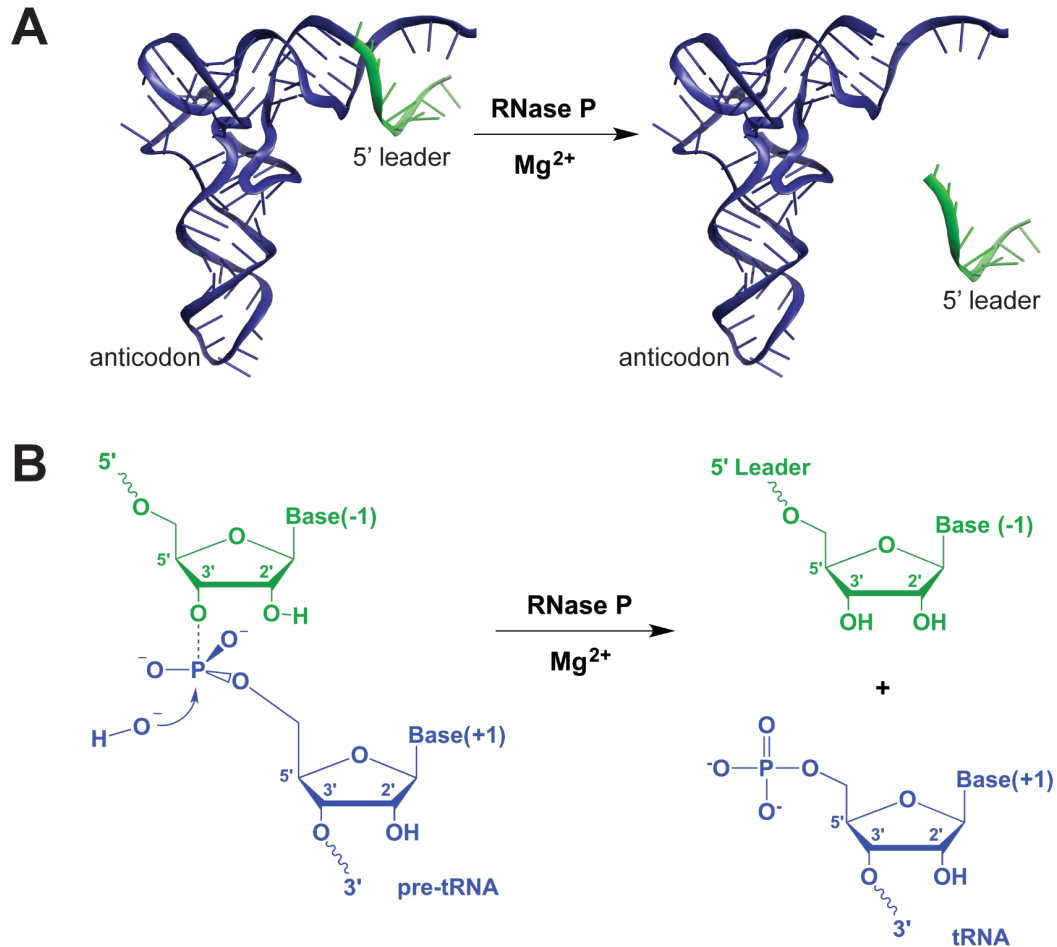


**Figure 1-1 Precursor tRNA hydrolysis is catalyzed by RNase P**

(A) RNase P cleavage of pre-tRNA shown in its tertiary structure. The tRNA body is shown in blue and the 5' leader is shown in green. (B) Depiction of the hydrolysis of a specific phosphodiester bond between nucleotide in position (-1) and position (+1) on pre-tRNA, producing a 5' leader molecule with a 3' hydroxyl group and tRNA containing a 5' phosphate group. Adapted with permission from (15).

RNase P RNAs (~400 nucleotides) exist primarily as one of two major types based on secondary structure: type A (Ancestral type) found in most bacteria and type B (*Bacillus* type) found in low-GC Gram-positive bacteria (16,17). A third class, type C, is found in some Chloroflexi (green non-sulfur bacteria) and resembles an intermediate of types A and B (17). Bacterial RNase P RNAs share a consensus sequence with a conserved secondary structure,

which is divided into two separate domains: the catalytic and specificity domains (18). The consensus sequence across all bacterial P RNAs contains five conserved regions with CR-I, IV, and V within the catalytic domain, and CR-II and III within the specificity domain. Within CR-V of the catalytic domain, the active site P4 helix contains core nucleotide base and backbone interactions important for positioning the  $Mg^{2+}$  ions required for catalysis (19). The specificity domain, while not essential for catalysis, enhances substrate affinity through interactions with the D- and T $\psi$ C-domains of pre-tRNA (20-22) (Figure 1-2). The catalytic domain can perform catalysis without the specificity domain in the presence of the protein subunit, albeit with a 100- to 500-fold reduction in activity and a 100-fold reduction in substrate affinity compared to full-length P RNA (23-25).

Archaeal and eukaryotic RNase P RNAs lack some of the structural features in their bacterial counterparts (Figure 1-3). In Archaea, Type A P RNAs typically lack the P8 and P13/14 stems. Type M P RNAs, found in *Methanococcus*, lack the P6 pseudoknot, P8 and P16 stems, and the P15 3' CCA recognition loop. Type T P RNAs, found in *Thermoproteaceae*, are missing a large portion of the specificity domain (26,27). Eukaryotic P RNA in the nucleus retains a conserved secondary structure, however, the nonhomologous regions deviate considerably in sequence and length compared to Bacteria and Archaea (28). A typical eukaryotic P RNA is about two-thirds the length of bacterial RNase P RNA, lacking structures that are important for tRNA binding and structural stability (28). The additional protein subunits are proposed to take over these roles (29).

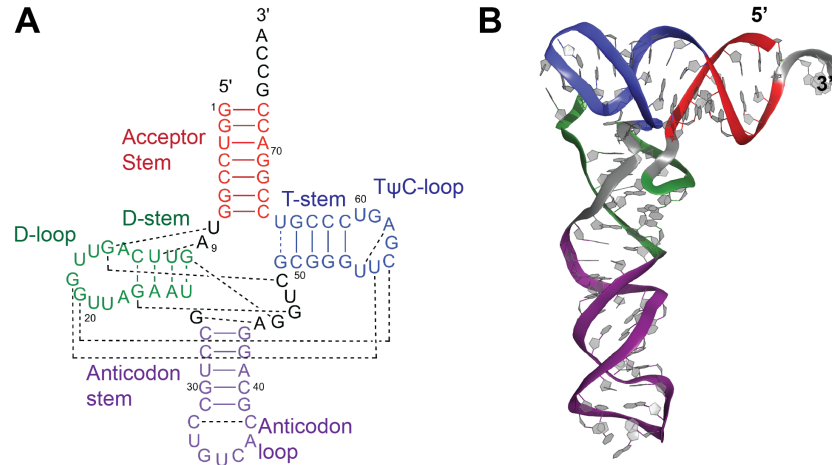


**Figure 1-2 Secondary and tertiary structures of canonical tRNA**

(A) Secondary structure of a canonical Type 0 tRNA from *B. subtilis* (adapted with permission from (15)). tRNA folds into a conserved cloverleaf secondary structure with distinct domains essential for substrate recognition, structure and function. The colored solid lines represent Watson Crick base pairs and colored dotted lines represent Wobble base pairs within the stem structures. Tertiary interactions are shown with black dotted lines. (B) Crystal structure of structure of *E. coli* tRNA<sup>Phe</sup> (PDB 3L0U) (30).

### Structural studies of RNP RNase P

Structural studies on RNP RNase P have led to a greater understanding of its molecular mechanism. Crystal structures of individual P RNA and P protein subunits in addition to holoenzyme-substrate complexes have been solved. P RNA structures have been solved in type A *Thermotoga maritima* (PDB ID: 2A2E (31)) in addition to the isolated specificity domain (PDB ID: 1U9S (32)), type B *B. subtilis* specificity domain (PDB ID: 1NBS (33)) and *B. stearothermophilus* (PDB ID: 2A64 (34)). Bacterial RNase P protein is the simplest (~120 amino acids). Structures of RNase P protein have been solved in type A *T. maritima* (PDB ID: 1NZ0 (35)), and in type B *B. subtilis* (PDB ID: 1A6F (36)) and *Staphylococcus aureus* (PDB: 1D6T (37)). P protein contains a central cleft with an arginine-rich binding site for single stranded RNA, referred to as an RNR motif (37). In

bacteria, the RNR motif in RNase P protein contacts the pre-tRNA leader sequence to stabilize an active enzyme-substrate conformation (38).

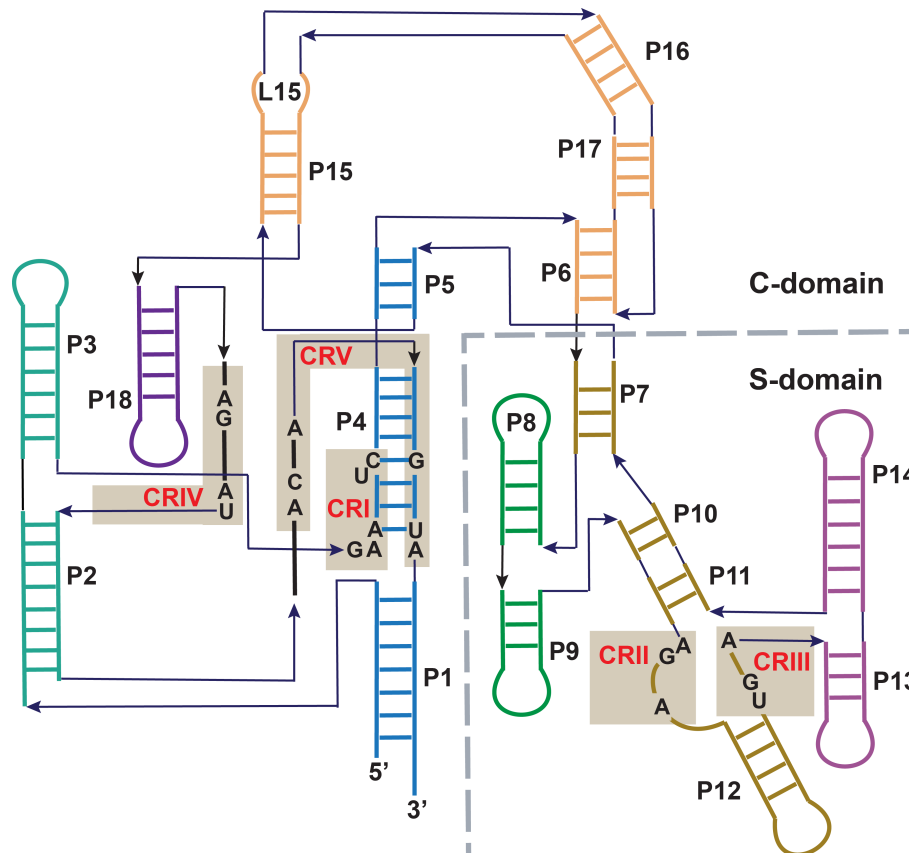


**Figure 1-3 Secondary structure of RNase P RNA from *T. maritima***

The catalytic (C-) and specificity (S-) domains are divided by a dashed grey line. Conserved regions are numbered and shaded in light brown. The C-domain includes helices P1/P4/P5 (blue), P2/P3 (teal), P6/P15/P16/P17 (orange), and P18 (purple). The S-domain includes P7/P10/P11/P12 (brown), P8/P9 (green), and P13/P14 (pink). (This figure was adapted with permission from (39)) (40,41).

A 4.3 Å resolution crystal structure of RNase P in complex with tRNA and 5' leader products revealed important substrate-protein, protein-P RNA, and P RNA-substrate contacts (PDB: 3Q1R and 3Q1Q (40)) (Figure 1-4). The RNR motif of P protein makes specific contacts with the 5' leader of pre-tRNA consistent with biochemical data (38) in addition to contacts with CR-IV and CR-V in P RNA, which contain the active site P4 helix. From this structure, metal ions

important for catalysis and pre-tRNA binding are proposed near the active site P4 helix and the cleavage site of tRNA (40). Conserved regions in the specificity domain of P RNA are involved in base stacking interactions with the D- and T $\psi$ C-loops of tRNA (42). The catalytic domain base pairs with the 3' CCA sequence and the acceptor stem in tRNA (43).

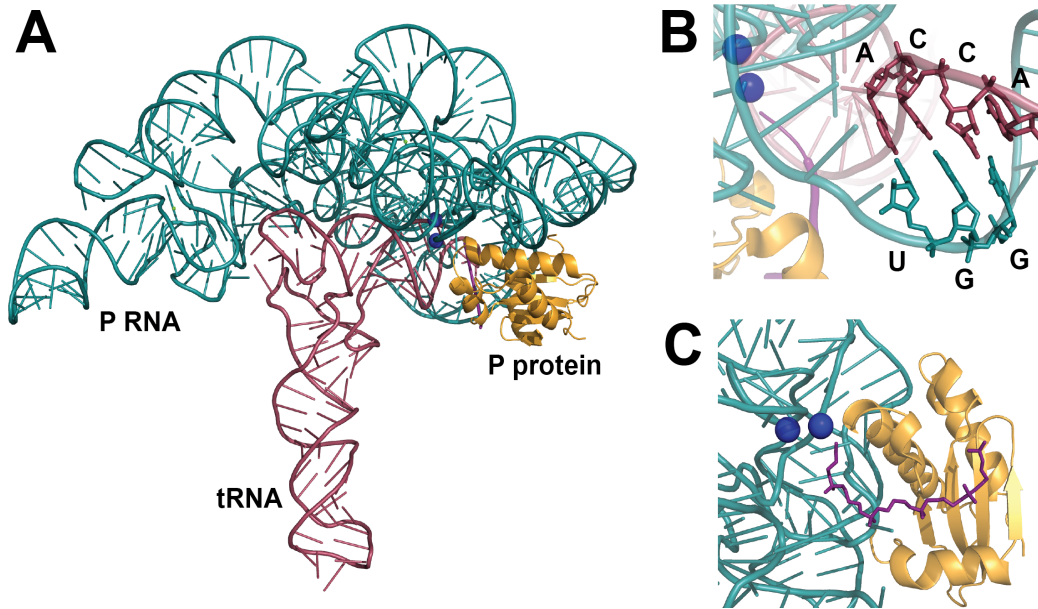


**Figure 1-4 Structure of *T. maritima* RNase P in complex with tRNA and 5'-leader**  
 Crystal structure of ribonucleoprotein RNase P in complex with tRNA and 5' leader products from *T. maritima* (PDB 3Q1R, PyMOL) (40). (A) The tertiary complex displays the catalytic RNA component (shown in teal), a protein subunit (shown in gold), bound tRNA molecule (shown in pink) and bound metal ions (shown as blue spheres). (B) The 3'-CCA sequence in tRNA (shown in red) makes hydrogen-bonding interactions with GGU nucleotides in the specificity domain of P RNA (shown in teal). (C) The 5' leader of pre-tRNA (shown in purple) interacts with the RNR motif in P protein and is located close to the active site of RNase P, represented by the two bound active site metal ions (shown in dark blue).

### PROTEIN-ONLY RNASE P (PRORP)

Some eukaryotes, including humans, have both RNP RNase P and PRORP. Humans have a RNP RNase P in the nucleus and a PRORP in the mitochondria. The PRORP holoenzyme consists of three nuclear-encoded



protein subunits: mitochondrial RNase P protein (MRPP) 1, 2 and 3. MRPP3 represents a novel class of endonuclease, containing an N-terminal pentatricopeptide repeat (PPR) RNA-binding domain, a central structural Zn<sup>2+</sup> binding domain, and a Nedd4-BP1, YacP nuclease (NYN) domain with homology to the flap endonucleases (44) (Figure 1-5). In mammals, there seven mitochondrial PPR domain proteins including MRPP3 (45). PPR domain proteins are generally involved in regulating gene expression in mitochondria (45). An ortholog of MRPP3, plant PRORP1, is a model system for studying structure and function and is discussed in the next section.

### **Single-subunit PRORP**

Plants, algae, and some trypanosomes encode homologs of MRPP3 that catalyze the hydrolysis of pre-tRNA as single-subunit proteins (46-48). Given its homology to MRPP3 in human mitochondria, PRORP1 in *Arabidopsis thaliana* has served as a model enzyme for elucidating important structural and functional characteristics of PRORP enzymes across species. There are three isozymes of PRORP in *A. thaliana*: PRORP1 localizes in the mitochondria and chloroplasts, and PRORP2 and 3 co-localize in the nucleus (46). PRORP2 and 3 are closely related enzymes, sharing 80% sequence identity and 88% sequence homology. Deletion of PRORP1 or double deletion of PRORP2 and PRORP3 are lethal, however single deletions of PRORP2 or PRORP3 retain cell viability. These results indicate that PRORP2 and PRORP3 have redundant yet essential roles in the nucleus (46,49). PRORP genes are found across plant genomes, whereas

genes encoding RNP RNase P RNA have not been found, suggesting that plants may be devoid of RNP RNase P (50-52). PRORP1 in *A. thaliana* can replace RNP RNase P in bacteria. Recombinant expression of PRORP1 in an *E. coli* strain with stunted RNase P RNA expression is viable, highlighting the ability of PRORP1 to substitute for RNP RNase P *in vivo* (46).

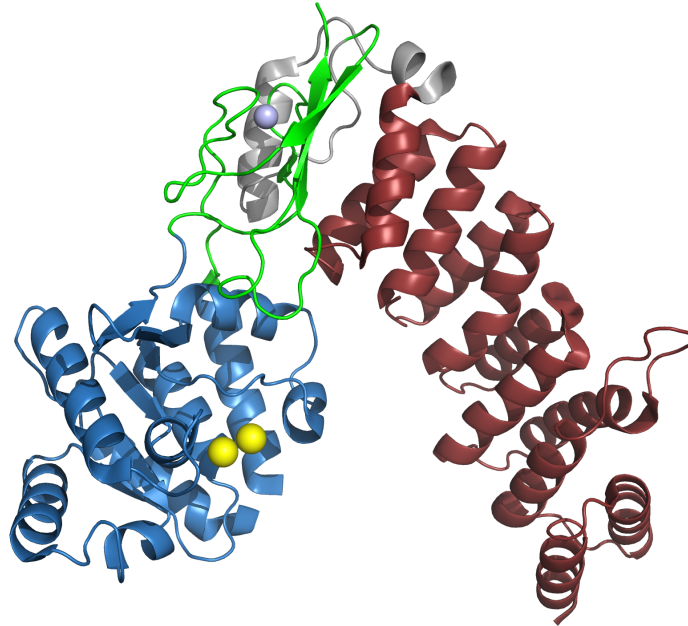


**Figure 1-5 Crystal structure of *A. thaliana* PRORP1**

The PPR domain is shown in red, the central domain is shown in green, and the NYN metallonuclease domain is shown in blue. The central domain coordinates a structural zinc ion shown as a gray sphere. The NYN metallonuclease domain coordinates two active site manganese ions shown as yellow spheres (PDB 4G24, image made in PyMOL (44)).

### **Multi-subunit PRORP**

PRORP enzymes in humans and other metazoans are multi-subunit complexes. MRPP1, 2, and 3 share no sequence homology with any of the identified protein subunits in RNP RNase P and all three subunits are required for RNase P activity (6). MRPP3 is homologous to the plant PRORP and is the metallonuclease subunit that houses the active site for RNase P. However, two

additional proteins, MRPP1 (TRMT10C) and MRPP2 (SDR5C1), are required for activity. Nuclear encoded MRPP1 and 3 contain N-terminal mitochondrial localization sequences and are trafficked from the cytosol to the mitochondria (53). Knockdowns via siRNA of either MRPP1 or MRPP3 in HeLa cells resulted in pre-tRNA transcript accumulation in mitochondria (54). Furthermore, mutations of each of the individual mitochondrial PRORP proteins in *Drosophila* are lethal, in part as a result of defective tRNA processing demonstrating the importance of each of these subunits for catalytic efficiency (55).

MRPP1 is a homolog of Trm10 in *Saccharomyces cerevisiae* and catalyzes N1-methylation of A or G at position 9 of tRNA (56). Trm10 belongs to the SpoU-TrmD (SPOUT) family of S-adenosylmethionine (SAM) dependent methyltransferases (56,57). MRPP1 is one of three human Trm10 homologues: TRMT10A and TRMT10B in the cytosol and TRMT10C (MRPP1) in the mitochondria. One study identified at least one methylation site at the Watson-Crick face for all human mitochondrial tRNAs (mt-tRNA) except for mt-tRNA<sup>Ser(AGY)</sup> and mt-tRNA<sup>Met</sup> (58). The methyltransferase responsible for the methylation of each mt-tRNA has yet to be identified. A likely candidate is MRPP1, which uniquely methylates A or G at position 9 of tRNA, as shown with mitochondrial tRNA<sup>Ile</sup> and tRNA<sup>Lys</sup> *in vitro* (59,60). MRPP1 forms a stable complex with MRPP2, a dehydrogenase/reductase that is essential for RNase P activity (59). No direct binding interactions between MRPP2 and pre-tRNA have been observed (59). In addition, the dehydrogenase activity of MRPP2 is not needed for methyltransferase or endonuclease activity, suggesting it likely has a

structural role in providing stability for the methyltransferase subcomplex composed of MRPP1 and MRPP2 (MRPP1/2) (59).

MRPP2 is a homotetramer and the stability of MRPP2 is proposed to affect MRPP1 protein levels and pre-tRNA processing. Pathogenic mutations located at the interacting interfaces of MRPP2 monomer could potentially destabilize the tetramer and affect MRPP1 stability. Recombinant pathogenic MRPP2 mutants mixed with the lysate of a bacterial strain expressing MRPP1 resulted in reduced levels of the MRPP1/2 complex compared to wild type (61). Fibroblasts from patients with HSD10 disease, which affects intellectual abilities and motor skills, contained a MRPP2 mutation that resulted in lower protein levels of both MRPP1 and MRPP2 (62). Furthermore, the loss of MRPP1 and impaired mitochondrial tRNA processing in due to knockdown of MRPP2 were partially restored with ectopic expression of wild type MRPP2 in human fibroblast cells (62). In another study, mutations were identified in MRPP1 from two patients with birth defects. Both died after 5 months due to respiratory failure. Investigations revealed reduced levels of MRPP1 and protein subunits of complex I and IV in the respiratory chain complex in fibroblast cells, increased pre-tRNA transcripts, impaired mitochondrial RNA processing, and defective mitochondrial protein synthesis, an essential process for production of vital electron transport chain complexes (63).

The stoichiometry of human MRPP subunits remains unclear. A ratio of 2:4 MRPP1-MRPP2 was initially proposed from studies quantifying the MRPP1 and MRPP2 complex from a denaturing PAGE stained with Coomassie Blue

(59). Additional work using gel filtration resulted in a complex with a molecular weight of 170 kDa, consistent with a 1:4 MRPP1-MRPP2 ratio (159 kDa) (64). However the authors concluded a 2:4 ratio, which has a molecular weight of 202 kDa (64). The work in this thesis (Chapter 2) provides evidence that a 1:4 complex forms and is catalytically active.

Plant PRORP1 and human mitochondrial PRORP are similar in structure in terms of their metallonuclease subunits; however, additional proteins, namely MRPP1 and 2, in human mitochondrial PRORP present an interesting case for studying the similarities and differences in mechanism and substrate specificity employed between single- and multi-subunit PRORP enzymes. The following section discusses the current research done to reveal the structure and catalytic mechanism of PRORP.

### **Structural studies of PRORP**

Structures of individual subunits of PRORP have enhanced understanding of its mechanism and function. There is not yet a structure of MRPP1, however structures exist for the full-length archaeal Trm10 homologue (PDB ID: 5A7Y (65)) (Figure 1-6), the methyltransferase domain of archaeal (PDB ID: 4JWF (57)), and human TRMT10A (PDB ID: 4FMW). The archaeal TRMT10 structure reveals a central SPOUT domain bound to *S*-Adenosyl-L-homocysteine (SAH) in between the N- and C-terminal domains. The structure of MRPP2 has been solved, revealing a tetramer complex (PDB ID: 1U7T (66)) (Figure 1-6).

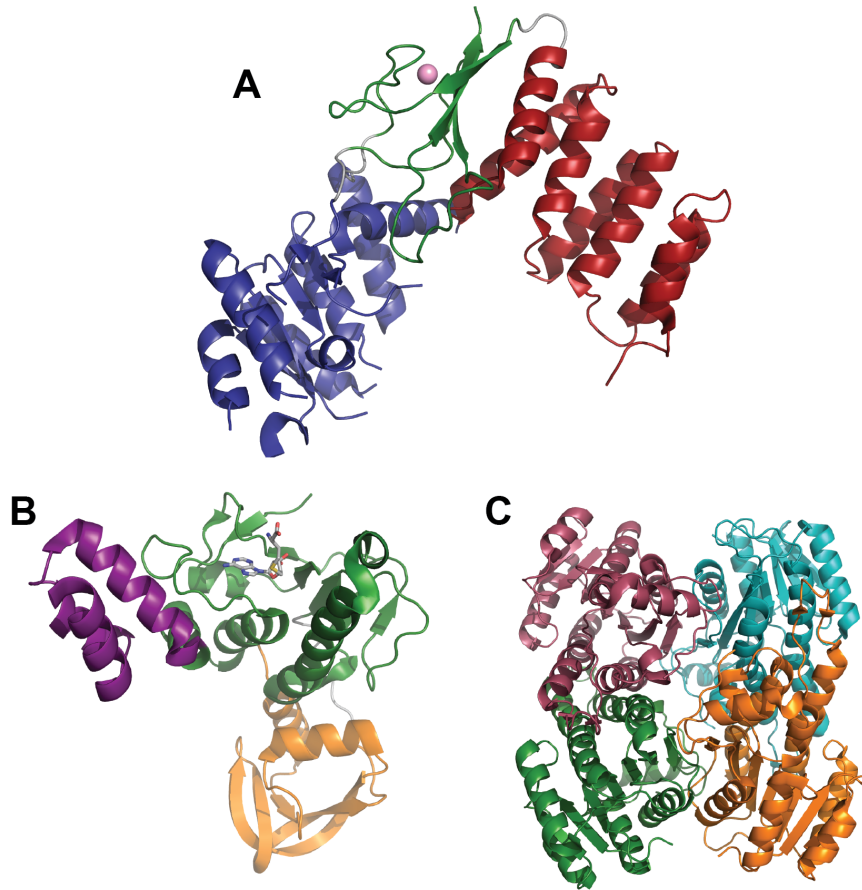


**Figure 1-6 Crystal structures of human mitochondrial RNase P proteins (MRPP)**

(A) Structure of N-terminal truncation of human MRPP3 ( $\Delta 206$ ) showing the PPR domain in red, the central domain in green with a Zn ion (pink sphere), and the NYN metallonuclease domain in blue (67). (B) Structure of archael TRMT10, a MRPP1 homologue with the C-domain in purple, SPOUT domain in green bound to SAH shown in sticks, and N-terminal domain in orange (65). (C) Structure of MRPP2 tetramer is shown with each subunit in a different color (66).

The structures of plant PRORP1 and PRORP2 reveal similar three-domain architectural folds (44,68). *A. thaliana* PRORP1 has a three-domain architecture homologous to human MRPP3, with an NYN metallonuclease domain, a bipartite central  $Zn^{2+}$ -binding domain, and a PPR RNA-binding domain (PDB ID: 4G24 (44)) (Figure 1-5). *A. thaliana* PRORP1 was crystallized in the presence of  $Mn^{2+}$  ions, which activates the enzyme, revealing two metal ion binding sites in the active site. The active site, located within the NYN

metallonuclease domain, contains four aspartates (*At* PRORP1 Asp 399, 474, 475, and 493) that are fully conserved across the available PRORP sequences, with a fifth aspartate (*At* PRORP1 Asp 497) that is conserved except in some metazoan homologs. Additional mechanistic work has led to a proposed 2-metal ion mechanism for PRORP1, which is discussed in the following section.

Structural and biochemical studies on plant PRORP1 and human MRPP3 have revealed both striking similarities and differences between the two enzymes. Both exhibit a V-shaped structure and contain PPR motifs and a NYN metallonuclease domain. Two structures of human MRPP3 were solved with an N-terminal truncation that excludes either two or four of the PPR motifs (PDB ID: 4XGL (67) and PDB ID: 4ROU (69)) (Figure 1-6). These structures are disordered in the NYN domain and the authors describe this as an inactive conformation. Given that no metal ion density was observed in these structures, the authors proposed that a possible role for MRPP1/2, the methyltransferase subcomplex required for RNase P activity, is to position active site metal ions (67,69). However, the MRPP3 constructs with the N-terminal truncations were not activated by addition of MRPP1/2, thus the disordered structure and lack of metal ion density may be due to the loss of PPR motifs at the N-terminus. Similar deletions of PPR motifs in PRORP1 are detrimental to the activity of the enzyme (44,70). Crystal structures reveal similarities in structure with 22% sequence identity between PRORP1 and MRPP3 (6,44,67,69). It is likely that PRORP1 and MRPP3 perform catalysis using similar mechanisms. However, more biochemical information is required for a full comparison.

## CATALYTIC MECHANISM OF RNASE P

Studies on the bacterial RNP RNase P and *A. thaliana* PRORP1 reveal a potential convergence in catalytic mechanisms between RNA and protein enzymes (71,72). These enzymes are different in composition, but perform the same function in the cell with comparable catalytic efficiencies *in vitro* (72). To gain insight into the mechanisms of pre-tRNA hydrolysis catalyzed by PRORP, previous research on elucidating the catalytic mechanism of bacterial RNP RNase P is discussed.

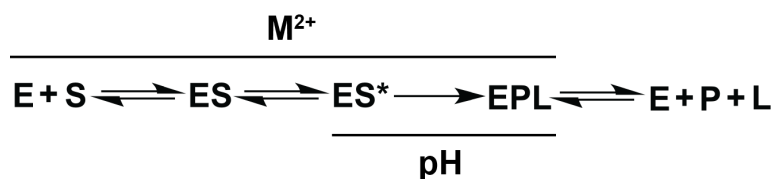
### Catalytic mechanism of RNP RNase P

The mechanism for the hydrolysis of a phosphodiester bond within pre-tRNA involves the proper orientation of substrate and essential catalytic metal ions (73-75). Bacterial RNase P uses a metal-bound water as the nucleophile, as shown by solvent isotope effects (71). RNase P can be activated by a number of metals ions *in vitro* including  $Mg^{2+}$ ,  $Mn^{2+}$ , and  $Zn^{2+}$ , but prefers  $Mg^{2+}$  *in vivo* (74-77). A minimal kinetic model of pre-tRNA hydrolysis has been proposed for RNP RNase P (Scheme 1-1) (14,78). Additional studies revealed a conformational change step following binding to form an active enzyme-substrate conformer (ES\*) that is coupled with divalent metal ion binding. Evidence of this conformation change was obtained using time-resolved fluorescence resonance



energy transfer (tr-FRET) revealing structural rearrangements between P protein and the 5' leader of pre-tRNA (14,78).

Hydrolysis of pre-tRNA catalyzed by bacterial RNase P is mediated by a metal ion that is proposed to contact the nonbridging *pro-R<sub>P</sub>* oxygen of the cleavage site scissile bond; a phosphorothioate substitution at this position blocks cleavage (Figure 1-7) (79). Similar results were found in human nuclear RNase P (80). PRORP purified from spinach chloroplasts was not inhibited by phosphorothioate substitution at the nonbridging *pro-R<sub>P</sub>* oxygen at the pre-tRNA scissile bond, indicative of a difference in mechanism between RNP RNase P and PRORP enzymes (Figure 1-6) (81,82).



**Scheme 1-1 A minimal kinetic mechanism of bacterial RNase P.**

The first step is bimolecular, followed by a conformational change step and a pH dependent cleavage step. All steps up to and including the cleavage step are metal dependent.

**Catalytic mechanism of PRORP**

Structural studies of RNP RNase P and PRORP reveal similarities that suggest convergent catalytic mechanisms. Catalytic metal ions are proposed to be bound by nonbridging oxygen atoms in the RNA of RNP RNase P while aspartate residues in PRORP bind catalytic metal ions (83). RNP RNase P is proposed to use a metal-bound water nucleophile to catalyze hydrolysis (71) and mechanistic studies of reveal a similar mechanism for *A. thaliana* PRORP (Figure 1-7) (72). The pH dependence on the activity of PRORP1 indicates a single

ionizable group, that activates catalysis upon protonation (72). This likely represents ionization of a metal-bound water since there are no additional groups in the active site that could ionize (72). However, the apparent  $pK_a$  for this group is 7.9, lower than the expected  $pK_a$  for a metal-bound water. One possible explanation for this result is a change in rate limiting steps from cleavage to a step prior to cleavage, such as a conformational change observed for RNP RNase P (14,78). More work will need to be done in order to elucidate the presence and function of a conformational change step in PRORP1.

The catalytic mechanism of human mitochondrial PRORP is currently under investigation. In the current proposal, the three MRPP proteins form a complex with a stoichiometry of 2:4:1 (MRPP1:2:3) to catalyze pre-tRNA cleavage, with qualitative proposals that MRPP1/2 binding to MRPP3 induces formation of an active enzyme (6,69). However the functional role of MRPP1/2 is still in question.

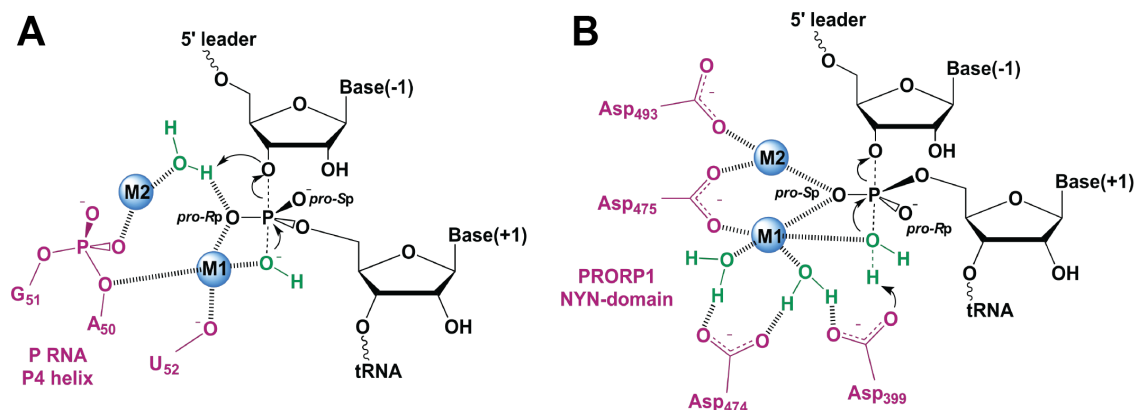


**Figure 1-7 Proposed chemical mechanism of pre-tRNA hydrolysis catalyzed by RNP RNase P and PRORP**

(A) bacterial RNase P proposed in (40) and (B) *A. thaliana* PRORP, adapted from (72). The active site metal ions are shown as blue spheres, and the active site of RNase P is shown in purple. The catalytic metal ion coordinates the nonbridging *pro-Rp* oxygen in RNP RNase P and the nonbridging *pro-Sp* oxygen in PRORP1 to activate a water nucleophile to catalyze cleavage of a phosphodiester bond.

## MITOCHONDRIAL tRNA PROCESSING

Mitochondria play a vital role in generating the energy for the cell through oxidative phosphorylation. The human mitochondrial genome is a closed, circular double-stranded DNA 16,569 bp in length, encoding genes for proteins responsible for maintaining membrane potential and catalyzing oxidative phosphorylation. The genome is transcribed into three long polycistronic transcripts with 22 tRNAs interspersed between 13 mRNAs that encode essential protein subunits for respiratory complexes I, III, IV, and V, 3 long noncoding RNAs (lncRNAs), and two mitochondrial ribosomal RNAs (rRNAs). Mitochondria have their own translation machinery and contain all of the RNA components required for translation: 22 tRNAs with two each for Leucine and Serine and rRNAs. Additionally, a nuclear encoded tRNA<sup>Gln</sup> was detected in the mitochondria, indicative of a pathway for tRNA trafficking into the mitochondria (84). The protein components for RNA processing and translation are missing from the mitochondrial genome. They are encoded in the nuclear genome and trafficked to the mitochondria. Among these proteins are the human mitochondrial RNase P subunits, ribosomal proteins, and various factors required for the biogenesis of tRNAs and rRNAs.

Given that tRNAs are transcribed into long polycistronic segments interspersed between rRNA, mRNA, and lncRNAs, the 5' and 3' end processing of tRNAs also releases these other transcripts. Mutations that decrease the

MRPP1 protein level affect both precursor RNA transcript levels and protein levels of respiratory chain complexes (63). Thus tRNA processing has effects beyond the 5'- or 3'-end maturation of the tRNA transcript, impacting downstream synthesis of essential proteins.

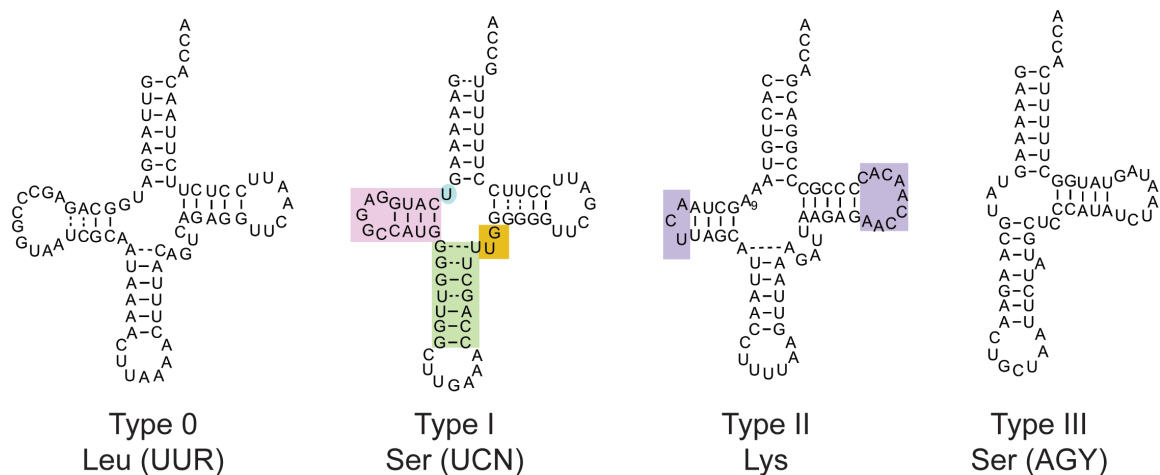


**Figure 1-8 Human mitochondrial tRNA structures.**

The canonical Type 0 tRNA is present in Leu (UUR) (shown), Leu (CUN), Asn, and Gln. Ser (UCN) is a Type I tRNA (shown), which has a shorter D loop (pink), one base between the acceptor and D steps instead of 2 (blue), an extended anticodon stem (green), and a shortened variable loop (orange). The majority of human mt-tRNAs are Type II, including Ala, Arg, Asp, Cys, Glu, Gly, His, Ile, Lys (shown), Met, Phe, Pro, Thr, Trp, Tyr, and Val. A<sub>9</sub> in tRNA<sup>Lys</sup> is methylated to stabilize the cloverleaf secondary structure. Type 2 tRNAs have variable D- and T-loop sizes and lack canonical tertiary interactions between the D and T loops (purple). Type III tRNA deviates the most from the canonical tRNA, missing the entire D-stem loop region and only exists in Ser (AGY).

### Structural characteristics of mammalian mt-tRNAs

In order to perform their biological role as adapter molecules, tRNAs must retain a specific structure that is recognized by enzymes in maturation pathways and protein synthesis. Proper folding of tRNAs, especially to form tertiary interactions in the D and T domains, is important for structure and stability as well as recognition by tRNA processing enzymes (40). A canonical cloverleaf

secondary structure and “L-shaped” tertiary structure (Type 0) is found in most tRNAs across all domains of life (Figure 1-1) (85). Type 0 tRNAs typically have two nucleotides between the acceptor- and D-stems, 5 nucleotides in the variable loop between the T- and anticodon stems. All of these features participate in tertiary interactions within tRNA (Figure 1-1).

The canonical type 0 tRNA is present in tRNA<sup>Leu(UUR)</sup> (shown in Figure 1-8), tRNA<sup>Leu(CUN)</sup>, tRNA<sup>Asn</sup>, and tRNA<sup>Gln</sup>. (Figure 1-8). Mammalian mt-tRNAs deviate in varying degrees from the canonical Type 0 tRNA. Type I tRNAs have a shortened D-loop, only one base instead of two between the acceptor and D-stems, an extended anticodon stem, and a shortened variable loop between the acceptor and T-stems (86). The majority of human mt-tRNAs are grouped under the category of Type II, with variable D- and T-loop sizes and sequences. Type II tRNAs lack canonical tertiary interactions between the D- and T-loops. Instead, the D-loop interacts with the variable loop to stabilize the tRNA core as shown for human mt-tRNA<sup>Asp</sup> (87) and bovine mt-tRNA<sup>Phe</sup> (88). Posttranscriptional modifications are important for structural stability of many Type II tRNAs, as in the example of tRNA<sup>Lys</sup>, which adopts an inactive bulged hairpin conformation in the absence of *N*1-methylation at A9 (89-91). Methylation at A9 disrupts Watson-Crick base pair interactions thus destabilizing the nonfunctional stem-looped structure and as a result, the cloverleaf structure is formed instead.

The most drastic deviation from the conserved canonical tRNA structure is mt-tRNA<sup>Ser(AGY)</sup>, which lacks the D-domain completely (Figure 1-8). This tRNA is missing important secondary and tertiary interactions that formed with the D-

domain. Regardless of the minimal structural features of this tRNA, biochemical studies have shown that mt-tRNA<sup>Ser(AGY)</sup> is aminoacylated, mainly recognized at the T-loop region, and is functional for translation *in vitro* (92,93). Additional covalent modifications are also important for the function of mt-tRNAs. However, tRNA processing catalyzed by RNase P is the first step in the maturation pathway. Thus, these modifications are not essential for the work done in this thesis.

### **Mitochondrial tRNA in disease**

Mitochondrial dysfunction is implicated in human aging, neurodegenerative diseases, cancer, diabetes, and various rare diseases (94). This often originates from damage to or mutations in mitochondrial DNA; nearly half of the mutations map to mt-tRNA genes; which make up only 10% of the genome (95,96). Mitochondrial DNA is highly susceptible to mutation and while some mutations contribute to the diversity of the genome, some are pathogenic, leading to disease (97). Since mitochondria are particularly important for energy-consuming tissues, such as the brain and muscle, mitochondrial diseases often result in encephalomyopathies from defective oxidative phosphorylation (85). These diseases can lead to symptoms that range from exercise intolerance and limb weakness to more severe phenotypes such as cardiopathies, diabetes, deafness, and blindness.

Disease-related mutations have been found in almost all tRNA genes, but cluster in genes encoding mt-tRNA<sup>Leu(UUR)</sup> (20 mutations), mt-tRNA<sup>Lys</sup> (10

mutations), and mt-tRNA<sup>Ile</sup> (10 mutations). They are found in any structural domain of tRNA but rarely in the anticodon triplet since these mutations would likely be lethal. To highlight a few mutations, a single A-to-G mutation in the D-loop of mt-tRNA<sup>Leu(UUR)</sup> is correlated with MELAS (mitochondrial epilepsy with lactic acidosis and stroke-like episodes) syndrome and a A-to-G mutation in the T-loop of mt-tRNA<sup>Lys</sup> is correlated with MERRF (myoclonic epilepsy with ragged red fibers) syndrome (95). Certain mutations can be found in a number of different pathologies.

The pathogenic mutations in tRNA have been shown to affect the tertiary structure, 3'-end processing efficiency, amino-acylation, and/or binding to elongation factors using *in vitro* studies of unmodified tRNA (95,98,99). However, these studies may not encompass the entire story because posttranscriptional modifications play a role in tRNA folding, stability, and function. To study tRNA maturation *in vivo*, molecular probes and tools such as small compound inhibitors and/or activators should be developed. This work can draw connections between the defects observed on a molecular level to the phenotypes exhibited in patients with mitochondrial dysfunction.

## **CONCLUSIONS AND SIGNIFICANCE**

RNase P presents an exciting case for comparing the molecular mechanisms employed by RNP and protein-only enzymes. Since the discovery of RNP RNase P as a ribozyme, many groups have investigated its substrate recognition, catalytic mechanisms, and molecular composition. Further research

has broadened our view of RNase P from an RNA-dependent enzyme to one that is composed of proteins only in Eukarya. Work with both RNP RNase P and PRORP provide valuable insight into the mechanism and function of these enzymes in the context of the cell. In addition to pre-tRNA processing, human mitochondrial RNase P affects the processing of non-tRNA transcript levels and the levels of essential proteins. Furthermore, a larger understanding of the molecular mechanisms employed by PRORP will provide insight into dysfunctional mitochondrial RNA processing that lead to disease. Work has been done to characterize the effects of a number of mutations on mitochondrial biogenesis. However, we still lack a fundamental mechanistic understanding of the roles of protein subunits in human mitochondrial RNase P, an enzyme shown to have a profound effect on RNA processing and protein levels in the mitochondria.

## **OBJECTIVE**

Work has been done to elucidate the molecular function of the plant ortholog of MRPP3, PRORP1. However human mitochondrial RNase P requires two additional proteins (MRPP1 and MRPP2) for catalysis. Therefore, Chapter 2 describes a model for pre-tRNA hydrolysis catalyzed by human mtRNase P that highlights the importance of the MRPP1/2 subcomplex on the recognition and processing of mt-tRNA transcripts. Chapter 3 presents inhibitors that are potent against plant and human mitochondrial PRORP, identified from a high throughput screen. These inhibitors could be developed into tools to investigate tRNA



processing pathways in mitochondria *in vivo*. Taken together, this work provides a mechanistic approach for investigating the function of PRORP in the human mitochondria and multi-subunit RNA-protein complexes. We also present a framework for studying mitochondrial diseases that arise from dysfunctional RNA processing.

## REFERENCES

1. Walker, S. C., and Engelke, D. R. (2006) Ribonuclease P: the evolution of an ancient RNA enzyme. *Crit Rev Biochem Mol Biol* **41**, 77-102
2. Phizicky, E. M., and Hopper, A. K. (2010) tRNA biology charges to the front. *Genes & Development* **24**, 1832-1860
3. Frank, D. N., and Pace, N. R. (1998) Ribonuclease P: unity and diversity in a tRNA processing ribozyme. *Annu Rev Biochem* **67**, 153-180
4. Randau, L. (2012) RNA processing in the minimal organism *Nanoarchaeum equitans* *Genome Biology* **13**, 1-11
5. Guerrier-Takada, C., Gardiner, K., Marsh, T., Pace, N., and Altman, S. (1983) The RNA moiety of ribonuclease P is the catalytic subunit of the enzyme. *Cell* **35**, 849-857
6. Holzmann, J., Frank, P., Löffler, E., Bennett, K. L., Gerner, C., and Rossmann, W. (2008) RNase P without RNA: Identification and Functional Reconstitution of the Human Mitochondrial tRNA Processing Enzyme. *Cell* **135**, 462-474
7. Chamberlain, J. R., Lee, Y., Lane, W. S., and Engelke, D. R. (1998) Purification and characterization of the nuclear RNase P holoenzyme complex reveals extensive subunit overlap with RNase MRP. *Genes Dev* **12**, 1678-1690
8. Smith, J. K., Hsieh, J., and Fierke, C. A. (2007) Importance of RNA-protein interactions in bacterial ribonuclease P structure and catalysis. *Biopolymers* **87**, 329-338
9. Pannucci, J. A., Haas, E. S., Hall, T. A., Harris, J. K., and Brown, J. W. (1999) RNase P RNAs from some Archaea are catalytically active. *Proc Natl Acad Sci U S A* **96**, 7803-7808
10. Kikovska, E., Svard, S. G., and Kirsebom, L. A. (2007) Eukaryotic RNase P RNA mediates cleavage in the absence of protein. *Proc Natl Acad Sci U S A* **104**, 2062-2067
11. Kurz, J. C., Niranjanakumari, S., and Fierke, C. A. (1998) Protein component of *Bacillus subtilis* RNase P specifically enhances the affinity for precursor-tRNA<sup>Asp</sup>. *Biochemistry* **37**, 2393-2400
12. Kurz, J. C., and Fierke, C. A. (2002) The affinity of magnesium binding sites in the *Bacillus subtilis* RNase P x pre-tRNA complex is enhanced by the protein subunit. *Biochemistry* **41**, 9545-9558
13. Hsieh, J., Andrews, A. J., and Fierke, C. A. (2004) Roles of protein subunits in RNA-protein complexes: lessons from ribonuclease P. *Biopolymers* **73**, 79-89
14. Hsieh, J., Rueda, D., Koutmos, K. S., Koutmos, M., Walter, N. G., and Fierke, C. A. (2010) A divalent cation stabilizes the active conformation of the *B. subtilis* RNase P•pre-tRNA complex: a role for an inner-sphere metal ion in RNase P *in preparation*
15. Liu, X. (2014) Molecular recognition of inhibitors, metal ions and substrates by ribonuclease P. University of Michigan

16. Haas, E. S., Banta, A. B., Harris, J. K., Pace, N. R., and Brown, J. W. (1996) Structure and evolution of ribonuclease P RNA in Gram-positive bacteria. *Nucleic acids research* **24**, 4775-4782
17. Haas, E. S., and Brown, J. W. (1998) Evolutionary variation in bacterial RNase P RNAs. *Nucleic acids research* **26**, 4093-4099
18. Chen, J. L., and Pace, N. R. (1997) Identification of the universally conserved core of ribonuclease P RNA. *Rna* **3**, 557-560
19. Kazantsev, A. V., Krivenko, A. A., and Pace, N. R. (2009) Mapping metal-binding sites in the catalytic domain of bacterial RNase P RNA. *Rna* **15**, 266-276
20. Harris, M. E., Nolan, J. M., Malhotra, A., Brown, J. W., Harvey, S. C., and Pace, N. R. (1994) Use of photoaffinity crosslinking and molecular modeling to analyze the global architecture of ribonuclease P RNA. *Embo J* **13**, 3953-3963
21. Westhof, E., and Altman, S. (1994) Three-dimensional working model of M1 RNA, the catalytic RNA subunit of ribonuclease P from Escherichia coli. *Proc Natl Acad Sci U S A* **91**, 5133-5137
22. Pan, T., Loria, A., and Zhong, K. (1995) Probing of tertiary interactions in RNA: 2'-hydroxyl-base contacts between the RNase P RNA and pre-tRNA. *Proc Natl Acad Sci U S A* **92**, 12510-12514
23. Green, C. J., Rivera-León, R., and Vold, B. S. (1996) The catalytic core of RNase P. *Nucleic acids research* **24**, 1497-1503
24. Loria, A., and Pan, T. (2001) Modular construction for function of a ribonucleoprotein enzyme: the catalytic domain of Bacillus subtilis RNase P complexed with B. subtilis RNase P protein. *Nucleic acids research* **29**, 1892-1897
25. Wu, S., Kikovska, E., Lindell, M., and Kirsebom, L. A. (2012) Cleavage Mediated by the Catalytic Domain of Bacterial RNase P RNA. *Journal of Molecular Biology* **422**, 204-214
26. Harris, J. K., Haas, E. S., Williams, D., Frank, D. N., and Brown, J. W. (2001) New insight into RNase P RNA structure from comparative analysis of the archaeal RNA. *Rna* **7**, 220-232
27. Lai, L. B., Chan, P. P., Cozen, A. E., Bernick, D. L., Brown, J. W., Gopalan, V., and Lowe, T. M. (2010) Discovery of a minimal form of RNase P in Pyrobaculum. *Proc Natl Acad Sci USA* **107**
28. Marquez, S. M., Harris, J. K., Kelley, S. T., Brown, J. W., Dawson, S. C., Roberts, E. C., and Pace, N. R. (2005) Structural implications of novel diversity in eucaryal RNase P RNA. *Rna* **11**, 739-751
29. Marquez, S. M., Chen, J. L., Evans, D., and Pace, N. R. (2006) Structure and Function of Eukaryotic Ribonuclease P RNA. *Molecular Cell* **24**, 445-456
30. Byrne, R. T., Konevega, A. L., Rodnina, M. V., and Antson, A. A. (2010) The crystal structure of unmodified tRNA Phe from Escherichia coli. *Nucleic acids research* **38**, 4154-4162

31. Torres-Larios, A., Swinger, K. K., Krasilnikov, A. S., Pan, T., and Mondragon, A. (2005) Crystal structure of the RNA component of bacterial ribonuclease P. *Nature* **437**, 584-587
32. Krasilnikov, A. S., Xiao, Y., Pan, T., and Mondragon, A. (2004) Basis for structural diversity in homologous RNAs. *Science* **306**, 104-107
33. Krasilnikov, A. S., Yang, X., Pan, T., and Mondragon, A. (2003) Crystal structure of the specificity domain of ribonuclease P. *Nature* **421**, 760-764
34. Kazantsev, A. V., Krivenko, A. A., Harrington, D. J., Holbrook, S. R., Adams, P. D., and Pace, N. R. (2005) Crystal structure of a bacterial ribonuclease P RNA. *Proc Natl Acad Sci U S A* **102**, 13392-13397
35. Kazantsev, A. V., Krivenko, A. A., Harrington, D. J., Carter, R. J., Holbrook, S. R., Adams, P. D., and Pace, N. R. (2003) High-resolution structure of RNase P protein from *Thermotoga maritima*. *Proc Natl Acad Sci U S A* **100**, 7497-7502
36. Stams, T., Niranjanakumari, S., Fierke, C. A., and Christianson, D. W. (1998) Ribonuclease P protein structure: evolutionary origins in the translational apparatus. *Science* **280**, 752-755
37. Spitzfaden, C., Nicholson, N., Jones, J. J., Guth, S., Lehr, R., Prescott, C. D., Hegg, L. A., and Eggleston, D. S. (2000) The structure of ribonuclease P protein from *Staphylococcus aureus* reveals a unique binding site for single-stranded RNA. *J Mol Biol* **295**, 105-115
38. Koutmou, K. S., Day-Storms, J. J., and Fierke, C. A. (2011) The RNR motif of *B. subtilis* RNase P protein interacts with both PRNA and pre-tRNA to stabilize an active conformer. *Rna* **17**, 1225-1235
39. Chen, Y. (2015) Ribonuclease P catalysis: Metal ion interaction and conformational dynamics. University of Michigan, Ann Arbor, MI
40. Reiter, N. J., Osterman, A., Torres-Larios, A., Swinger, K. K., Pan, T., and Mondragón, A. (2010) Structure of a bacterial ribonuclease P holoenzyme in complex with tRNA. *Nature* **468**, 784-789
41. Lim, W. H. (2011) Importance of substrate recognition and metal ions in the Ribonuclease P catalysis, Ph.D. Thesis. University of Michigan, Ann Arbor, MI, USA
42. Christian, E. L., Zahler, N. H., Kaye, N. M., and Harris, M. E. (2002) Analysis of substrate recognition by the ribonucleoprotein endonuclease RNase P. *Methods* **28**, 307-322
43. Kirsebom, L. A., and Svard, S. G. (1994) Base pairing between *Escherichia coli* RNase P RNA and its substrate. *Embo J* **13**, 4870-4876
44. Howard, M. J., Lim, W. H., Fierke, C. A., and Koutmos, M. (2012) Mitochondrial ribonuclease P structure provides insight into the evolution of catalytic strategies for precursor-tRNA 5' processing. *PNAS* **109**, 16149-16154
45. Rackham, O., and Filipovska, A. (2012) The role of mammalian PPR domain proteins in the regulation of mitochondrial gene expression. *Biochimica et Biophysica Acta (BBA) - Gene Regulatory Mechanisms* **1819**, 1008-1016

46. Gobert, A., Butmann, B., Taschner, A., Gößringer, M., Holzmann, J., Hartmann, R. K., Rossmannith, W., and Giegé, P. (2010) A single Arabidopsis organellar protein has RNase P activity. *Nature Structural and Molecular Biology* **17**, 740-744
47. Lai, L. B., Bernal-Bayard, P., Mohannath, G., Lai, S. M., Gopalan, V., and Vioque, A. (2011) A functional RNase P protein subunit of bacterial origin in some eukaryotes. *Molecular Genetics and Genomics* **286**, 359-369
48. Taschner, A., Weber, C., Buzet, A., Hartmann, Roland K., Hartig, A., and Rossmannith, W. (2012) Nuclear RNase P of Trypanosoma brucei: A Single Protein in Place of the Multicomponent RNA-Protein Complex. *Cell Reports* **2**, 19-25
49. Gutmann, B., Gobert, A., and Giegé, P. (2012) PRORP proteins support RNase P activity in both organelles and the nucleus in Arabidopsis. *Genes & Development* **26**, 1022-1027
50. Hartmann, E., and Hartmann, R. K. (2003) The enigma of ribonuclease P evolution. *Trends Genet* **19**, 561-569
51. Piccinelli, P., Rosenblad, M. A., and Samuelsson, T. (2005) Identification and analysis of ribonuclease P and MRP RNA in a broad range of eukaryotes. *Nucleic acids research* **33**, 4485-4495
52. Rosenblad, M. A., López, M. D., Piccinelli, P., and Samuelsson, T. (2006) Inventory and analysis of the protein subunits of the ribonucleases P and MRP provides further evidence of homology between the yeast and human enzymes. *Nucleic acids research* **34**, 5145-5156
53. Lopez Sanchez, M. I. G., Shearwood, A.-M. J., Chia, T., Davies, S. M. K., Rackham, O., and Filipovska, A. (2014) Estrogen-Mediated Regulation of Mitochondrial Gene Expression. *Molecular Endocrinology* **29**, 14-27
54. Lopez Sanchez, M. I. G., Mercer, T. R., Davies, S. M. K., Shearwood, A.-M. J., Nygård, K. K. A., Richman, T. R., Mattick, J. S., Rackham, O., and Filipovska, A. (2011) RNA processing in human mitochondria. *Cell Cycle* **10**, 2904-2916
55. Sen, A., Karasik, A., Shanmuganathan, A., Mirkovic, E., Koutmos, M., and Cox, R. T. (2016) Loss of the mitochondrial protein-only ribonuclease P complex causes aberrant tRNA processing and lethality in Drosophila. *Nucleic acids research* **44**, 6409-6422
56. Jackman, J. E., Montange, R. K., Malik, H. S., and Phizicky, E. M. (2003) Identification of the yeast gene encoding the tRNA m1G methyltransferase responsible for modification at position 9. *Rna* **9**, 574-585
57. Shao, Z., Yan, W., Peng, J., Zuo, X., Zou, Y., Li, F., Gong, D., Ma, R., Wu, J., Shi, Y., Zhang, Z., Teng, M., Li, X., and Gong, Q. (2014) Crystal structure of tRNA m1G9 methyltransferase Trm10: insight into the catalytic mechanism and recognition of tRNA substrate. *Nucleic acids research* **42**, 509-525
58. Clark, W. C., Evans, M. E., Dominissini, D., Zheng, G., and Pan, T. (2016) tRNA base methylation identification and quantification via high-throughput sequencing. *Rna* **22**, 1771-1784

59. Vilardo, E., Nachbagauer, C., Buzet, A., Taschner, A., Holzmann, J., and Rossmann, W. (2012) A subcomplex of human mitochondrial RNase P is a bifunctional methyltransferase-extensive moonlighting in mitochondrial tRNA biogenesis. *Nucleic acids research* **40**, 11583-11593
60. Swinehart, W. E., and Jackman, J. E. (2015) Diversity in mechanism and function of tRNA methyltransferases. *RNA Biology* **12**, 398-411
61. Vilardo, E., and Rossmann, W. (2015) Molecular insights into HSD10 disease: impact of SDR5C1 mutations on the human mitochondrial RNase P complex. *Nucleic acids research* **43**, 5112-5119
62. Deutschmann, A. J., Amberger, A., Zavadil, C., Steinbeisser, H., Mayr, J. A., Feichtinger, R. G., Oerum, S., Yue, W. W., and Zschocke, J. (2014) Mutation or knock-down of 17beta-hydroxysteroid dehydrogenase type 10 cause loss of MRPP1 and impaired processing of mitochondrial heavy strand transcripts. *Human molecular genetics* **23**, 3618-3628
63. Metodiev, M. D., Thompson, K., Alston, Charlotte L., Morris, Andrew A. M., He, L., Assouline, Z., Rio, M., Bahi-Buisson, N., Pyle, A., Griffin, H., Siira, S., Filipovska, A., Munnich, A., Chinnery, Patrick F., McFarland, R., Rötig, A., and Taylor, Robert W. (2016) Recessive Mutations in TRMT10C Cause Defects in Mitochondrial RNA Processing and Multiple Respiratory Chain Deficiencies. *The American Journal of Human Genetics* **98**, 993-1000
64. Falk, M. J., Gai, X., Shigematsu, M., Vilardo, E., and Takase, R. (2016) A novel HSD17B10 mutation impairing the activities of the mitochondrial RNase P complex causes X-linked intractable epilepsy and neurodevelopmental regression. *RNA Biology* **13**, 477-485
65. Van Laer, B., Roovers, M., Wauters, L., Kasprzak, J. M., Dyzma, M., Deyaert, E., Kumar Singh, R., Feller, A., Bujnicki, J. M., Droogmans, L., and Versées, W. (2016) Structural and functional insights into tRNA binding and adenosine N1-methylation by an archaeal Trm10 homologue. *Nucleic acids research* **44**, 940-953
66. Kissinger, C. R., Rejto, P. A., Pelletier, L. A., Thomson, J. A., Showalter, R. E., Abreo, M. A., Agree, C. S., Margosiak, S., Meng, J. J., Aust, R. M., Vanderpool, D., Li, B., Tempczyk-Russell, A., and Villafranca, J. E. (2004) Crystal Structure of Human ABAD/HSD10 with a Bound Inhibitor: Implications for Design of Alzheimer's Disease Therapeutics. *Journal of Molecular Biology* **342**, 943-952
67. Reinhard, L., Sridhara, S., and Hallberg, B. M. (2015) Structure of the nuclease subunit of human mitochondrial RNase P. *Nucleic acids research*
68. Karasik, A., Shanmuganathan, A., Howard, M. J., Fierke, C. A., and Koutmos, M. (2016) Nuclear Protein-Only Ribonuclease P2 Structure and Biochemical Characterization Provide Insight into the Conserved Properties of tRNA 5' End Processing Enzymes. *Journal of Molecular Biology* **428**, 26-40

69. Li, F., Liu, X., Zhou, W., Yang, X., and Shen, Y. (2015) Auto-inhibitory Mechanism of the Human Mitochondrial RNase P Protein Complex. *Scientific reports* **5**, 9878
70. Imai, T., Nakamura, Maeda, Nakayama, Gao, Nakashima, Kakuta, and Kimura. (2014) Pentatricopeptide repeat motifs in the processing enzyme PRORP1 in *Arabidopsis thaliana* play a crucial role in recognition of nucleotide bases at T $\psi$ C loop in precursor tRNAs. *Biochemical and Biophysical Research Communications* **450**, 1541-1546
71. Cassano, A. G., Anderson, V. E., and Harris, M. E. (2004) Analysis of solvent nucleophile isotope effects: evidence for concerted mechanisms and nucleophilic activation by metal coordination in nonenzymatic and ribozyme-catalyzed phosphodiester hydrolysis. *Biochemistry* **43**, 10547-10559
72. Howard, M. H., Klemm, B. P., and Fierke, C. A. (2015) Mechanistic Studies Reveal Similar Catalytic Strategies for Phosphodiester Bond Hydrolysis by Protein-only and RNA-dependent Ribonuclease P. *Journal of Biological Chemistry* **290**, 13454-13464
73. Smith, D., and Pace, N. R. (1993) Multiple magnesium ions in the ribonuclease P reaction mechanism. *Biochemistry* **32**, 5273-5281
74. Perreault, J. P., and Altman, S. (1993) Pathway of activation by magnesium ions of substrates for the catalytic subunit of RNase P from *Escherichia coli*. *J Mol Biol* **230**, 750-756
75. Beebe, J. A., Kurz, J. C., and Fierke, C. A. (1996) Magnesium ions are required by *Bacillus subtilis* ribonuclease P RNA for both binding and cleaving precursor tRNA<sup>Asp</sup>. *Biochemistry* **35**, 10493-10505
76. Brannvall, M., and Kirsebom, L. A. (1999) Manganese ions induce miscleavage in the *Escherichia coli* RNase P RNA-catalyzed reaction. *J Mol Biol* **292**, 53-63
77. Cuzic, S., and Hartmann, R. K. (2005) Studies on *Escherichia coli* RNase P RNA with Zn<sup>2+</sup> as the catalytic cofactor. *Nucleic acids research* **33**, 2464-2474
78. Hsieh, J., and Fierke, C. A. (2009) Conformational change in the *Bacillus subtilis* RNase P holoenzyme-pre-tRNA complex enhances substrate affinity and limits cleavage rate. *Rna* **15**, 1565-1577
79. Li, X., and Gegenheimer, P. (1997) Ribonuclease P Catalysis Requires Mg<sup>2+</sup> Coordinated to the pro-RP Oxygen of the Scissile Bond. *Biochemistry* **36**, 2425-2438
80. Thomas, B. C., Chamberlain, J., Engelke, D. R., and Gegenheimer, P. (2000) Evidence for an RNA-based catalytic mechanism in eukaryotic nuclear ribonuclease P. *Rna* **6**, 554-562
81. Thomas, B. C., Li, X., and Gegenheimer, P. (2000) Chloroplast ribonuclease P does not utilize the ribozyme-type pre-tRNA cleavage mechanism. *Rna* **6**, 545-553
82. Walczyk, D., Gößringer, M., Rossmannith, W., Zatsopin, T. S., Oretskaya, T. S., and Hartmann, R. K. (2016) Analysis of the Cleavage Mechanism by Protein-Only RNase P Using Precursor tRNA Substrates with

- Modifications at the Cleavage Site. *Journal of Molecular Biology* **428**, 4917-4928
83. Crary, S. M., Kurz, J. C., and Fierke, C. A. (2002) Specific phosphorothioate substitutions probe the active site of *Bacillus subtilis* ribonuclease P. *Rna* **8**, 933-947
  84. Rubio, M. A. T., Rinehart, J. J., Krett, B., Duvezin-Caubet, S., Reichert, A. S., Söll, D., and Alfonzo, J. D. (2008) Mammalian mitochondria have the innate ability to import tRNAs by a mechanism distinct from protein import. *Proceedings of the National Academy of Sciences* **105**, 9186-9191
  85. Suzuki, T., Nagao, A., and Suzuki, T. (2011) Human mitochondrial tRNAs: biogenesis, function, structural aspects, and diseases. *Annual review of genetics* **45**, 299-329
  86. Watanabe, Y., Kawai, G., Yokogawa, T., Hayashi, N., Kumazawa, Y., Ueda, T., Nishikawa, K., Hirao, I., Miura, K., and Watanabe, K. (1994) Higher-order structure of bovine mitochondrial tRNA(SerUGA): chemical modification and computer modeling. *Nucleic acids research* **22**, 5378-5384
  87. Messmer, M., Pütz, J., Suzuki, T., Suzuki, T., Sauter, C., Sissler, M., and Catherine, F. (2009) Tertiary network in mammalian mitochondrial tRNA<sup>Asp</sup> revealed by solution probing and phylogeny. *Nucleic acids research* **37**, 6881-6895
  88. Wakita, K., Watanabe, Y., Yokogawa, T., Kumazawa, Y., Nakamura, S., Ueda, T., Watanabe, K., and Nishikawa, K. (1994) Higher-order structure of bovine mitochondrial tRNA(Phe) lacking the 'conserved' GG and T psi CG sequences as inferred by enzymatic and chemical probing. *Nucleic acids research* **22**, 347-353
  89. Helm, M., Brulé, H., Degoul, F., Capanec, C., Leroux, J.-P., Giegé, R., and Florentz, C. (1998) The presence of modified nucleotides is required for cloverleaf folding of a human mitochondrial tRNA. *Nucleic acids research* **26**, 1636-1643
  90. Helm, M., Giegé, R., and Florentz, C. (1999) A Watson-Crick Base-Pair-Disrupting Methyl Group (m<sup>1</sup>A<sub>9</sub>) Is Sufficient for Cloverleaf Folding of Human Mitochondrial tRNA<sup>Lys</sup> *Biochemistry* **38**, 13338-13346
  91. Voigts-Hoffmann, F., Hengesbach, M., Kobitski, A. Y., van Aerschot, A., Herdewijn, P., Nienhaus, G. U., and Helm, M. (2007) A Methyl Group Controls Conformational Equilibrium in Human Mitochondrial tRNA<sup>Lys</sup>. *Journal of the American Chemical Society* **129**, 13382-13383
  92. Ueda, T., Yotsumoto, Y., Ikeda, K., and Watanabe, K. (1992) The T-loop region of animal mitochondrial tRNA(Ser)(AGY) is a main recognition site for homologous seryl-tRNA synthetase. *Nucleic acids research* **20**, 2217-2222
  93. Hanada, T., Suzuki, T., Yokogawa, T., Takemoto - Hori, C., Sprinzl, M., and Watanabe, K. (2001) Translation ability of mitochondrial tRNAs<sup>Ser</sup> with unusual secondary structures in an in vitro translation system of bovine mitochondria. *Genes to Cells* **6**, 1019-1030



94. Shutt, T. E., and Shadel, G. S. (2010) A compendium of human mitochondrial gene expression machinery with links to disease. *Environmental and molecular mutagenesis* **51**, 360-379
95. Florentz, C., Sohm, B., Tryoen-Toth, P., Putz, J., and Sissler, M. (2003) Human mitochondrial tRNAs in health and disease. *Cellular and molecular life sciences : CMLS* **60**, 1356-1375
96. Wittenhagen, L. M., and Kelley, S. O. (2003) Impact of disease-related mitochondrial mutations on tRNA structure and function. *Trends Biochem Sci* **28**, 605-611
97. Pesole, G., Gissi, C., De Chirico, A., and Saccone, C. (1999) Nucleotide Substitution Rate of Mammalian Mitochondrial Genomes. *Journal of Molecular Evolution* **48**, 427-434
98. Yarham, J. W., Elson, J. L., Blakely, E. L., McFarland, R., and Taylor, R. W. (2010) Mitochondrial tRNA mutations and disease. *Wiley Interdisciplinary Reviews - RNA* **1**, 304-324
99. Enriquez, J. A., Chomyn, A., and Attardi, G. (1995) MtDNA mutation in MERRF syndrome causes defective aminoacylation of tRNA<sup>Lys</sup> and premature translation termination. *Nat Genet* **10**, 47-55

## CHAPTER 2<sup>3</sup>

### **Methyltransferase subcomplex of human mitochondrial RNase P activates the metallonuclease subunit by enhancing catalytic efficiency and pre-tRNA affinity**

#### **ABSTRACT**

Ribonuclease P (RNase P) is essential for catalyzing cleavage at the 5' end of precursor tRNA (pre-tRNA) to remove extra nucleotides. In many organisms, RNase P is a ribonucleoprotein (RNP) complex with a catalytic RNA subunit. One of the exceptions is human mitochondrial RNase P (mtRNase P), which is composed of three protein subunits: mitochondrial RNase P protein (MRPP) 1, 2 and 3. MRPP3 contains the active site that catalyzes pre-tRNA cleavage. MRPP3 catalysis requires MRPP1 and MRPP2, which form a methyltransferase subcomplex (MRPP1/2) that catalyzes methylation at position 9 (m<sup>1</sup>R9) of mitochondrial tRNAs. To understand the mechanism of MRPP3 activation by MRPP1/2, we performed steady-state kinetics and fluorescence anisotropy (FA) binding measurements, demonstrating that the MRPP1/2 subcomplex enhances the catalytic activity of MRPP3 at least 100,000-fold and the apparent substrate affinity at least 300-fold. In addition, *in vitro* pull-down

---

<sup>3</sup> Nancy Wu performed the binding and metal-dependence experiments, purified the enzymes and substrates, Xin Liu performed the MTO and STO experiments. N.W. and X. L. designed the experiments, interpreted the results, developed the models, wrote the paper and made the figures. Aranganathan Shanmuganathan purified MRPP1/2 for the pull down experiment and conducted the AUC experiments.

results indicate that MRPP3 forms a complex with MRPP1/2 that is stabilized by the presence of pre-tRNA, suggesting that MRPP3 recognizes the MRPP1/2-bound pre-tRNA or that pre-tRNA induces structural rearrangements in MRPP1/2 and/or MRPP3 that increase the binding affinity between MRPP1/2 and 3. We propose that binding of MRPP1/2 to pre-tRNA alters the pre-tRNA structure, yielding a pre-tRNA structure that is recognized by MRPP3 at a higher affinity and efficiently cleaved. We propose a new model for pre-tRNA cleavage catalyzed by human mtRNase P that highlights the importance of the MRPP1/2 subcomplex for recognition and processing of mitochondrial pre-tRNA transcripts.

## **BACKGROUND**

Mitochondrial dysfunction is implicated in human aging, neurodegenerative diseases, cancer, diabetes, and various rare diseases (1). This dysfunction often originates from damage and mutations in mitochondrial DNA, with more than half of these disease-related point mutations mapped to tRNA genes (2-5). The human mitochondrial genome is transcribed into three polycistronic transcripts, all of which are processed by nuclear-encoded mitochondrial RNase P and RNase Z that recognize pre-tRNA to generate 5' and 3' end matured tRNA, respectively, thus releasing interspersed mRNA, ribosomal RNA and long noncoding RNA transcripts (6). RNase P is a divalent metal-ion dependent endonuclease found in all domains of life and uses magnesium as the *in vivo* metal to properly fold and bind to pre-tRNA substrates and catalyze

hydrolysis (7). RNase P catalyzes the hydrolysis of a specific phosphodiester bond in precursor tRNA (pre-tRNA), removing a 5' leader sequence with a 3'-OH group and leaving a tRNA molecule with a 5'-phosphate group. In many organisms, RNase P is a RNP complex with a catalytic RNA subunit and accessory proteins (8,9). Our view of RNase P expanded with the identification of protein-only RNase P (PRORP) found in plants and human mitochondria. In plant mitochondria, nuclei, and chloroplasts, PRORP functions as a single-subunit enzyme (10,11). In contrast, human mtRNase P is composed of three protein subunits: MRPP 1, 2 and 3 (12). MRPP3 is the catalytic subunit containing the active site for pre-tRNA hydrolysis. MRPP3, which is homologous to plant PRORP1, requires two other proteins (MRPP1 and MRPP2) to activate RNase P activity (12).

Apart from their roles in human mtRNase P, MRPP1, a tRNA methyltransferase, and MRPP2, a hydroxysteroid (17- $\beta$ ) dehydrogenase, function together in a stable complex (MRPP1/2) to catalyze methylation of A or G at position 9 in mitochondrial tRNA (mt-tRNA) (13). MRPP2 is an NAD-dependent member of the short-chain dehydrogenase/reductase superfamily involved in isoleucine metabolism and other cellular functions (14,15). MRPP1 requires MRPP2 for stability and function, but the dehydrogenase activity and NAD binding capability of MRPP2 are dispensable for methyltransferase activity (12,16). MRPP2 mutations and knockdown experiments indicate that MRPP2 is required for stable expression of MRPP1 (17). Furthermore, the data suggests that the enzymatic activities of MRPP1 and MRPP2 are not essential to activate

cleavage catalyzed by MRPP3 (16). Thus, MRPP1 and MRPP2 are proposed to play a structural role that is independent of their primary catalytic functions. However, more work needs to be done to test this hypothesis.

MRPP1, 2, and 3 are important for proper RNA processing of mitochondrial transcripts and for the expression of respiratory chain complexes in mitochondria. The disruption of these processes result in mitochondrial dysfunction and disease (18-20). Recessive MRPP1 mutations lead to low levels of assembled respiratory chain complexes, possibly due to the instability of the mutant protein and respiratory chain complexes and inadequate processing of mt-tRNA (19). Furthermore, pathogenic mutations located at the subunit interface of MRPP2 could potentially destabilize the tetramer complex, leading to a reduction in MRPP1 protein levels and reduced tRNA processing (21). A MRPP2 mutation found in patient fibroblasts led to lower protein levels of both MRPP1 and MRPP2 (17). Both MRPP1 and MRPP3 knockdown experiments result in enrichment of precursor transcripts indicating a reduction in tRNA and RNA processing (6). Furthermore, the loss of the mitochondrial PRORP in *Drosophila* causes aberrant tRNA processing and lethality (20).

MRPP1/2 is proposed to play a structural role in activating MRPP3 and RNase P activity. Two crystal structures of MRPP3 with N-terminal truncations show the active site is in a distorted, inactive conformation with no active site metals bound. The authors independently proposed that MRPP1 and MRPP2 mediate metal binding at the active site to facilitate a conformational change forming the active MRPP3 conformer (22,23). However, the truncated MRPP3

constructs are not activated by MRPP1/2. Thus, an investigation into the function of MRPP1/2 in mitochondrial RNase P activity will enhance our mechanistic understanding of multi-subunit PRORP.

In this chapter, we report the first multiple-turnover kinetic data catalyzed by human mtRNase P and demonstrate that the MRPP1/2 subcomplex enhances the catalytic activity of MRPP3 by increasing substrate affinity. Consistent with this, pull-down results show that pre-tRNA stabilizes the formation of MRPP1/2/3 complex. We therefore propose a model of catalysis that provides a framework for interpreting published results regarding the effects of MRPP on RNA transcript levels, novel insights into understanding mt-tRNA-related diseases, and will guide future work in dissecting the enzymatic mechanism and function of human mtRNase P in the context of a cell.

## **RESULTS**

### **MRPP1/2 enhances catalysis by MRPP3**

Previous studies demonstrated that MRPP3 requires the MRPP1/2 subcomplex for efficient catalysis, but the mechanism behind this observation is poorly understood (12,16). We investigated the activity of human mtRNase P using a previously described bacterial fluorescein-labeled pre-tRNA<sup>Asp</sup> (Fl-pre-tRNA) substrate, which has a canonical cloverleaf secondary structure. Fl-pre-tRNA is processed efficiently by PRORP1 from *A. thaliana*, a homolog of MRPP3, and was used to elucidate the catalytic mechanism of PRORP1 (24).

Therefore, FI-pre-tRNA<sup>Asp</sup> is suitable for studying the mechanism of human mtRNase P and the role of MRPP1/2 in catalysis.

To investigate the mechanism of MRPP3 activation by the MRPP1/2 subcomplex, we measured the initial rates of FI-pre-tRNA cleavage at various concentrations of MRPP1/2 and substrate using low nanomolar concentrations of MRPP3 under multiple-turnover (MTO) conditions. FI-pre-tRNA is completely cleaved at the correct site under saturating concentrations of MRPP1/2 (Figure 2-1A). This is the first study to demonstrate MTO activity of human mtRNase P *in vitro*; previous work has measured single turnover (STO) activity. The addition of MRPP1/2 alters all of the apparent Michaelis-Menten parameters ( $k_{cat,app}$ ,  $K_{M,app}$ , and  $k_{cat}/K_{M,app}$ ), which are listed in Table 2-1. Equation 2-5 was fit to the dependence of  $k_{cat,app}$  on MRPP1/2 concentration to determine  $k_{chem}$  at saturating MRPP1/2 concentration ( $0.25\text{ s}^{-1}$ , Figure 2-1D). Equation 2-6 was fit to the MRPP1/2 dependence on  $K_{M,app}$  to determine  $K_4$ ,  $K_5$ , and  $\frac{K_1 K_6}{K_7}$  (Scheme 2-3, Figure 2-1E). At saturating concentrations of MRPP1/2, the value for  $K_{M,app}$  approaches  $K_5$  (Equation 2-6). The catalytic efficiency ( $k_{cat}/K_{M,app}$ ) of MRPP1/2/3 with 1200 nM MRPP1/2 is  $4 \times 10^5\text{ M}^{-1}\text{s}^{-1}$  (Figure 2-1E and Table 2-1), which is comparable to PRORP1 ( $1 \times 10^5\text{ M}^{-1}\text{s}^{-1}$  (24)). In contrast, no significant product formation was observed after 20 h incubation of pre-tRNA with a high concentration of MRPP3 (25  $\mu\text{M}$ ) under STO conditions. The value of  $k_{cat}/K_M$  catalyzed by MRPP3 alone is estimated to be less than  $4\text{ M}^{-1}\text{s}^{-1}$ , assuming less than 10% product formation was observed on urea-PAGE. To make this approximation, we also assume a mechanism for which product release is not

rate limiting and under sub-saturating ( $k_{cat}/K_M$ ) conditions. Thus, MRPP1/2 enhances the catalytic efficiency by more than 100,000-fold (from  $<4 \text{ M}^{-1}\text{s}^{-1}$  to  $4 \times 10^5 \text{ M}^{-1}\text{s}^{-1}$ , Table 2-1).

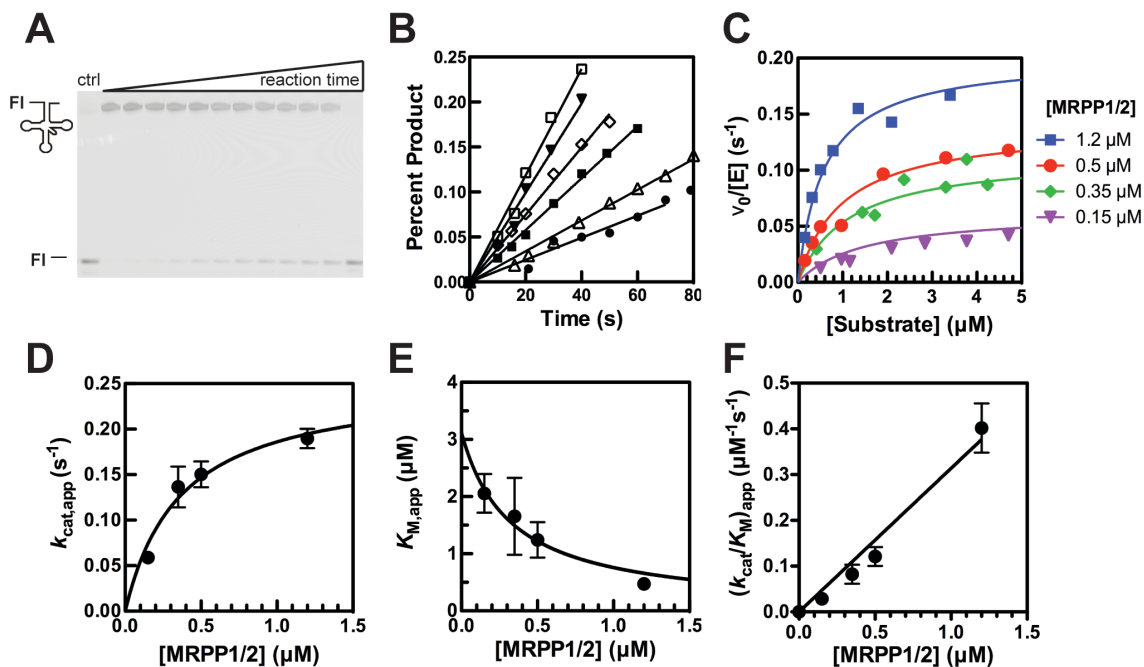


**Figure 2-1 Steady-state activity of human mitochondrial RNase P.**

(A) A representative fluorescence scan ( $\lambda_{ex} = 488 \text{ nm}$ ,  $\lambda_{em} = 525 \text{ nm}$ ) of a 22% polyacrylamide gel with samples from a MTO assay containing 1200 nM MRPP1/2, 25 nM MRPP3, 1300 nM pre-tRNA (containing 40 nM FI-pre-tRNA). Time points are: 10s, 15s, 20s, 30s, 40s, 49s, 1min, 1m11s, 1m20s, 1m29s, 2m, and 1hr. Control lane is reaction of 20 nM PRORP1 with 100 nM substrate (containing 40 nM FI-pre-tRNA) at 1hr. (B) representative initial rates of percent cleavage under MTO conditions as described in (A) at varying substrate concentration (300 nM  $\square$ ; 500 nM  $\blacktriangledown$ ; 800 nM  $\diamond$ ; 1300 nM  $\blacksquare$ ; 2100 nM  $\triangle$ ; 3400 nM  $\bullet$ ). (C) The dependence of the initial velocities of MRPP activity on pre-tRNA concentration (150–4700 nM) and varying MRPP1/2 concentrations. The Michaelis-Menten equations derived from Scheme 2-3 (Equations 2-5, 2-6, and 2-7) was fit to obtain values for  $K_4$ ,  $K_6$ , and  $k_{chem}$ . Equations 2-5, 2-6 and 2-7 were fit independently to the data to obtain the dependence of  $k_{cat,app}$  (D),  $K_{M,app}$  (E), and  $(k_{cat}/K_M)_{app}$  (F) on MRPP1/2 concentration, respectively. All the reactions were performed in 50 mM MOPS pH 7.8, 100 mM NaCl, 4.5 mM  $\text{MgCl}_2$  and 1 mM TCEP at 37 °C. The kinetic parameters are reported in Table 2-1.



**Table 2-1 Steady-state kinetic parameters as a function of MRPP1/2 concentration as described in Figure 2-1**

MRPP1/2 (nM)	$k_{cat,app}$ ( $s^{-1}$ )	$K_{M,app}$ ( $\mu M$ )	$(k_{cat}/K_M)_{app}$ ( $M^{-1}s^{-1}$ )
1200	$0.19 \pm 0.01$	$0.47 \pm 0.08$	$(4.0 \pm 0.1) \times 10^5$
500	$0.15 \pm 0.01$	$1.2 \pm 0.3$	$(1.2 \pm 2.0) \times 10^5$
350	$0.14 \pm 0.02$	$1.7 \pm 0.7$	$(8.2 \pm 2.1) \times 10^4$
150	$0.064 \pm 0.005$	$2.1 \pm 0.3$	$(2.9 \pm 0.3) \times 10^4$
0	ND	ND	< 4

ND: not determined

Reactions contained MRPP3 (25–50 nM), varying concentrations of MRPP1/2 (150–1200 nM) and FI-pre-tRNA substrate (150–5000 nM of total pre-tRNA with 40 nM of FI-pre-tRNA and varying unlabeled pre-tRNA). Reactions were initiated by mixing FI-pre-tRNA with MRPP proteins in 50 mM MOPS pH 7.8, 100 mM NaCl, 4.5 mM  $MgCl_2$  and 1 mM TCEP at 37 °C.

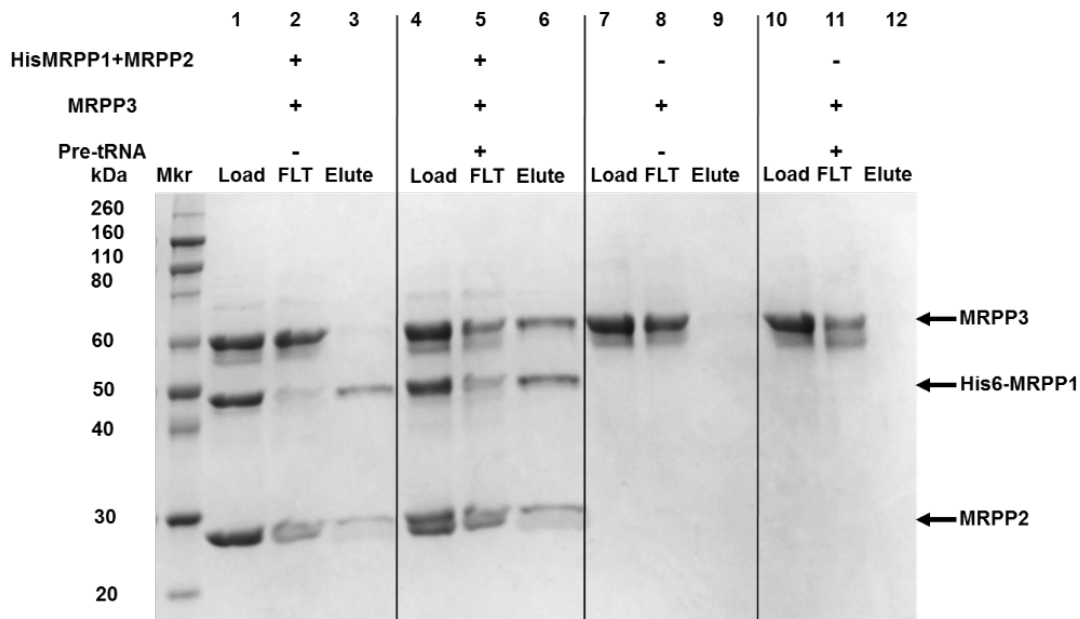


**Figure 2-2 MRPP1/2/3/pre-tRNA complex forms in the presence of pre-tRNA.**

12% SDS-PAGE stained with Coomassie Blue showing results from pull-down assays performed with 2.1  $\mu M$  MRPP3 in the absence of pre-tRNA (Lane 1–3, 7–9) or in the presence of pre-tRNA (Lane 4–6, 10–12) and with the His-MRPP1/2 complex (Lane 1–6) or without the HisMRPP1/2 complex (Lane 7–12). MRPP3 controls with or without pre-tRNA are in Lanes 7–9 and 10–12, respectively. Samples (Lanes 1, 4, 7, and 10) were loaded on to Ni-NTA magnetic agarose beads in loading buffer (50 mM MOPS pH 7.8, 100 mM NaCl, 4.5 mM  $CaCl_2$ , 1 mM TCEP, and 50 mM imidazole). After a 35-min incubation at room temperature, the flow-through (FLT) was collected (Lanes 2, 5, 8, and 11). 100 mM EDTA pH 8 was used to elute the protein and RNA from the beads (Lanes 3, 6, 9, and 12).

### **Pre-tRNA substrate enhances formation of mtRNase P holo-complex**

To understand the interactions between MRPP1/2/3 and pre-tRNA, we performed *in vitro* magnetic capture experiments using nickel (II)-coated magneto-beads to evaluate whether MRPP3 can be pulled down with the His-MRPP1/MRPP2 complex (Figure 2-2). Under near-physiological salt conditions (100 mM NaCl), His-MRPP1/2 subcomplex does not pull down a quantifiable amount of MRPP3 even with high concentrations of MRPP1/2 and MRPP3 (2.1  $\mu$ M) (Figure 2-2, Lane 3). This result is consistent with a previous report under similar conditions (150 mM NaCl) (12). There is a faint MRPP3 band in Lane 3 without pre-tRNA, which suggests that there are weak interactions between MRPP3 and His-MRPP1/2. The amount of MRPP3 found to His-MRPP1/2 is significantly enriched in the presence of pre-tRNA (Lane 6). MRPP3 is not eluted in the absence of HisMRPP1/2, indicating that this enhancement is not due to pre-tRNA enhancing the binding of MRPP3 to the resin (Lane 12). These data demonstrate that a quaternary complex composed of MRPP3, MRPP1/2 and pre-tRNA is formed and that pre-tRNA stabilizes the interaction between MRPP1/2 and MRPP3.

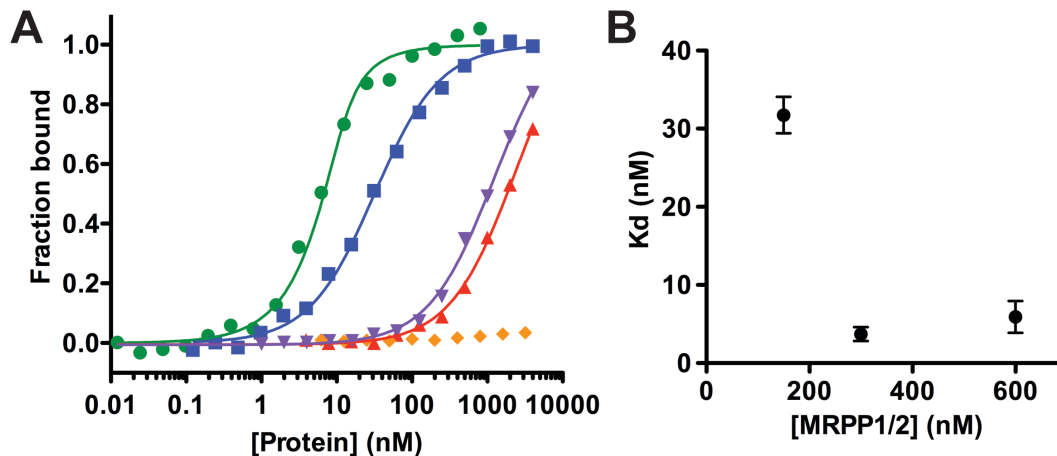


**Figure 2-3 Binding affinity of mitochondrial RNase P proteins to FI-pre-tRNA.**

(A) The FA binding assay was used to measure the binding affinity of 10 nM FI-pre-tRNA with MRPP1/2 (purple), MRPP3 (red), MRPP2 (orange), and MRPP3 with 150 nM MRPP1/2 (blue). The binding affinity of PRORP1 (green) was measured with 2 nM FI-pre-tRNA. FA is measured after a 2-5 min incubation at 37 °C in 50 mM MOPS, pH 7.8, 100 mM NaCl, 4.5 mM CaCl<sub>2</sub>, and 1 mM TCEP, with 10nM FI-pre-tRNA. Fraction bound was calculated from FA values (Equation 2-11). A binding isotherm (Equation 2-12) was fit to the data except for PRORP1, which was fit to a quadratic equation (Equation 2-13). Dissociation constants are listed in Table 2-2. (B) The FA was measured using 10 nM FI-pre-tRNA with varying MRPP3 concentrations at a constant MRPP1/2 concentration (150, 300, or 600 nM). The  $K_D$  values are plot as a function of MRPP1/2 concentration. The errors reported are from the fit of the FA data.

**Table 2-2 Dissociation constants ( $K_D$ ) of FI-pre-tRNA for mtRNase P proteins**

	$K_D$ (nM)	
	CaCl <sub>2</sub>	MgCl <sub>2</sub>
MRPP1/2	1200 ± 100	40 ± 4 <sup>a</sup>
MRPP3	2300 ± 200	1800 ± 200 <sup>a</sup>
MRPP3 with MRPP1/2	7 ± 2	
PRORP1 <sup>b</sup>	1.8 ± 0.3	

Experiments were done as described in Figure 2-3. The reported errors are the standard error of the mean obtained from the fit of the FA data.

<sup>a</sup> Experiments were in the presence of MgCl<sub>2</sub>, which does not activate pre-tRNA cleavage when MRPP1/2 or MRPP3 are present alone.

<sup>b</sup> The binding affinity of PRORP1 was measured with 2 nM FI-pre-tRNA and a quadratic equation (Equation 2-13) was used to fit the data.

### Evidence of synergistic binding between MRPP subunits and pre-tRNA

To understand the interactions between MRPP subunits and pre-tRNA, we measured apparent dissociation constants ( $K_{D,app}$ ) using a FA binding assay as previously described (11,25). MRPP3 ( $K_D = 2300$  nM) binds to FI-pre-tRNA 1,000-fold weaker than PRORP1 ( $K_D = 1.8$  nM) and 2-fold weaker than the MRPP1/2 subcomplex ( $K_{D,app} = 1200$  nM) in  $CaCl_2$  (Figure 2-3, Table 2-2). MRPP3 binds to FI-pre-tRNA with similar  $K_D$  values in  $MgCl_2$  and  $CaCl_2$ , but MRPP1/2 subcomplex binds FI-pre-tRNA tighter in  $MgCl_2$  the ( $K_{D,app} = 40$  nM) compared to  $CaCl_2$  ( $K_{D,app} = 1200$  nM). No significant change in FP was observed upon addition of MRPP2 alone, consistent with a gel shift assay study indicating that MRPP2 does not bind pre-tRNA (16). Interestingly, the presence of sub-saturating concentrations of MRPP1/2 increases the binding affinity of MRPP3 for FI-pre-tRNA by nearly 300-fold ( $K_{D,app} = 7 \pm 2$  nM) in  $CaCl_2$  (Figure 2-3, Table 2-2). The binding affinity is measured in the presence of  $CaCl_2$  because PRORP1 and MRPP1/2/3 does not catalyze cleavage under these conditions.

### **MRPP1/2/3 complex ratio**

To evaluate the functional subunit complex of human mitochondrial RNase P, the MRPP1/MRPP2 subunits the subcomplex was determined using analytical ultracentrifugation (AUC) in collaboration with the Koutmos lab at the Uniformed Services University. A single sharp peak, indicative of a single population, corresponding to a sedimentation coefficient of 6.5 was observed. The Svedberg equation (Equation 2-17) was used to estimate the molecular weight (174 kDa), which is close to the molecular weight of MRPP1/2 in a 1-to-4 MRPP1-to-MRPP2

subunit ratio (153 kDa) (Figure 2-4). The expected weight for a 2-to-4 MRPP1-to-MRPP2 ratio is 202 kDa. This is in contrast to the reported literature ratio of 2:4. We also demonstrate that the 1:4 complex activates the cleavage activity of MRPP3.

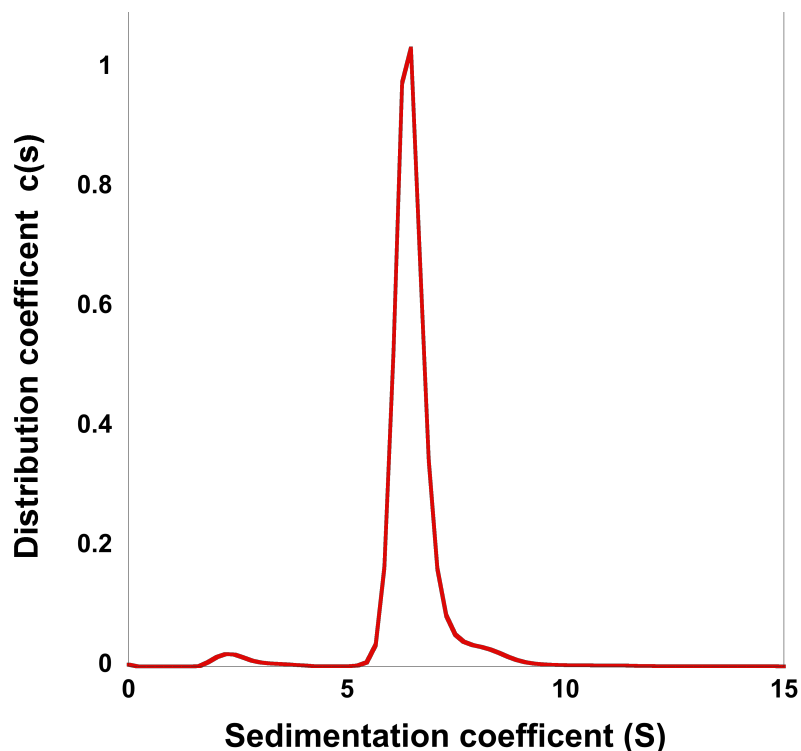


**Figure 2-4 The MRPP1/2 subunit ratio determined by analytical ultracentrifugation.**

A single peak corresponding to a sedimentation coefficient of 6.5 was observed, which has an estimated molecular weight of 174 kDa calculated using the Svedberg equation (Equation 2-17). The expected molecular weight is 153 kDa for a 1:4 MRPP1:MRPP2 ratio and 202 kDa for a 2:4 MRPP1:MRPP2 ratio.

To gain insight into the activation of MRPP3 by the MRPP1/2 subcomplex, we measured the MRPP1/2 dependence on MRPP3 activity under STO conditions. The STO activity was fit to a single exponential decay (Equation 2-14) and the  $k_{\text{obs}}$  was measured at varying concentrations of MRPP1/2 and MRPP3 (Figure 2-5). The maximum observed rate constant ( $k_{\text{max}}$ ) was determined as a function of MRPP1/2 concentration with three MRPP3 concentrations (Figure 2-

5B). Increasing the MRPP3 concentration decreases the  $K_{1/2}$  for MRPP1/2 more than 3-fold (from 1.0 to 0.3  $\mu\text{M}$ ). These data show that the concentration of MRPP1/2 required for half-maximal STO catalytic activity ( $K_{1/2}^{\text{MRPP1/2}}$ ) depends on the concentration of MRPP3. At 1  $\mu\text{M}$  MRPP3 where  $K_{1/2}^{\text{MRPP1/2}}$  is 0.5  $\mu\text{M}$ , the optimum ratio of MRPP1/2 to MRPP3 is about 1:1 (MRPP1:2:3 = 1:4:1). At a lower concentration of MRPP3 (0.1  $\mu\text{M}$ ),  $K_{1/2}^{\text{MRPP1/2}}$  is 1  $\mu\text{M}$  and more MRPP1/2 is required for saturation (MRPP1:2:3 = 10:40:1). At a higher concentration of MRPP3 (10  $\mu\text{M}$ ) where  $K_{1/2}^{\text{MRPP1/2}}$  is 0.3  $\mu\text{M}$ , a lower concentration of MRPP1/2 is sufficient for activity. Furthermore, the  $k_{\text{max,app}}$  values as a function of MRPP3 concentration was fit to Equation 2-15 to determine  $K_{1/2}$  for MRPP3 ( $0.094 \pm 0.003 \mu\text{M}$ ) and  $k_{\text{max}}$  ( $0.21 \pm 0.001 \text{ s}^{-1}$ ) (Figure 2-5C). Equation 2-15 was also fit to the  $k_{\text{max,app}}$  at different concentrations of MRPP1/2 to determine the  $K_{1/2}$  for activation of activity by MRPP1/2 at saturating MRPP3 concentration ( $K_{1/2}^{\text{MRPP1/2}} = 0.3 \pm 0.2 \mu\text{M}$ ) (Figure 2-5E). The STO activity ( $k_{\text{max}}$ ) approaches maximum at 1.6  $\mu\text{M}$  MRPP1/2.

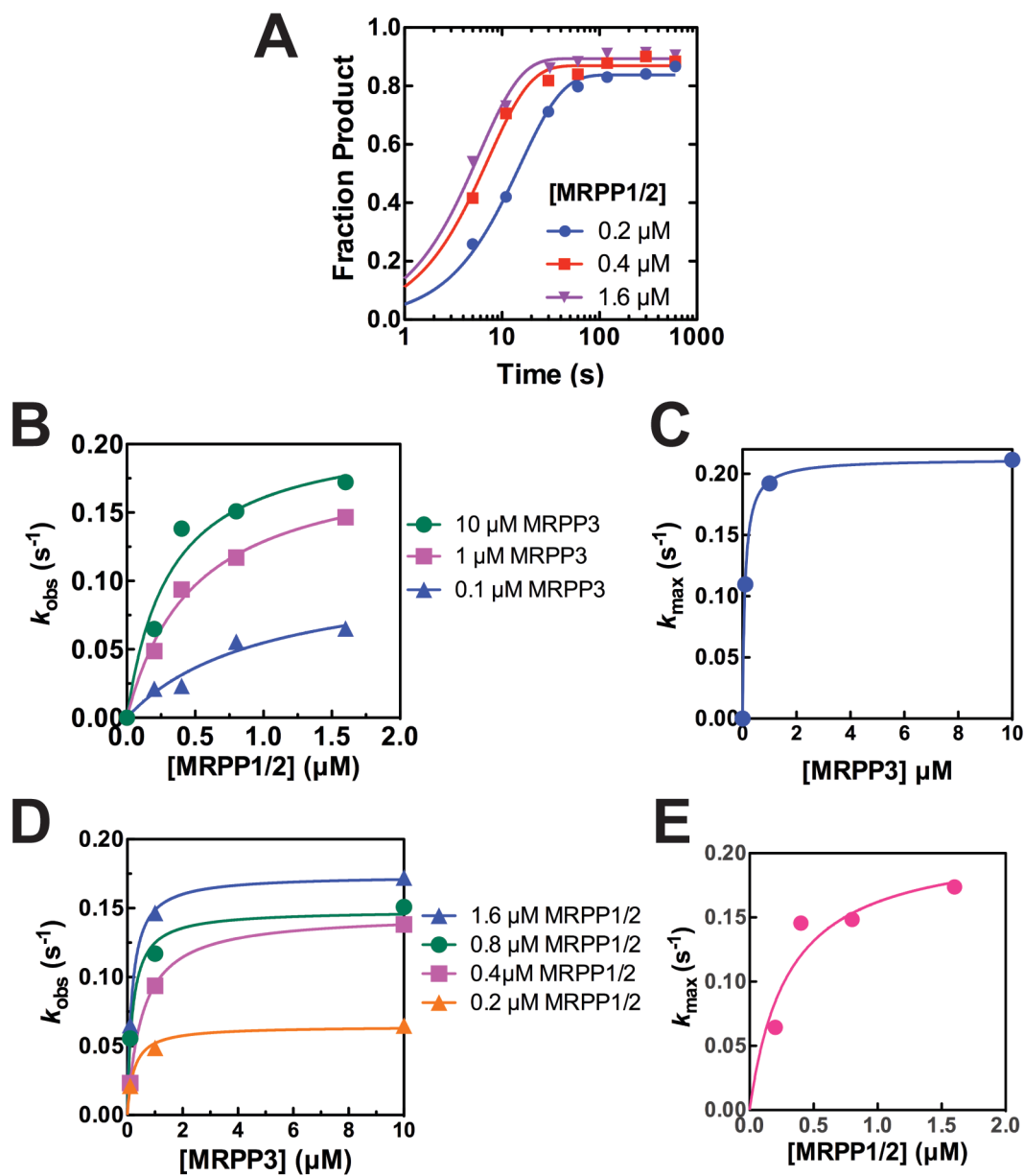


**Figure 2-5 Single-turnover activity of mtRNase P.**

(A) A representative time-course of single-turnover activity of MRPP1/2/3 complex using 10  $\mu\text{M}$  MRPP3 and varying concentrations of MRPP1/2 in 50 mM MOPS pH 7.8, 100 mM NaCl, 4.5 mM  $\text{MgCl}_2$ , and 1mM TCEP at 37  $^\circ\text{C}$ . A single exponential equation (Equation 2-14) was fit to the data to obtain  $k_{\text{obs}}$ . (B) Equation 2-13 was fit to the MRPP1/2 dependence of  $k_{\text{obs}}$  at various concentrations of MRPP3 to determine values for  $k_{\text{max,app}}$ . (C) Equation 2-15 is fit to the MRPP3 dependence of  $k_{\text{max,app}}$  to determine the apparent  $K_{1/2}^{\text{MRPP3}}$  ( $94 \pm 3$  nM) and  $k_{\text{max}}$  ( $0.21 \pm 0.001$  s $^{-1}$ ). (D) Equation 2-15 was fit to the MRPP3 dependence of  $k_{\text{obs}}$  at various concentrations of MRPP1/2 to determine  $k_{\text{max,app}}$ . (E) Equation 2-15 was fit to the MRPP3 dependence of  $k_{\text{max,app}}$  to determine an apparent  $K_{1/2}^{\text{MRPP1/2}}$  ( $300 \pm 200$  nM) and  $k_{\text{max}}$  ( $0.21 \pm 0.04$  s $^{-1}$ ). The reported errors are the standard error of the mean values obtained from fitting the data.

## The MRPP1/2 subcomplex does not enhance the apparent MRPP3 metal affinity

A possible role for MRPP1/2 is to enhance active site metal ion binding, proposed by recent structural studies of MRPP3 (22,23). Both crystal structures are truncated forms of MRPP3 in an inactive conformation with no metal ions in the active site (22,23). To test whether MRPP1/2 activates MRPP3 catalysis by positioning catalytic metal ions in the active site, we measured the apparent  $K_{1/2}$  for MRPP3 activation by  $Mg^{2+}$  ( $K_{1/2}^{Mg}$ ) under MTO conditions at various MRPP1/2 concentrations and a sub-saturating pre-tRNA concentration (500 nM) representing  $k_{cat}/K_M$  conditions (Figure 2-6). If MRPP1/2 enhances the affinity of the active site for  $Mg^{2+}$ , we predict that the value of  $K_{1/2}^{Mg}$  would decrease with increasing MRPP1/2 concentration. However,  $K_{1/2}^{Mg}$  remains unchanged between 150 nM and 500 nM MRPP1/2 ( $K_{1/2}^{Mg} = 1.9 \pm 0.2$  mM and  $2.5 \pm 0.6$  mM, respectively). Thus, these data do not support the hypothesis that the MRPP1/2 subcomplex positions catalytic  $Mg^{2+}$  ions to activate MTO activity of MRPP3.

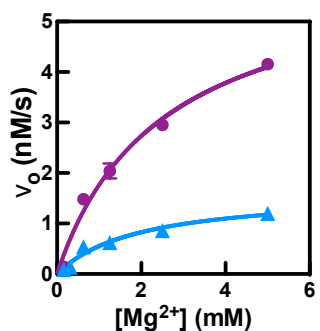


**Figure 2-6 Magnesium dependence on the steady-state activity of mtRNase P.**

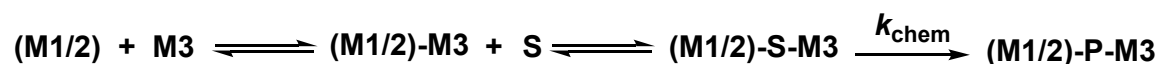
Initial velocities were measured in the same conditions as in Figure 2-1 at varying concentrations of  $MgCl_2$  and MRPP1/2 (500 nM, purple; 150 nM, blue) with sub-saturating pre-tRNA (500 nM). Equation 2-16 was fit to the data to calculate  $K_{1/2}^{Mg}$  values of  $2.5 \pm 0.6$  mM and  $1.9 \pm 0.2$  mM for 500 nM and 150 nM MRPP1/2, respectively. The error bars are the standard error of the mean values obtained from fitting the data.



## DISCUSSION

### Kinetic model for mitochondrial RNase P catalysis

The previous model for pre-tRNA cleavage catalyzed by human mtRNase P involves the formation of a tertiary complex (MRPP1/2/3), which then binds to pre-tRNA (Scheme 2-1). MRPP1/2 binding is proposed to induce formation of an active MRPP3 enzyme (22,23). The data presented in this chapter challenges that model. Under physiological conditions, our data and others show that MRPP3 does not strongly associate with MRPP1/2 (12). Scheme 2-1 predicts a constant  $k_{\text{cat}}$  value as a function of MRPP1/2, but  $k_{\text{cat,app}}$  increases hyperbolically with MRPP1/2 concentration (Figure 2-1D). The previous model also proposed a tertiary complex with a stoichiometry of 2:4:1 (MRPP1:2:3) (12). Here, analytic ultracentrifugation and STO experiments suggest a stoichiometry of 1:4:1 (MRPP1:2:3) (Figures 2-4 and 2-5).

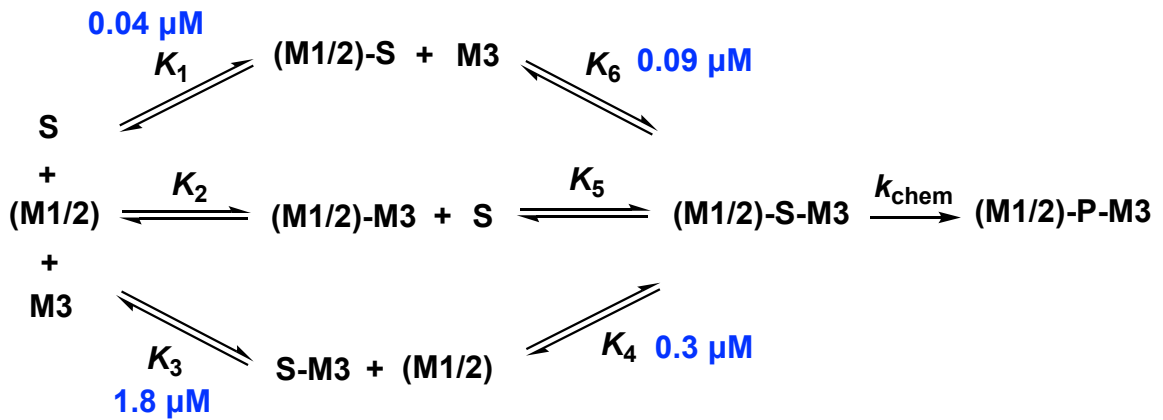


#### Scheme 2-1 Current kinetic model for human mitochondrial RNase P catalysis

MRPP3 is denoted by M3, MRPP1/2 subcomplex is denoted by (M1/2), pre-tRNA is denoted by S, and tRNA and 5' leader products are denoted by P. (M1/2) binds to M3, after which (M1/2)-M3 binds to S to catalyze cleavage and generate P.

We propose a kinetic model that is consistent with the data (Scheme 2-2). In this model, pre-tRNA binds to either M1/2 or M3 first, or to (M1/2)-M3 complex to form the active MRPP1/2-S-M3 complex. This model is consistent with the MRPP1/2 dependence observed for  $k_{\text{cat,app}}$ ,  $K_{M,app}$ , and  $(k_{\text{cat}}/K_M)_{\text{app}}$  (Figure 2-1,

Equations 2-1, 2-2, and 2-3), and with the role of pre-tRNA in MRPP1/2/3/pre-tRNA complex formation. Furthermore, MRPP3 alone does not catalyze cleavage of pre-tRNA (12), but binds to pre-tRNA with 1.8  $\mu\text{M}$  affinity to form an inactive complex (M3-S) (Figure 2-3, Table 2-2). The M3-S complex is not a dead end complex since increasing the MRPP3 concentration under STO conditions does not result in inhibition of MRPP1/2/3 activity (Figure 2-5). These data indicated that M3-S binds MRPP1/2 productively to form an active M1/2-S-M3 complex. Therefore, this model qualitatively describes the data. However, the thermodynamic box in Scheme 2-2 requires that  $K_1K_6 = K_3K_4$  and this is not currently true.



**Scheme 2-2 Random Binding Model**

The (M1/2)-S-M3 ternary complex can be formed through three pathways. In one pathway, S binds to (M1/2) first, followed by binding to M3 (top). In the second pathway, S binds to a (M1/2)-M3 complex to form the (M1/2)-S-M3 ternary complex (center). In the third pathway, S binds to M3 followed by addition of the (M1/2) complex (bottom).

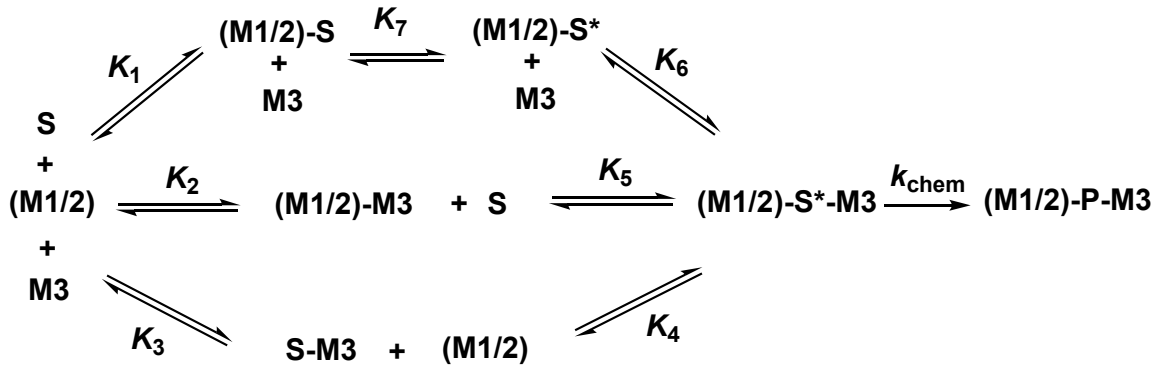
$$k_{cat,app} = \frac{k_{chem}[M1/2]}{K_4 + [M1/2]} \quad \text{Equation 2-1}$$

$$K_{M,app} = \frac{K_1K_6 + K_5[M1/2]}{K_4 + [M1/2]} \quad \text{Equation 2-2}$$

$$\left(\frac{k_{cat}}{K_M}\right)_{app} = \frac{k_{chem}[M1/2]}{K_1K_6+K_5[M1/2]} \quad \text{Equation 2-3}$$

$$\frac{v_0}{[MRPP3]} = k_{chem} \left( \frac{k_{cat,app}[S]}{\frac{K_1K_6+K_5[M1/2]}{K_4+[M1/2]}+[S]} \right) \quad \text{Equation 2-4}$$

One possibility for this discrepancy is that the values for  $K_1$ ,  $K_3$ ,  $K_4$ , or  $K_6$  are not correct.  $K_1$  the dissociation constant between pre-tRNA and MRPP1/2 (0.04  $\mu\text{M}$ ).  $K_3$  is the dissociated constant for pre-tRNA binding to MRPP3 (1.8  $\mu\text{M}$ ). At saturating substrate, the  $K_{1/2}$  for the MRPP1/2 dependence of  $k_{cat}$  is  $K_4$  (0.3  $\mu\text{M}$ ) (Equation 2-1). The value for  $K_4$  was also confirmed under STO by measuring the value for  $K_{1/2}$  of MRPP1/2 (Figure 2-5E).  $K_6$  is the  $K_{1/2}$  for activation of activity by MRPP3 at saturating MRPP1/2 under STO conditions (0.09  $\mu\text{M}$ ). Thus, the values for  $K_1$ ,  $K_3$ ,  $K_4$ , and  $K_6$  are correct. A second possibility is that the model (Scheme 2-2) is not correct. We therefore present a slightly modified kinetic model that includes one additional step; a conformational change following MRPP1/2 binding to pre-tRNA (Scheme 2-3).



**Scheme 2-3 New kinetic model for human mitochondrial RNase P catalysis**

There are three possible paths to form an active (M1/2)-S\*-M3 complex followed by the cleavage step to form P. In the first path, S binds to (M1/2) through  $K_1$ , followed by a conformational change step ( $K_7$ ) to form (M1/2)-S\*, and binding to M3 through  $K_6$  to form an active (M1/2)-S\*-M3 complex. The values for  $K_1$  and  $K_7$  are calculated using Equation 2-9. In the second path, S binds to a pre-formed (M1/2)-M3 complex ( $K_5$ ) to form (M1/2)-S\*-M3. In the third path, S binds M3 through  $K_3$ , and then binds to (M1/2) through  $K_4$  to form (M1/2)-S\*-M3. The thermodynamic constants are listed in Table 2-3.

$$k_{cat,app} = \frac{k_{chem} [M1/2]}{K_4 + [M1/2]} \quad \text{Equation 2-5}$$

$$K_{M,app} = \frac{\left(\frac{K_1 K_6}{K_7}\right) + K_5 [M1/2]}{K_4 + [M1/2]} \quad \text{Equation 2-6}$$

$$\left(\frac{k_{cat}}{K_M}\right)_{app} = \frac{k_{chem} [M1/2]}{\left(\frac{K_1 K_6}{K_7}\right) + K_5 [M1/2]} \quad \text{Equation 2-7}$$

$$\frac{v_0}{[MRPP3]} = \frac{k_{cat,app} [S]}{K_{M,app} + [S]} = \frac{\left(\frac{k_{chem} [M1/2]}{K_4 + [M1/2]}\right) [S]}{\left(\frac{\frac{K_1 K_6}{K_7} + K_5 [M1/2]}{K_4 + [M1/2]}\right) + [S]} \quad \text{Equation 2-8}$$

$$K_{1,app} = \frac{K_1}{(1 + K_7)} \quad \text{Equation 2-9}$$

$$\frac{K_1 K_6}{K_7} = K_3 K_4 = K_2 K_5 \quad \text{Equation 2-10}$$

The values for the equilibrium constants of this model (Scheme 2-3) are determined using binding measurements, and MTO and STO data.  $K_3$  is the dissociation constant for pre-tRNA binding to MRPP3 (1.8  $\mu\text{M}$ ). At saturating substrate,  $K_4$  is the  $K_{1/2}$  for the MRPP1/2 dependence of  $k_{cat,app}$  (0.3  $\mu\text{M}$ ) (Equation 2-5, Figure 2-1), which is consistent with the value of  $K_{1/2}$  for the MRPP1/2 dependence on STO  $k_{max}$  (0.3  $\mu\text{M}$ , Figure 2-5E).  $K_6$  is the  $K_{1/2}$  for the MRPP3 dependence of STO  $k_{max}$  (0.09  $\mu\text{M}$ , Figure 2-5C).  $K_{1,app}$  is the apparent binding affinity of pre-tRNA for MRPP1/2 measured using fluorescence anisotropy (0.04  $\mu\text{M}$ ).  $K_1$  (~0.0404  $\mu\text{M}$ ) and  $K_7$  (~0.0067  $\mu\text{M}$ ) are calculated using  $K_{1,app}$  and Equation 2-9. The value for  $K_5$ , which describes the binding of pre-tRNA to an MRPP1/2/3 tertiary complex, is estimated to be less than 0.007  $\mu\text{M}$  (Figure 2-3B, Table 2-2). The binding constant between MRPP1/2 and MRPP3 ( $K_2$ ) is estimated to be a minimum of 80  $\mu\text{M}$ . The thermodynamic box in Scheme

2-3 holds true (Equation 2-10). These values are consistent with the values determined by fitting the data independently. The values for  $k_{\max}$  ( $0.21 \pm 0.001 \text{ s}^{-1}$ ) and  $k_{\text{cat}}$  ( $0.25 \pm 0.04 \text{ s}^{-1}$ ) are comparable, which suggests that the rate-limiting step in human mitochondrial RNase P catalysis is not product release.

**Table 2-3 Thermodynamic constants listed in Scheme 2-3**

$K_1$	0.0404 $\mu\text{M}$
$K_2$	1.8 $\mu\text{M}$
$K_3$	0.3 $\mu\text{M}$
$K_4$	0.36 $\mu\text{M}$
$K_5$	0.007 $\mu\text{M}$
$K_6$	0.09 $\mu\text{M}$
$K_7$	0.0067

According to Scheme 2-3, at saturating concentrations of pre-tRNA, the rate of human mtRNase P catalysis is linearly dependent on both MRPP1/2 and MRPP3. A hyperbolic decrease in  $K_{M,\text{app}}$  is consistent with more productive binding between MRPP3 and pre-tRNA substrate following addition of MRPP1/2. We propose that MRPP1/2 facilitates catalysis by changing the contacts between MRPP3 and pre-tRNA through a conformational change. The addition of MRPP1/2 also increases  $k_{\text{cat,app}}$ , which suggests that it participates in protein-protein or protein-RNA contacts within MRPP3, or stabilizes pre-tRNA and/or MRPP3 for catalysis. Interactions between MRPP1/2 and MRPP3 were not observed (Figure 2-2), suggesting that the conformational change is mediated through pre-tRNA. The mechanism through  $K_1$ ,  $K_6$ , and  $K_7$  may be the preferred path. Future experiments to test this model include transient kinetics experiments to measure the rate constants of pre-tRNA binding to MRPP1/2. Kinetic

simulations of the data using our proposed model (Scheme 2-3) will be done to provide more information on the mechanism of human mtRNase P catalysis.

### **MRPP1/2 may play a structural role in mitochondrial RNase P activity**

Crystallographic studies on truncated MRPP3 led to the proposal that MRPP1/2 induces conformational changes in MRPP3 to orient active site metal ions for activation of mtRNase P activity (22,23). We observe no change in the value of the  $K_{1/2}$  for the  $Mg^{2+}$  dependence on the initial rate between 150 nM and 500 nM MRPP1/2, which does not support this hypothesis (Figure 2-6). However, magnesium dependence experiments with saturating concentrations of MRPP1/2 or measuring the binding affinity, as a function of metal ion concentration may be able to test this hypothesis. Our data supports a model wherein the MRPP1/2 complex plays a structural role in MRPP3 and pre-tRNA interactions instead. The MRPP1/2 subcomplex is not only required for MRPP3 cleavage activity, but also increases the apparent affinity of MRPP3 to pre-tRNA by nearly 300-fold, which is comparable to the affinity of pre-tRNA for PRORP1 (Figure 2-3, Table 2-2). In the absence of MRPP1/2, there is a large difference in pre-tRNA cleavage activity between PRORP1 and MRPP3, indicative of different substrate recognition mechanisms.

### **Pre-tRNA stabilizes the MRPP1/2/3 complex**

Pre-tRNA stabilizes the quaternary enzyme-substrate complex (Figure 2-2, lanes 3 and 6). Three models can be proposed: (1) MRPP3 recognizes the complex or interface of MRPP1/2-pre-tRNA, (2) MRPP1/2 alters the structure of

pre-tRNA to a conformation with higher affinity to MRPP3 or (3) pre-tRNA binding alters the structure of MRPP1/2, which then binds MRPP3 with higher affinity.

## CONCLUSION

This is the first report of MTO kinetics for human mitochondrial RNase P, conditions likely used *in vivo* (26,27). Our results highlight the functional importance of MRPP1/2 in processing pre-tRNA in human mitochondria. Optimal mitochondrial RNase P MTO activity is achieved with catalytic amounts of MRPP3 (25 nM) and high concentration MRPP1/2 (low micromolar) (Figure 2-1). This result is consistent with the differential effects of siRNA knockdowns of MRPP1 and MRPP3 in cells (6). MRPP1 and MRPP3 were reduced to similar levels ( $1.8\% \pm 0.8\%$  and  $1.8\% \pm 0.7\%$ , respectively), but the MRPP1 knockdown resulted in a larger accumulation of pre-tRNA transcripts (100-fold increase) compared to the MRPP3 knockdown (10-fold increase). Based on our data, reduced MRPP3 levels have less of an effect on transcript levels because only catalytic amounts of MRPP3 are needed for sufficient activity. Conversely, when MRPP1/2 is reduced, there is a significant decrease in catalytic efficiency (100,000-fold, Table 2-1) and substrate affinity (300-fold, Table 2-2).

The tRNA maturation pathway involves the removal of extraneous ends catalyzed by endonucleases such as RNase P at the 5' end, but also includes specific base modifications. A common modification found in almost all mitochondrial tRNAs is *N1* methylation catalyzed by MRPP1. MRPP1 is

expressed in the cytosol and then imported to the mitochondria via a mitochondrial localization sequence. Possible reasons for the high dependence on MRPP1/2 are: (1) MRPP1 in the cytosol gets degraded or imported to the mitochondria before it binds to MRPP2 or (2) in some cases, tRNA methylation may occur before cleavage catalyzed by RNase P and/or methylation could be the rate-limiting step for some tRNAs.

In summary, we present data that shows MRPP1/2 significantly enhances the catalytic efficiency and substrate binding of the metallo-nuclease subunit, MRPP3, and provide the framework for further investigation of the mechanisms employed by these MRPP1, 2, and 3 in tRNA-related mitochondrial pathogenesis.

## **METHODS**

### **Pre-tRNA preparation**

Fluorescein-labeled pre-tRNA<sup>Asp</sup> (FI-pre-tRNA) was prepared as previously described with a 5-nucleotide leader and a discriminator base at the 3' end without the 3' CCA sequence (24). The template was produced from plasmid DNA containing a T7 promoter region and *B. subtilis* pre-tRNA<sup>Asp</sup> sequence by PCR amplification. The *in vitro* transcription reaction was performed using 3 µg PCR product as the template with 4 mM adenosine triphosphate (ATP), 4 mM cytidine triphosphate (CTP), 4 mM uridine triphosphate, 5 mM Guanosine 5'-monothiophosphate (GMPS), 0.8 mM guanosine triphosphate (GTP), 25 mM



MgCl<sub>2</sub>, 1 mM spermidine, 5 mM dithiothreitol (DTT), 50 mM Tris-HCl, pH 8.0, 1 µg/ml pyrophosphatase, and 0.1 mg/ml T7 RNA polymerase. The 5'-GMPS-pre-tRNA<sup>Asp</sup> was labeled with fluorescein by incubation with 40-fold excess 5-iodoacetamido-fluorescein (5-IAF, Life Technologies) overnight at 37 °C to obtain FI-pre-tRNA. The RNA was purified by 10% polyacrylamide/bis (39:1) denaturing gel with 7 M urea (28). Unlabeled pre-tRNA was prepared using *in vitro* transcription as described above without the addition of GMPS and with the concentration of GTP increased from 0.8 mM to 4 mM. Nucleoside triphosphates (NTPs) and chemicals were purchased from Sigma at the highest purity. Inorganic pyrophosphatase was purchased from Roche Applied Science. GMPS was synthesized from 2', 3' isopropylidene-guanosine and thiophosphoryl chloride as described previously (29). Recombinant His<sub>6</sub>-T7 RNA polymerase was expressed in *E. coli* and purified by Ni-NTA chromatography as described previously (30). Before each assay, pre-tRNA was denatured at 95 °C for 2 min in water, incubated at 37 °C for 15 min followed by addition of the desired buffer and incubation for another 30 min at 37 °C. This ensures that pre-tRNA substrate is folded into its canonical tertiary structure.

### **Purification of recombinant human mitochondrial RNase P subunits**

To prepare a plasmid for the co-expression and co-purification of MRPP1 and MRPP2, DNA encoding an N-terminal truncation of the MRPP1 gene (*TRMT10C*) (residues 40-403, Δ39MRPP1) with an N-terminal His<sub>6</sub>-tag followed by a TEV protease site and the full-length MRPP2 gene (*SDR5C1*) were cloned

into a pCDFDuet-1 (Novagen) co-expression vector as previously described (32). The plasmid was transformed and expressed in Rosetta (DE3) *E. coli* cells. Cells were grown in Terrific Broth or auto-induction media (Novagen) containing 50 mg/L streptomycin and 34 mg/L chloramphenicol at 37 °C to an OD<sub>600</sub> of 0.6-0.8, and then induced by addition of 500 µM β-D-1-thiogalactopyranoside (IPTG) followed by growth for 16 h at 18°C (24 h for auto-induction media). Cells were harvested and lysed using a microfluidizer in 20 mM Tris-HCl pH 7.5 or 50 mM MOPS (pH 7.5), 1 mM Tris(2-carboxyethyl)phosphine (TCEP), pH 7.5, 10% glycerol, 1 M NaCl, 15 mM imidazole and one tablet of Complete EDTA free protease inhibitor cocktail (Roche). Cell lysate was pelleted for 60 min at 30,600 × g at 4 °C. The soluble fraction was then applied to a Ni-Sepharose column preequilibrated with buffer A. The column was washed with buffer A containing 150 mM NaCl over 10 column volumes (CV). Bound proteins were eluted by gradient from 50-500 mM imidazole in buffer A over 10 CV. Fractions containing MRPP1/2 were pooled, His<sub>6</sub>TEV protease was added, and the reaction was dialyzed against buffer A containing 150 mM NaCl. The sample was then applied to a second Ni-Sepharose column. The flow-through was collected, concentrated, and dialyzed into 50 mM MOPS pH 7.5, 300 mM NaCl, and 1 mM TCEP. The sample was loaded onto a Sephacryl-200 gel-filtration column (GE Healthcare) preequilibrated with 20 mM MOPS, 1 mM TCEP, and 300 mM NaCl. Protein was eluted at 1 mL/min and the A<sub>280</sub> was monitored. Peak fractions were analyzed by SDS-PAGE and Coomassie Blue stain. Fractions containing MRPP1 and MRPP2 were pooled. The molecular extinction coefficients (ε<sub>280</sub>) of the

individual subunits are  $62,130 \text{ M}^{-1}\text{cm}^{-1}$  and  $4,720 \text{ M}^{-1}\text{cm}^{-1}$  for  $\Delta 39\text{MRPP1}$  and  $\text{MRPP2}$ , respectively.

The  $\text{MRPP3}$  gene (*KIAA0391*) with an N-terminal truncation (residues 46-583,  $\Delta 45\text{MRPP3}$ ) was cloned into a pETM-11 vector that adds an N-terminal  $\text{His}_6$ -tag as previously described (31). The plasmid was transformed and expressed in Rosetta (DE3) *E. coli* cells. Cells were grown in LB medium at  $37^\circ\text{C}$  to an  $\text{OD}_{600}$  of 0.6-0.8, and then induced by addition of 500 or 660  $\mu\text{M}$  IPTG followed by growth for 16 h at  $18^\circ\text{C}$ . Cells were lysed using a microfluidizer and centrifuged for 60 min at  $30,000 \times g$  at  $4^\circ\text{C}$ . The soluble fraction was then applied to a Ni-Sepharose column or prepacked HisTrap FF column (GE Healthcare Life Sciences) preequilibrated in buffer B (50 mM MOPS, pH 7.5, 10% glycerol, 150 mM NaCl, 1 mM  $\text{MgCl}_2$ , 1 mM TCEP) with 15 mM imidazole. Buffer B containing 1 M NaCl was used to elute nucleic acid contaminants. Bound proteins were eluted using an imidazole gradient (50-500 mM) in buffer B over 10 CV. Fractions containing  $\text{MRPP3}$  were pooled and TEV protease (1 mg per 40 mg of substrate protein) was added and the sample was dialyzed overnight against Buffer B at  $4^\circ\text{C}$ . The sample was then applied to a second Ni-Sepharose column. The flow-through was collected, concentrated, and dialyzed into 50 mM MOPS (pH 7.5), 1 mM TCEP, 150 mM NaCl, and 10 % glycerol. Full-length  $\text{MRPP2}$  was purified in a similar manner to that for  $\Delta 45\text{MRPP3}$ . The concentrations of  $\Delta 45\text{MRPP3}$  and  $\text{MRPP2}$  were determined by absorbance ( $\Delta 45\text{MRPP3}$ ,  $\epsilon_{280} = 85,830 \text{ M}^{-1}\text{cm}^{-1}$ ;  $\text{MRPP2}$ ,  $\epsilon_{280} = 4720 \text{ M}^{-1}\text{cm}^{-1}$ ).  $\text{PRORP1}$  was purified as previously described (11).

### Multiple-turnover (MTO) cleavage measurements

MTO assays were performed at limiting concentrations of MRPP3 (25–50 nM) and varied concentrations of MRPP1/2 (150-1200 nM) and FI-pre-tRNA substrate (150-5000 nM of total pre-tRNA containing 40 nM of FI-pre-tRNA). Reactions were initiated by mixing FI-pre-tRNA with MRPP proteins at 37 °C in reaction buffer (50 mM MOPS pH 7.8, 100 mM NaCl, 4.5 mM MgCl<sub>2</sub> and 1 mM TCEP). Reaction time points were quenched with an equal volume of 8 M urea, 100 mM EDTA pH 8, 0.05% bromophenol blue, and 0.05% xylene cyanol). Quenched reactions were resolved on a 22% PAGE containing 7 M urea, and imaged by a Typhoon scanner ( $\lambda_{\text{ex}} = 488 \text{ nm}$ ,  $\lambda_{\text{em}} = 535 \text{ nm}$ ). Gels were analyzed using ImageJ software. The initial velocities were divided by the MRPP3 concentration, plotted against MRPP1/2 concentration, and fit to the Michaelis-Menten equation (Equation 2-8) to obtain the apparent kinetic parameters  $k_{\text{cat,app}}$ ,  $(K_{\text{M}})_{\text{app}}$ , and  $(k_{\text{cat}}/K_{\text{M}})_{\text{app}}$ . The steady-state kinetics equation were derived for  $k_{\text{cat,app}}$  (Equation 2-5),  $(K_{\text{M}})_{\text{app}}$  (Equation 2-6), and  $(k_{\text{cat}}/K_{\text{M}})_{\text{app}}$  (Equation 2-7) from the model in Scheme 2-3 and used to determine  $k_{\text{chem}}$ ,  $K_4$ ,  $K_5$ , and  $\frac{K_1 K_6}{K_7}$ . The values of  $K_{1,\text{app}}$  and  $K_3$  were measured by FA binding assays. The values for  $K_1$  and  $K_7$  were calculated using  $K_{1,\text{app}}$  and Equations 2-9 and 2-10.

### Magnetic capture assay

We performed *in vitro* experiments using magnetic capture methods (33). Ni-NTA magnetic beads (Qiagen) were pre-equilibrated in binding buffer (50mM HEPES pH 7.8, 100 mM NaCl, 4.5 mM CaCl<sub>2</sub>, and 1 mM TCEP) before incubation with 2.1 μM His<sub>6</sub>-MRPP1/2 subcomplex and 2.1 μM MRPP3 with or without 2.1 μM pre-tRNA. The Ni-NTA magnetic beads were incubated with samples for 35 min at room temperature before the flow-through was collected and the beads were washed with binding buffer twice. The samples were eluted with 100 mM EDTA (pH 7.5). The samples were run on SDS-PAGE and the gel was stained using Coomassie Blue.

#### **Fluorescence anisotropy (FA) binding assay**

Binding experiments using 10 nM FI-pre-tRNA and varying concentrations of proteins were carried out in 50 mM MOPS (pH 7.8), 100 mM NaCl, 1 mM TCEP, and 4.5 mM MgCl<sub>2</sub> or CaCl<sub>2</sub>. Proteins and FI-pre-tRNA were incubated at 37 °C for 2 min in a 384-well black-bottom plate (Corning Incorporation, #3575) prior to FA measurement using a TECAN plate reader (Infinite 500, G-factor = 0.951). The FA binding data were converted to fraction bound ( $Y_b$ ) using Equation 2-11, where  $A_0$  is the FA value of unbound FI-pre-tRNA and  $A_b$  is the FA value of fully bound protein-FI-pre-tRNA complex (Figure 2-3). The value of  $A_b$  varied with different proteins. All fraction bound data, with the exception of PRORP1, were fit to a binding isotherm (Equation 2-12, where [P] is the protein concentration) and PRORP1 data were fit to a quadratic equation (Equation 2-13) because the FI-pre-tRNA concentration was close to the  $K_D$  value, where  $L$  is the concentration of the FI-pre-tRNA (2 nM).

$$Y_b = \frac{A-A_0}{A_b-A_0} \quad \text{Equation 2-11}$$

$$Y_b = \frac{[P]}{K_D+[P]} \quad \text{Equation 2-12}$$

$$Y_b = \frac{[P]+L+K_D-\sqrt{([P]+K_D+L)^2-4[P]L}}{2L} \quad \text{Equation 2-13}$$

### Single-turnover (STO) experiments

STO activity was measured using 10 nM FI-pre-tRNA and MRPP3 (0.1 – 10  $\mu$ M) pre-incubated with 0.2–1.6  $\mu$ M MRPP1/2 subcomplex in 50 mM MOPS (pH 7.8), 150 mM NaCl, 4.5 mM MgCl<sub>2</sub>, 2 mM TCEP at 37 °C. Time points were taken and analyzed by urea-PAGE as described for MTO experiments. A single exponential equation (Equation 2-14) was fit to the percent cleavage ( $Y_c$ ) time course to calculate the single-turnover rate constant ( $k_{obs}$ ). Equation 2-15 was fit to the MRPP1/2 concentration dependence of  $k_{obs}$  to calculate  $k_{max}$  and the apparent affinity of MRPP1/2 ( $K_{1/2}^{MRPP1/2}$ ) and MRPP3 ( $K_{1/2}^{MRPP3}$ ), where  $k$  is  $k_{obs}$  or  $k_{max,app}$ . The dependence of  $k_{max,app}$  on MRPP3 concentration was fit to Equation 2-15 where [P] refers to either the concentration of MRPP1/2 or MRPP3, to obtain  $k_{max}$  and  $K_{1/2}^{MRPP1/2}$  or  $K_{1/2}^{MRPP3}$ .

$$Y_c = Y_{\infty}(1 - e^{-k_{obs}t}) \quad \text{Equation 2-14}$$

$$k = \frac{k_{max}[P]}{K_{1/2}+[P]} \quad \text{Equation 2-15}$$

### Derivation of rate law equations according to Scheme 2-2

$$rate = k_{chem}[M1/2 \cdot S \cdot M3]$$

$$[M3_{tot}] = [M3] + [S \cdot M3] + [M1/2 \cdot M3] + [M1/2 \cdot S \cdot M3]$$

$$K_1 = \frac{[M1/2][S]}{[M1/2 \cdot S]}; [M1/2 \cdot S] = \frac{[M1/2][S]}{K_1}$$

$$K_2 = \frac{[M1/2][M3]}{[M1/2 \cdot M3]}; [M1/2 \cdot M3] = \frac{[M1/2][M3]}{K_2}$$

$$K_3 = \frac{[M3][S]}{[S \cdot M3]}$$

$$K_4 = \frac{[M1/2][S \cdot M3]}{[M1/2 \cdot S \cdot M3]}; [S \cdot M3] = \frac{K_4[M1/2 \cdot S \cdot M3]}{[M12]}$$

$$K_5 = \frac{[M1/2 \cdot M3][S]}{[M1/2 \cdot S \cdot M3]}; [M1/2 \cdot M3] = \frac{K_5[M1/2 \cdot S \cdot M3]}{[S]}$$

$$K_6 = \frac{[M1/2 \cdot S][M3]}{[M1/2 \cdot S \cdot M3]}; [M3] = \frac{K_6[M1/2 \cdot S \cdot M3]}{[M1/2 \cdot S]}$$

$$[M3_{tot}] = \frac{K_6[M1/2 \cdot S \cdot M3]}{[M1/2 \cdot S]} + \frac{K_4[M1/2 \cdot S \cdot M3]}{[M12]} + \frac{K_5[M1/2 \cdot S \cdot M3]}{[S]} + [M1/2 \cdot S \cdot M3]$$

$$[M3_{tot}] = [M1/2 \cdot S \cdot M3] \left( \frac{K_1 K_6}{[M1/2][S]} + \frac{K_4}{[M1/2]} + \frac{K_5}{[S]} + 1 \right)$$

$$[M3_{tot}] = [M1/2 \cdot S \cdot M3] \left( \frac{K_1 K_6 + K_4[S] + K_5[M1/2] + [S][M1/2]}{[M1/2][S]} \right)$$

$$[M1/2 \cdot S \cdot M3] = \frac{[M1/2][M3_{tot}][S]}{K_1 K_6 + K_5[M1/2] + [S]([M1/2] + K_4)}$$

$$[M1/2 \cdot S \cdot M3] = \frac{\frac{[M1/2][M3_{tot}][S]}{K_4 + [M1/2]}}{\frac{K_1 K_6 + K_5[M1/2]}{K_4 + [M1/2]} + [S]}$$

$$rate = k_{chem} \left( \frac{\frac{[M1/2][M3_{tot}][S]}{K_4 + [M1/2]}}{\frac{K_1 K_6 + K_5[M1/2]}{K_4 + [M1/2]} + [S]} \right)$$

$$k_{cat,app} = \frac{k_{chem}[M1/2]}{K_4 + [M1/2]}$$

$$K_{M,app} = \frac{K_1 K_6 + K_5[M1/2]}{K_4 + [M1/2]}$$

$$\left( \frac{k_{cat}}{K_M} \right)_{app} = \frac{k_{chem}[M1/2]}{K_1 K_6 + K_5[M1/2]}$$

### Derivation of rate law equations according to Scheme 2-3

$$\text{rate} = k_{\text{chem}}[M1/2 \cdot S \cdot M3^*]$$

$$[M3_{\text{tot}}] = [M3] + [S \cdot M3] + [M1/2 \cdot M3] + [M1/2 \cdot S \cdot M3^*]$$

$$K_1 = \frac{[M1/2][S]}{[M1/2 \cdot S]}; [M1/2 \cdot S] = \frac{[M1/2][S]}{K_1}$$

$$K_2 = \frac{[M1/2][M3]}{[M1/2 \cdot M3]}; [M1/2 \cdot M3] = \frac{[M1/2][M3]}{K_2}$$

$$K_3 = \frac{[M3][S]}{[S \cdot M3]}$$

$$K_4 = \frac{[M1/2][S \cdot M3]}{[M1/2 \cdot S \cdot M3^*]}; [S \cdot M3] = \frac{K_4[M1/2 \cdot S \cdot M3^*]}{[M12]}$$

$$K_5 = \frac{[M1/2 \cdot M3][S]}{[M1/2 \cdot S \cdot M3^*]}; [M1/2 \cdot M3] = \frac{K_5[M1/2 \cdot S \cdot M3^*]}{[S]}$$

$$K_6 = \frac{[M1/2 \cdot S][M3]}{[M1/2 \cdot S \cdot M3^*]}; [M3] = \frac{K_6[M1/2 \cdot S \cdot M3^*]}{[M1/2 \cdot S]}$$

$$K_7 = \frac{[M1/2 \cdot S^*]}{[M1/2 \cdot S]}$$

$$[M3_{\text{tot}}] = \frac{K_6[M1/2 \cdot S \cdot M3^*]}{[M1/2 \cdot S^*]} + \frac{K_4[M1/2 \cdot S \cdot M3^*]}{[M1/2]} + \frac{K_5[M1/2 \cdot S \cdot M3^*]}{[S]} + [M1/2 \cdot S \cdot M3^*]$$

$$[M3_{\text{tot}}] = [M1/2 \cdot S \cdot M3^*] \left( \frac{K_6}{K_7[M1/2 \cdot S]} + \frac{K_4}{[M1/2]} + \frac{K_5}{[S]} + 1 \right)$$

$$[M3_{\text{tot}}] = [M1/2 \cdot S \cdot M3^*] \left( \frac{K_1 K_6}{K_7[M1/2][S]} + \frac{K_4}{[M1/2]} + \frac{K_5}{[S]} + 1 \right)$$

$$[M3_{\text{tot}}] = [M1/2 \cdot S \cdot M3^*] \left( \frac{\frac{K_1 K_6}{K_7} + K_4[S] + K_5[M1/2] + [S][M1/2]}{[M1/2][S]} \right)$$

$$[M12 \cdot S \cdot M3^*] = \frac{[M1/2][M3_{\text{tot}}][S]}{\left( \frac{K_1 K_6}{K_7} \right) + K_5[M1/2] + [S]([M1/2] + K_4)}$$

$$[M12 \cdot S \cdot M3^*] = \frac{\left( \frac{[M12][M3_{\text{tot}}]}{K_4 + [M12]} [S] \right)}{\left( \frac{\frac{K_1 K_6}{K_7} + K_5[M12]}{K_4 + [M12]} + [S] \right)}$$



$$rate = k_{chem} \left( \frac{[M12][M3_{tot}]}{K_4 + [M12]} [S] \right) / \left( \frac{\frac{K_1 K_6 + K_5 [M12]}{K_7}}{K_4 + [M12]} + [S] \right)$$

$$k_{cat,app} = \frac{k_{chem}[M1/2]}{K_4 + [M12]}$$

$$K_{M,app} = \frac{\frac{K_1 K_6 + K_5 [M1/2]}{K_7}}{K_4 + [M1/2]}$$

$$\left( \frac{k_{cat}}{K_M} \right)_{app} = \frac{k_{chem}[M1/2]}{\frac{K_1 K_6 + K_5 [M1/2]}{K_7}}$$

### Magnesium dependence

The magnesium dependence of cleavage of pre-tRNA by human mitochondrial RNase P was measured under MTO conditions using 500 nM pre-tRNA containing 40 nM FI-pre-tRNA, sub-saturating (150 nM) or saturating (500 nM) MRPP1/2, in 50 mM MOPS (pH 7.8) and 1 mM TCEP (pH 7.5). The initial velocity was measured over six concentrations of Mg<sup>2+</sup> holding the ionic strength constant by varying NaCl concentration ( $\mu = 115$  mM taking only the concentrations of NaCl and MgCl<sub>2</sub> into account). For reactions using 150 nM MRPP1/2, 30 nM MRPP3 was used and for reactions using 500 nM MRPP1/2, 40 nM MRPP3 was used. Equation 2-16 was fit to the Mg<sup>2+</sup> dependence of the apparent steady state parameters where  $v_o$  is the initial velocity,  $V_{max}$  represents the maximal velocity at saturating Mg<sup>2+</sup>, and  $K_{1/2}^{Mg}$  is the concentration of Mg<sup>2+</sup> at which  $V_{max}$  is half-maximal.

$$v_o = \frac{V_{max}[Mg^{2+}]}{K_{1/2}^{Mg} + [Mg^{2+}]} \quad \text{Equation 2-16}$$

## Analytical ultracentrifugation

To evaluate the homogeneity and stoichiometry of MRPP1/2 we employed the sedimentation velocity technique using a Beckman Optimal XL-I analytical ultracentrifuge with UV absorbance optical system. The sample or reference solvent was added to 12 mm double sector aluminium epoxy cells with sapphire windows. Solutions were centrifuged at 40,000 rpm at 20 °C. 400 scans were recorded. Solute distributions were captured using the UV absorbance optical system. The data were analyzed using the c(s) method of the SEDFIT suite (34,35). A single peak with an S value of 6.5 was obtained. Equation 2-17 was used to estimate the molecular weight (~147kDa), which is close to the stoichiometry ratio of 1:4 of MRPP1:2 (153 kDa).

$$MW = \frac{S^0 RT}{D^0(1-\bar{v}\rho)} \quad \text{Equation 2-17}$$

MW = molecular weight

$S^0$  = the sedimentation coefficient extrapolated to zero solute concentration

$D^0$  = the diffusion coefficient extrapolated to zero solute concentration

R = the gas constant

T = the temperature in K

$\rho$  = buffer density

$\bar{v}$  = solute partial specific volume, which is the volume excluded by the solute

## REFERENCES

1. Shutt, T. E., and Shadel, G. S. (2010) A compendium of human mitochondrial gene expression machinery with links to disease. *Environmental and molecular mutagenesis* **51**, 360-379
2. Florentz, C., Sohm, B., Tryoen-Toth, P., Putz, J., and Sissler, M. (2003) Human mitochondrial tRNAs in health and disease. *Cellular and molecular life sciences : CMLS* **60**, 1356-1375
3. Wittenhagen, L. M., and Kelley, S. O. (2003) Impact of disease-related mitochondrial mutations on tRNA structure and function. *Trends Biochem Sci* **28**, 605-611
4. Taylor, R. W., and Turnbull, D. M. (2005) Mitochondrial DNA mutations in human disease. *Nature reviews. Genetics* **6**, 389-402
5. Suzuki, T., Nagao, A., and Suzuki, T. (2011) Human mitochondrial tRNAs: biogenesis, function, structural aspects, and diseases. *Annual review of genetics* **45**, 299-329
6. Lopez Sanchez, M. I. G., Mercer, T. R., Davies, S. M. K., Shearwood, A.-M. J., Nygård, K. K. A., Richman, T. R., Mattick, J. S., Rackham, O., and Filipovska, A. (2011) RNA processing in human mitochondria. *Cell Cycle* **10**, 2904-2916
7. Smith, D., and Pace, N. R. (1993) Multiple magnesium ions in the ribonuclease P reaction mechanism. *Biochemistry* **32**, 5273-5281
8. Walker, S. C., and Engelke, D. R. (2006) Ribonuclease P: the evolution of an ancient RNA enzyme. *Crit Rev Biochem Mol Biol* **41**, 77-102
9. Klemm, P. B., Wu, N., Chen, Y., Liu, X., Kaitany, J. K., Howard, J. M., and Fierke, A. C. (2016) The Diversity of Ribonuclease P: Protein and RNA Catalysts with Analogous Biological Functions. *Biomolecules* **6**
10. Gobert, A., Butmann, B., Taschner, A., Gößringer, M., Holzmann, J., Hartmann, R. K., Rossmanith, W., and Giegé, P. (2010) A single Arabidopsis organellar protein has RNase P activity. *Nature Structural and Molecular Biology* **17**, 740-744
11. Howard, M. J., Lim, W. H., Fierke, C. A., and Koutmos, M. (2012) Mitochondrial ribonuclease P structure provides insight into the evolution of catalytic strategies for precursor-tRNA 5' processing. *PNAS* **109**, 16149-16154
12. Holzmann, J., Frank, P., Löffler, E., Bennett, K. L., Gerner, C., and Rossmanith, W. (2008) RNase P without RNA: Identification and Functional Reconstitution of the Human Mitochondrial tRNA Processing Enzyme. *Cell* **135**, 462-474
13. Jackman, J. E., Montange, R. K., Malik, H. S., and Phizicky, E. M. (2003) Identification of the yeast gene encoding the tRNA m1G methyltransferase responsible for modification at position 9. *Rna* **9**, 574-585
14. Yang, S.-Y., He, X.-Y., and Miller, D. (2007) HSD17B10: A gene involved in cognitive function through metabolism of isoleucine and neuroactive steroids. *Molecular Genetics and Metabolism* **92**, 36-42

15. Yang, S.-Y., He, X.-Y., and Schulz, H. (2005) Multiple functions of type 10 17 $\beta$ -hydroxysteroid dehydrogenase. *Trends in Endocrinology & Metabolism* **16**, 167-175
16. Vilardo, E., Nachbagauer, C., Buzet, A., Taschner, A., Holzmann, J., and Rossmann, W. (2012) A subcomplex of human mitochondrial RNase P is a bifunctional methyltransferase-extensive moonlighting in mitochondrial tRNA biogenesis. *Nucleic acids research* **40**, 11583-11593
17. Deutschmann, A. J., Amberger, A., Zavadil, C., Steinbeisser, H., Mayr, J. A., Feichtinger, R. G., Oerum, S., Yue, W. W., and Zschocke, J. (2014) Mutation or knock-down of 17 $\beta$ -hydroxysteroid dehydrogenase type 10 cause loss of MRPP1 and impaired processing of mitochondrial heavy strand transcripts. *Human molecular genetics* **23**, 3618-3628
18. Falk, M. J., Gai, X., Shigematsu, M., Vilardo, E., and Takase, R. (2016) A novel HSD17B10 mutation impairing the activities of the mitochondrial RNase P complex causes X-linked intractable epilepsy and neurodevelopmental regression. *RNA Biology* **13**, 477-485
19. Metodiev, M. D., Thompson, K., Alston, Charlotte L., Morris, Andrew A. M., He, L., Assouline, Z., Rio, M., Bahi-Buisson, N., Pyle, A., Griffin, H., Siira, S., Filipovska, A., Munnich, A., Chinnery, Patrick F., McFarland, R., Rötig, A., and Taylor, Robert W. (2016) Recessive Mutations in TRMT10C Cause Defects in Mitochondrial RNA Processing and Multiple Respiratory Chain Deficiencies. *The American Journal of Human Genetics* **98**, 993-1000
20. Sen, A., Karasik, A., Shanmuganathan, A., Mirkovic, E., Koutmos, M., and Cox, R. T. (2016) Loss of the mitochondrial protein-only ribonuclease P complex causes aberrant tRNA processing and lethality in Drosophila. *Nucleic acids research* **44**, 6409-6422
21. Vilardo, E., and Rossmann, W. (2015) Molecular insights into HSD10 disease: impact of SDR5C1 mutations on the human mitochondrial RNase P complex. *Nucleic acids research* **43**, 5112-5119
22. Li, F., Liu, X., Zhou, W., Yang, X., and Shen, Y. (2015) Auto-inhibitory Mechanism of the Human Mitochondrial RNase P Protein Complex. *Scientific reports* **5**, 9878
23. Reinhard, L., Sridhara, S., and Hallberg, B. M. (2015) Structure of the nuclease subunit of human mitochondrial RNase P. *Nucleic acids research*
24. Howard, M. H., Klemm, B. P., and Fierke, C. A. (2015) Mechanistic Studies Reveal Similar Catalytic Strategies for Phosphodiester Bond Hydrolysis by Protein-only and RNA-dependent Ribonuclease P. *Journal of Biological Chemistry* **290**, 13454-13464
25. Liu, X., Chen, Y., and Fierke, C. A. (2014) A real-time fluorescence polarization activity assay to screen for inhibitors of bacterial ribonuclease P. *Nucleic acids research* **42**, e159
26. Cha, S. (1968) Kinetics of Enzyme Reactions with Competing Alternative Substrates. *Molecular Pharmacology* **4**, 621

27. Schellenberger, V., Siegel, R. A., and Rutter, W. J. (1993) Analysis of enzyme specificity by multiple substrate kinetics. *Biochemistry* **32**, 4344-4348
28. Rueda, D., Hsieh, J., Day-Storms, J. J., Fierke, C. A., and Walter, N. G. (2005) The 5' Leader of Precursor tRNA(Asp) Bound to the *Bacillus subtilis* RNase P Holoenzyme Has an Extended Conformation. *Biochemistry* **44**, 16130-16139
29. Behrman, E. (2000) An improved synthesis of guanosine 5'-monothiophosphate. *J. Chem. Research (S)*, 446-447
30. He, B., Rong, M., Lyakhov, D., Gartenstein, H., Diaz, G., Castagna, R., McAllister, W. T., and Durbin, R. K. (1997) Rapid mutagenesis and purification of phage RNA polymerases. *Protein Expr Purif* **9**, 142-151
31. Lim, W. H. (2011) Importance of substrate recognition and metal ions in the Ribonuclease P catalysis, Ph.D. Thesis. University of Michigan, Ann Arbor, MI, USA
32. Liu, X. (2014) Molecular recognition of inhibitors, metal ions and substrates by ribonuclease P. University of Michigan
33. Day-Storms, J. J., Niranjanakumari, S., and Fierke, C. A. (2004) Ionic interactions between PRNA and P protein in *Bacillus subtilis* RNase P characterized using a magnetocapture-based assay. *Rna* **10**, 1595-1608
34. Schuck, P. (1998) Sedimentation Analysis of Noninteracting and Self-Associating Solutes Using Numerical Solutions to the Lamm Equation. *Biophysical Journal* **75**, 1503-1512
35. Schuck, P. (2000) Size-Distribution Analysis of Macromolecules by Sedimentation Velocity Ultracentrifugation and Lamm Equation Modeling. *Biophysical Journal* **78**, 1606-1619

## CHAPTER 3<sup>4</sup>

### Inhibition of protein-only RNase P with Gambogic acid and Juglone

#### ABSTRACT

One of many essential steps in transfer RNA (tRNA) maturation is the removal of the 5' ends of precursor transcripts (pre-tRNA). This is catalyzed by ribonuclease P (RNase P), a metal-dependent endonuclease present across all domains of life. To better understand the processing of tRNA, we screened for compounds that inhibit the activity of protein-only RNase P (PRORP) from *A. thaliana* mitochondria (PRORP1) using a high throughput fluorescence polarization (FP) assay. Compound hits were validated and dose response confirmatory assays were performed. Two compound hits, gambogic acid and juglone (5-hydroxy-1,4-naphthalenedione), inhibit PRORP enzymes in plant and human mitochondria with at least 50-fold higher potency compared to bacterial ribonucleoprotein (RNP) RNase P. Biochemical measurements indicate that gambogic acid is a rapidly-binding uncompetitive inhibitor that targets the enzyme-substrate complex and juglone is a time-dependent inhibitor. Furthermore, we have solved an x-ray crystal structure, revealing PRORP1 in a

---

<sup>4</sup> Nancy Wu optimized the FP assay, prepared the substrate, purified PRORP1 variants, MRPP1/2 and MRPP3, performed the high throughput screen and assays with PRORP1 and *B.s.* RNase P and analyzed the data. N.W. and Carol A. Fierke participated in the experimental design and interpretation of the results. Laura Muehlbauer performed the dose-response experiments with human mitochondrial RNase P. Markos Koutmos and Agnes Karasik performed the crystallographic studies and analyses.

covalent complex with juglone. This is the first report of inhibitors against a new class of metallonucleases, protein-only mitochondrial RNase Ps. Moving forward, gambogic acid and juglone have the potential to be developed into tools to understand mitochondrial disease states that arise from dysfunction in tRNA processing.

## **BACKGROUND**

Transfer RNAs are transcribed as precursor transcripts (pre-tRNA) with extra nucleotides at both ends and undergo modification before they are functional for protein synthesis. One of the first steps in tRNA maturation is the removal of the 5' leader through phosphodiester bond hydrolysis catalyzed by RNase P. RNase P can be activated by a number of metals *in vitro* including  $Mg^{2+}$  and  $Mn^{2+}$ , but prefers  $Mg^{2+}$  *in vivo* (1,2). The mechanism and function of RNase P has been studied for many years, beginning with the identification of ribonucleoprotein (RNP) RNase P as a ribozyme in bacteria and in the nucleus of some eukaryotes (3-5). Our view of this enzyme was then broadened with the discovery of protein-only RNase P (PRORP) in human mitochondria (6). The two types of RNase P enzymes, PRORP and RNP RNase P, have both been proposed to employ a two metal ion mechanism for the hydrolysis of a specific phosphodiester bond in pre-tRNA using a metal ion bound water nucleophile (7,8).

The composition of PRORP enzymes differs across species. PRORP1 in *A. thaliana* functions as a single-subunit protein while human mitochondrial PRORP require three proteins: mitochondrial RNase P protein (MRPP) 1, 2, and 3 (MRPP1/2/3). A model system for studying PRORP function is PRORP1 from *A. thaliana*, which is an ortholog of MRPP3, the metallo-nuclease subunit of PRORP in human mitochondria. PRORP1 and MRPP3 belong to a unique class of endonucleases that contain a Nedd4-BP1, Yac Nucleases (NYN) domain, a member of the PIN domain-like superfamily (9). In addition, PRORP1 and MRPP3 also have a pentatricopeptide repeat (PPR) domain that binds RNA and a structural zinc binding central domain. PRORP1 (10) and MRPP3 (11,12) are similar in structure, with 22% sequence identity. PRORP1 and MRPP3 have four completely conserved aspartate residues (*At* PRORP1 Asp 399, 474, 475, and 493) that are important for catalytic activity and metal ion binding in PRORP1 (6,8). MRPP3 houses the active site for pre-tRNA catalysis, but requires the addition of a tRNA R9 methyltransferase (MRPP1) and a short chain hydroxysteroid dehydrogenase (MRPP2) subcomplex for function (6,13).

RNA processing in mitochondria is essential and the disruption of this pathway can be detrimental. Mutations of individual mitochondrial protein-only RNase P proteins in *Drosophila* are lethal, in part due to defective tRNA processing (14). Knockdowns via siRNA of either MRPP1 or MRPP3 in HeLa cells also result in mitochondrial pre-tRNA transcript accumulation (15). Furthermore, the pathogenic mutations in MRPP1 and MRPP2 lead to dysfunctional mitochondrial RNA processing and decreased respiratory chain



complex proteins levels (16,17). MRPP1 mutations were identified in two patients with birth defects. Investigations revealed reduced protein levels in fibroblast cells, increased pre-tRNA transcripts, impaired mitochondrial RNA processing, and defective mitochondrial protein synthesis, an essential process for the production of vital electron transport chain complexes (17). Furthermore, point mutations in mitochondrial tRNA (mt-tRNA) genes and mitochondrial RNase P proteins are associated with a number of pathologies arising from mitochondrial dysfunction (18,19). To characterize how such mutations affect mt-tRNAs, various groups have shown that pathogenic mutations affect the tertiary structure of tRNA, 5'- and 3'-end processing efficiency, amino-acylation, and binding to elongation factors (18,20,21). However, *in vitro* studies of unmodified tRNA do not encompass the complete picture of tRNA processing since posttranscriptional modifications play a role in tRNA folding and stability (22). To better understand the mechanism of mitochondrial RNA processing *in vivo*, we propose to develop inhibitors to rapidly modulate the activity of PRORP enzymes.

To develop tools for studying human MRPP1/2/3 *in vivo*, I screened for inhibitors of the MRPP3 ortholog, PRORP1. There are currently no known inhibitors against PRORP enzymes and this work aims to identify and characterize inhibitors against plant PRORP1 and human MRPP1/2/3. An adapted FP assay was used to screen a small molecule compound library containing compounds extracted from microbes and pharmacologically active compounds (23). Biochemical measurements indicate that we have identified both rapidly binding uncompetitive and time-dependent inhibitors that are at least

50-fold more potent against plant and human MRPP1/2/3 relative to bacterial RNP RNase P. The compounds identified from this screen serve as lead compounds to be used to probe mitochondrial RNase P activity in the cell and to improve our understanding of the molecular recognition of mitochondrial RNase P.

## RESULTS

### A high throughput FP assay for PRORP1 activity

To identify potent inhibitors of PRORP1, we developed an FP assay that monitors the conversion of fluorescein 5' end-labeled pre-tRNA (FI-pre-tRNA) to a fluorescein-labeled leader sequence cleaved by PRORP1 (Figure 3-1). This assay was adapted from a recently developed FP assay for RNP RNase P from *B. subtilis* (23). To optimize this assay for use in a high throughput screen, buffer conditions were varied to enhance activity, including the addition of spermidine and bovine serum albumin (BSA). The PRORP1 concentration was varied to reach an optimal linear range for the high throughput assay. FP assays were performed under multiple turnover (MTO) conditions where pre-tRNA was used in excess compared to PRORP1 at concentrations close to the  $K_M$  value to identify both competitive and noncompetitive inhibitors.  $\text{CaCl}_2$  is used to quench the reaction since PRORP1 binds to FI-pre-tRNA but does not catalyze hydrolysis in the presence of  $\text{CaCl}_2$ . A time course of the PRORP1 reaction

quenched by the addition of CaCl<sub>2</sub> at various time points is shown in Figure 3-2A.

This FP assay (average plate  $Z' = 0.6 \pm 0.05$ , Figure 3-2) was used to screen a pilot compound library of small molecules (6046 compounds) to identify 88 compound hits that are above 3 standard deviations (SD) from the negative control (1.5% hit rate). A second cut off identified 42 compounds that inhibit PRORP1 activity greater than 40% (Table A-1). Finally, a gel-based confirmation assay was used to eliminate false positive hits. From the 42 hits, incubation of 23 compounds at 12.5  $\mu\text{M}$  with PRORP1 resulted in no product formation, observed on urea-PAGE after 1h. Next, we used the real-time FP assay to determine the dose-dependence of inhibition of these 23 compounds by measure initial velocities. Of the compounds tested, the two most potent compounds, gambogic acid and juglone (structures shown in Figure 3-3), were studied in an in-depth kinetic analysis to determine their modes of inhibition.

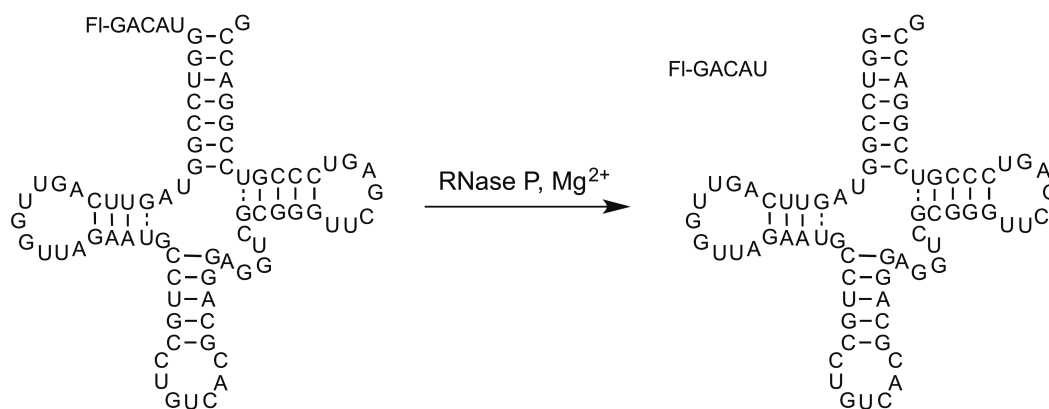


**Figure 3-1 Fluorescence polarization (FP) assay to measure RNase P activity**

Fluorescein 5' end-labeled *B.s.* pre-tRNA<sup>Asp</sup> is cleaved by RNase P to give products: fluorescein-labeled 5' leader and tRNA<sup>Asp</sup>.

## **Gambogic acid and juglone are more potent against PRORP compared to RNP RNase P**

To compare the potency of gambogic acid and juglone against PRORP and RNP RNase P, we determined the  $IC_{50}$  values of PRORP1, MRPP1/2/3, and *B. subtilis* RNase P using the FP assay. After a 30 min pre-incubation with PRORP1, gambogic acid inhibits PRORP1 activity with an  $IC_{50}$  value of  $0.99 \pm 0.04 \mu\text{M}$  (n=3) and MRPP1/2/3 with an  $IC_{50}$  value of  $0.26 \pm 0.06 \mu\text{M}$  (n=1), while juglone inhibits PRORP1 with an  $IC_{50}$  value of  $2.1 \pm 0.04 \mu\text{M}$  (n=1) and MRPP1/2/3 with an  $IC_{50}$  value of  $1.8 \pm 0.04 \mu\text{M}$  (n=1) (Figure 3-3 and Table 3-1). Gambogic acid and juglone are more than 50-fold less potent against *B. subtilis* RNP RNase P ( $IC_{50}$  value of gambogic acid is  $50 \pm 2 \mu\text{M}$ , n=4; and  $IC_{50}$  value of juglone is  $580 \pm 16 \mu\text{M}$ , n=4, Figure 3-3 and Table 3-1). These data suggest that gambogic acid and juglone may recognize common features of PRORP1 and MRPP1/2/3 that are not present to *B. subtilis* RNP RNase P. Understanding the mode of inhibition of these compounds will provide further insight into the molecular recognition mechanisms of PRORP and RNP RNase P.

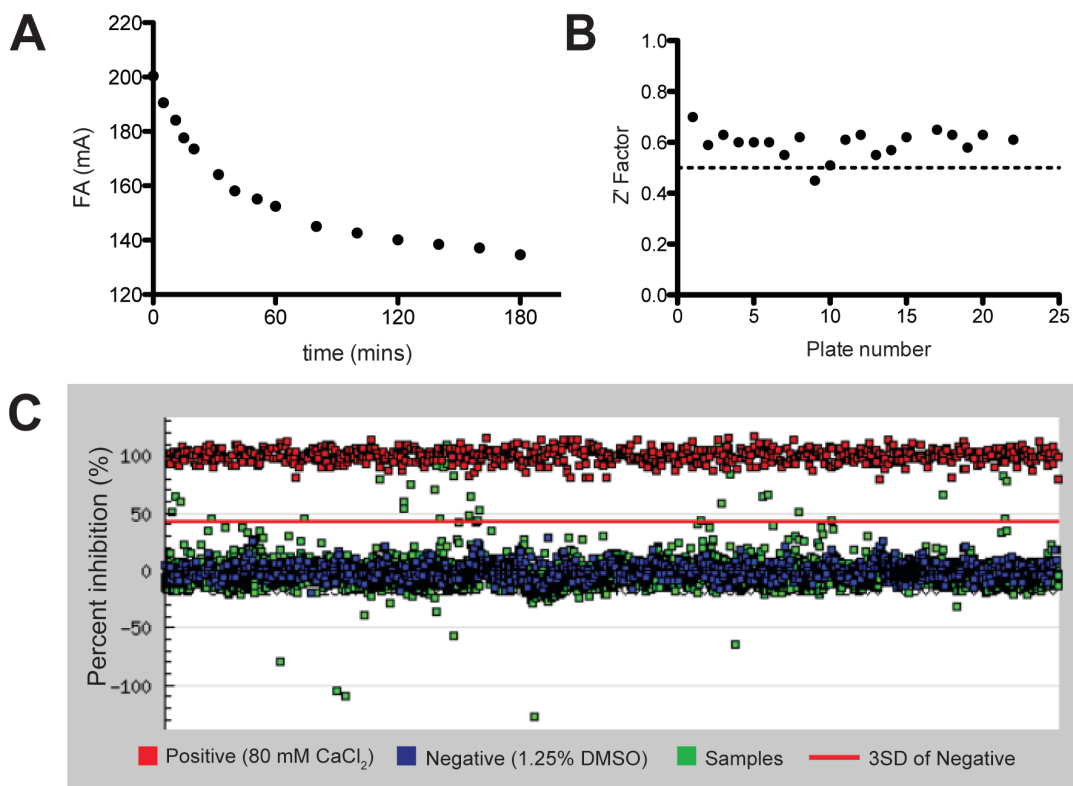


**Figure 3-2 A robust high throughput FP assay for identifying inhibitors of PRORP1**

(A) A time course of the FP assay using 0.3 nM PRORP1 and 800 nM pre-tRNA containing 40 nM FI-pre-tRNA at 25 °C in 30 mM MOPS pH 7.8, 5 mM MgCl<sub>2</sub>, 100 mM NaCl, 1 mM TCEP, 500 nM (12 µg/mL) yeast tRNA<sup>mix</sup>, 5 mM spermidine, 6.65 µg/ml BSA, and 0.01% NP-40. Samples were quenched with 80 mM CaCl<sub>2</sub> at various time points and the fluorescence anisotropy (FA) value was measured. (B) The Z' factor values across each 384-well microplate range from 0.45 to 0.7. The average Z' factor of this assay is 0.6 ± 0.05. (C) The percent inhibition of PRORP1 activity with compounds was determined from FA readout after 1 hr reaction time for each plate. Positive controls (80 mM CaCl<sub>2</sub>) are shown in red, negative controls (1.25% DMSO) are shown in blue, the samples are shown in green, and the red line represents 3SD above the negative control.

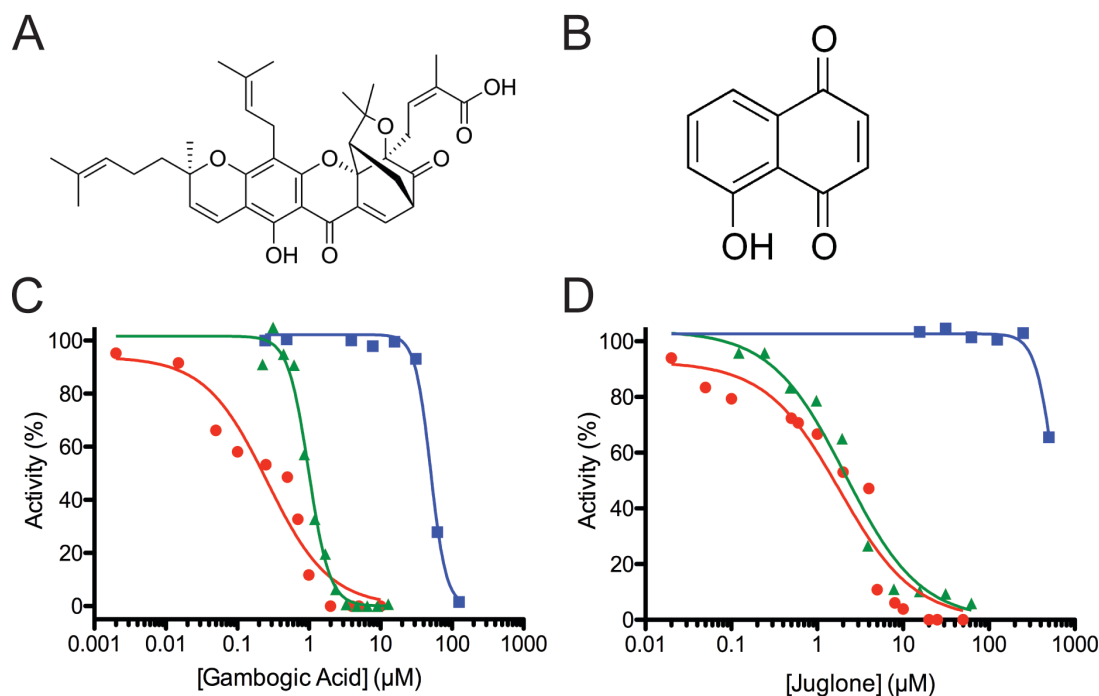


**Figure 3-3 Gambogic acid and juglone are inhibitors against protein-only RNase P in plant and human mitochondria**

(A) Structure of gambogic acid, (B) Structure of juglone, (C) Gambogic acid and (D) juglone inhibit PRORP1 from *A. thaliana* (green), human MRPP1/2/3, and *B. subtilis* RNP RNase P (blue). Compounds were incubated with enzyme at double the reaction concentration for 30 minutes prior the addition of equal volumes of substrate to initiate the reaction. PRORP1 experiments were done using the FP assay with 0.3 nM PRORP1, 800 nM pre-tRNA containing 40 nM FI-pre-tRNA, 30 mM MOPS (pH 7.8), 5 mM MgCl<sub>2</sub>, 1 mM TCEP, 100 mM NaCl, 500 nM yeast tRNA<sup>mix</sup>, 5 mM spermidine, 6.65 μg/ml BSA, and 0.01% NP-40 at 25 °C. MRPP1/2/3 experiments were done with 50 nM MRPP3, 500 nM MRPP1/2 in 50 mM MOPS (pH 7.8), 4.5 mM MgCl<sub>2</sub>, 100 mM NaCl, and 1 mM TCEP (pH 7.5). *B. subtilis* RNP RNase P experiments were done with 20 nM RNase P and 500 nM FI-pre-tRNA in 50 mM Tris (pH 7.2), 5 mM MgCl<sub>2</sub>, 100 mM KCl, 500 nM (12 μg/mL) yeast tRNA<sup>mix</sup>, 20 mM DTT, 10 mM spermidine, and 0.01% NP-40 at 37 °C. The *IC*<sub>50</sub> and *n* values are listed in Table 3-1. The data was fit with Equation 3-5.

### Gambogic acid is an uncompetitive inhibitor of PRORP1 activity

We evaluated the time-dependence of inhibition of gambogic acid. Pre-incubation of PRORP1 with gambogic acid prior to the addition of pre-tRNA to initiate the reaction does not affect the *IC*<sub>50</sub> value. To identify the mode of inhibition of gambogic acid, PRORP1 activity was measured using real-time FP assays under MTO conditions with varying pre-tRNA and gambogic acid

concentrations (Figure 3-4). Each curve was fit individually to Equation 3-6 to determine the apparent catalytic rate constant ( $k_{cat,app}$ ) and apparent substrate concentration at half maximal activity ( $K_{M,app}$ ). Increasing gambogic acid concentration decreased the value of  $k_{cat,app}$  with no significant change in  $(k_{cat}/K_M)_{app}$  (Figure 3-4). A global fit analysis (Equations 3-6, 3-7, and 3-8) was also used to determine the inhibition constant ( $K_I$ ). The data are well described by the uncompetitive inhibition model with a  $K_I$  value of  $1.1 \pm 0.03 \mu\text{M}$  ( $n=4$ ). A model for an uncompetitive inhibitor is shown in Figure 3-4B.

**Table 3-1** The  $IC_{50}$  values and Hill coefficients ( $n$ ) for the inhibition of PRORP1, MRPP1/2/3, and *B. subtilis* RNase P with gambogic acid and juglone.

	gambogic acid		juglone	
	$IC_{50}$ ( $\mu\text{M}$ )	$n$	$IC_{50}$ ( $\mu\text{M}$ )	$n$
<b>PRORP1</b>	$0.99 \pm 0.04$	3	$2.1 \pm 0.4$	1
<b>MRPP1/2/3</b>	$0.26 \pm 0.06$	1	$1.8 \pm 0.4$	1
<b><i>B. s.</i> RNase P</b>	$50 \pm 2$	4	$580 \pm 16$	4

The errors reported represent the standard error from the fit.

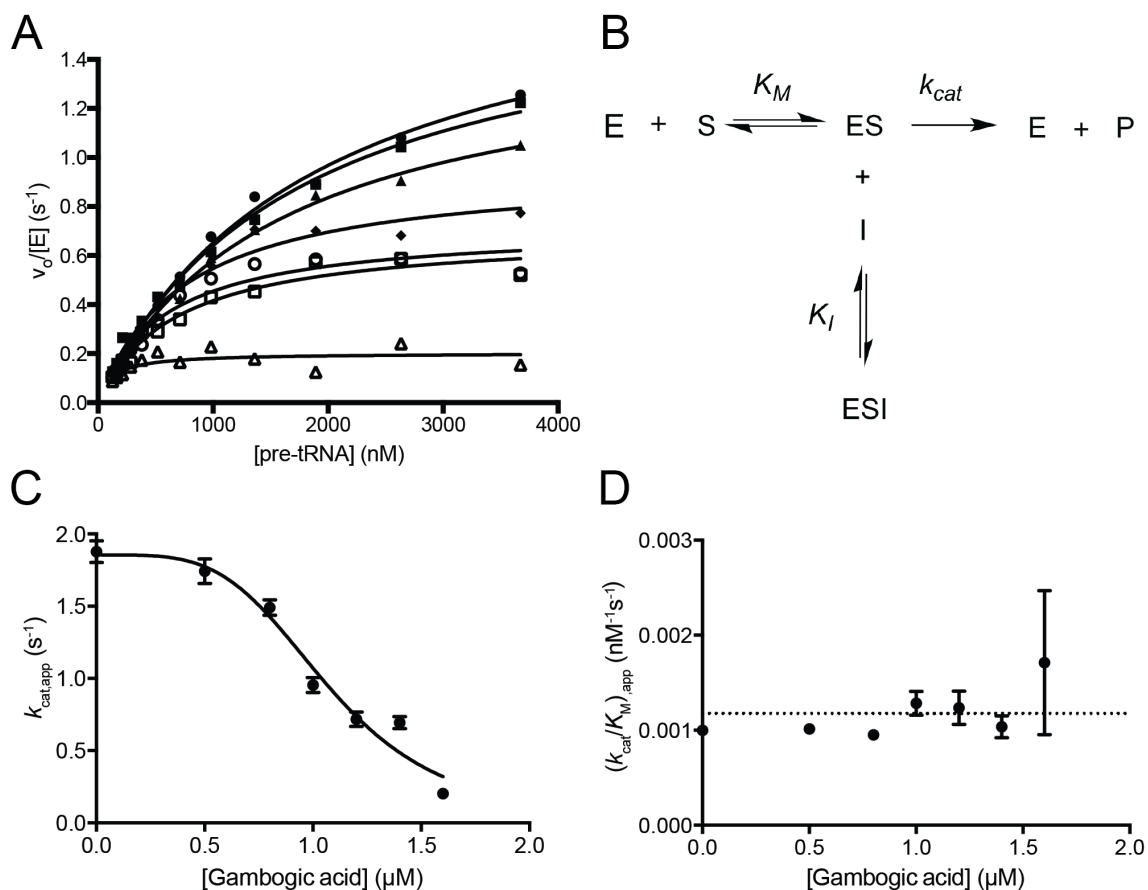


### Figure 3-4 Gambogic acid is an uncompetitive inhibitor of PRORP1

(A) The initial rate for PRORP1 catalyzed cleavage of FI-pre-tRNA is plotted as a function of substrate concentration over a range of concentrations of gambogic acid (filled circles, 0  $\mu\text{M}$ ; filled squares, 0.5  $\mu\text{M}$ ; filled triangles, 0.8  $\mu\text{M}$ ; filled diamonds, 1  $\mu\text{M}$ ; open circles, 1.2  $\mu\text{M}$ ; open squares, 1.4  $\mu\text{M}$ ; open triangles, 1.6  $\mu\text{M}$ ). Equation 3-6 was fit to each data set to calculate the values of  $k_{cat,app}$ , and  $K_{M,app}$ , and  $(k_{cat}/K_M)_{app}$  (B) Reaction scheme for an uncompetitive inhibitor. (C)  $k_{cat,app}$  values for PRORP1 activity obtained from the data in frame A ( $n=1$ ) as a function of gambogic acid concentration is fit with Equation 3-7, resulting in an inhibition constant ( $K_I$ ) of  $1.1 \pm 0.05 \mu\text{M}$  ( $n=4$ ). (D)  $k_{cat}/K_{M,app}$  values for PRORP1 activity are constant as a function of gambogic acid concentration. The errors shown are the standard errors obtained from fitting the data.

### Juglone is a time-dependent inhibitor of PRORP1 activity

We also evaluated the time-dependence of inhibition of juglone. Pre-incubation of PRORP1 with gambogic acid does not affect the  $IC_{50}$  value, however, the potency of juglone increases with pre-incubation time. To determine a minimal kinetic mechanism for the time-dependent inhibition of PRORP1 by



juglone, the pre-incubation time was varied for each juglone concentration measured (Figure 3-5). PRORP1 activity was measured using 250 nM pre-tRNA, which is well below the  $K_M$  in these reaction conditions. PRORP1 activity decreases with increasing pre-incubation time following a single exponential decay. The observed pseudo first order rate constant ( $k_{obs}$ ) for the inhibition of PRORP1 exhibits a hyperbolic dependence on juglone concentration (Figure 3-5C). The data were extrapolated to 0 min pre-incubation revealing a rapid step for inhibition as well as time-dependent inhibition (Figure 3-5B). These data are consistent with a two-step inhibition mechanism where juglone rapidly binds to and inhibits PRORP1, followed by a slow conversion from the enzyme-inhibitor complex (EI) to the inactive EI\* complex (Scheme 3-1). The apparent inhibition constant ( $K_I = 12.5 \pm 2.7 \mu\text{M}$ ) was determined by fitting Equation 3-5 to the dose response curve of the data extrapolated to 0 min pre-incubation where the  $K_I$  is represented by the  $IC_{50}$  (Figure 3-5B). This value of  $K_I$  (12  $\mu\text{M}$ ) was used in Equation 3-9 to fit the data for  $k_{inact}$  ( $0.018 \pm 0.001 \text{ min}^{-1}$ ). A global fit analysis (Equations 3-9 and 3-10) using a  $K_I$  value of 12  $\mu\text{M}$  was also done to determine  $k_{inact}$  ( $0.014 \pm 0.001 \text{ min}^{-1}$ ).

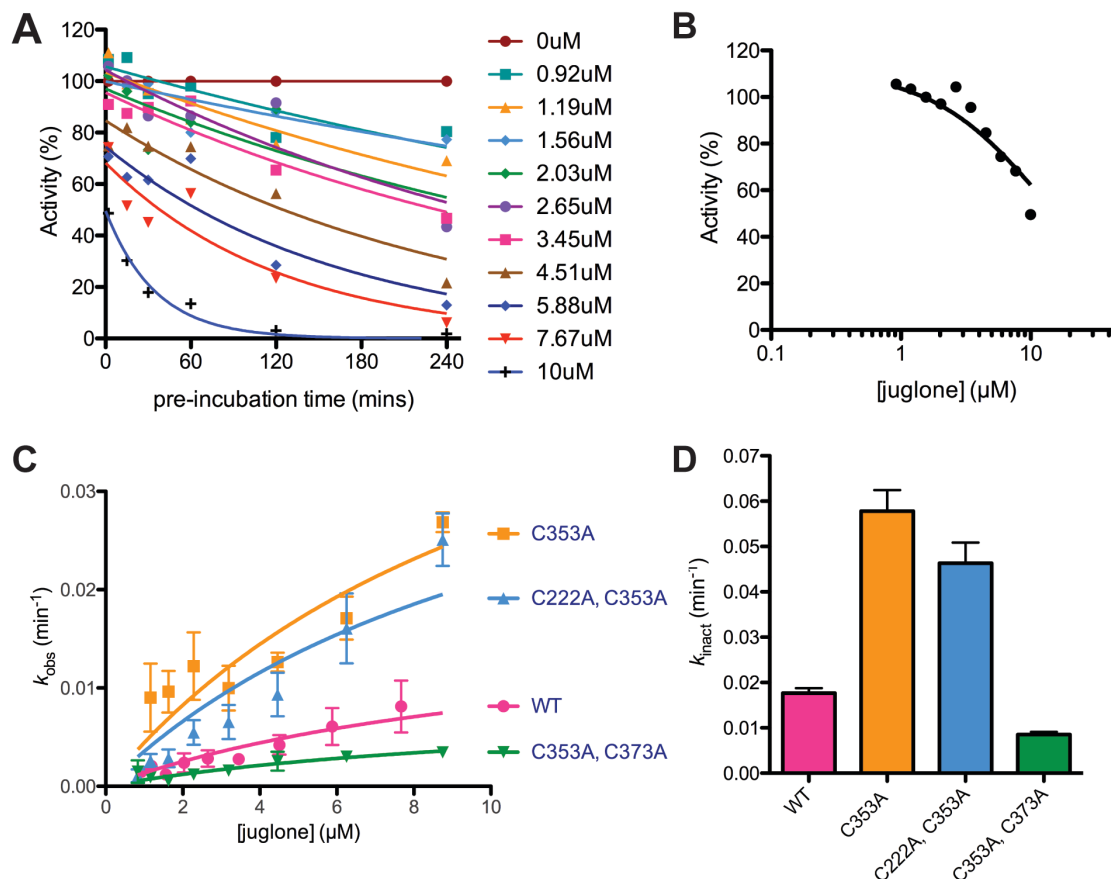


### Figure 3-5 Juglone is a time-dependent inhibitor of PRORP1

(A) The activity of PRORP1 is plotted with varying pre-incubation times with juglone. The range of juglone concentrations is shown in the legend on the right. Each data set was fit to a single exponential decay (Equation 3-9) to determine the observed rate constant for inactivation ( $k_{obs}$ ). (B) The dose response of juglone on PRORP1 activity extrapolated to 0-min pre-incubation. Equation 3-5 was fit to the data to calculate  $K_i$  ( $12.5 \pm 2.7 \mu\text{M}$ ,  $n=1$ ). (C) The observed rate constants for juglone inactivation ( $k_{obs}$ ) of PRORP1 variants are plotted with varying juglone concentration. Equation 3-10 was fit to the data where  $K_i$  is held at  $12 \mu\text{M}$  to determine the value for  $k_{inact}$ . (D) The  $k_{inact}$  values vary between PRORP1 mutants. The errors shown are standard errors obtained from the fit.

### Crystallographic studies reveal a PRORP1-juglone complex

To understand the molecular basis for time-dependent inhibition of PRORP1 by juglone, PRORP1 was crystallized with juglone. This work was done in collaboration with the Koutmos lab at the Uniformed Services University of the

Health Sciences. Crystals were formed without inhibitor present and then soaked for 45 min or overnight in the presence of juglone at 4 °C. In all crystallization conditions, PRORP1 was covalently modified by juglone at C353, which is located in a solvent accessible, flexible region within the zinc binding central domain (Figure 3-6). Overnight soaking with juglone revealed two additional modifications at C222 and 373 where partial juglone electron densities were observed.

To identify the site of modification that leads to inactivation, cysteine-to-alanine PRORP1 mutants were purified and inhibition studies were repeated. A C353A PRORP1 mutant did not abolish the time-dependent inhibition of juglone for PRORP1, but instead enhanced  $k_{\text{inact}}$  by 3-fold ( $0.058 \pm 0.004 \text{ min}^{-1}$ ) while  $K_i$  remained unchanged (Figure 3-5). A C222A/C353A double mutant of PRORP1 resulted in no inhibition without pre-incubation at the concentrations tested and a less than 2-fold decrease in  $k_{\text{inact}}$ , suggesting that loss of C222 affects the rapid inhibition of juglone, but not the time-dependent inhibition. Furthermore, a C353A/C373A double mutant of PRORP1 reduced  $k_{\text{inact}}$  by 7-fold compared to the C353A single mutant, suggesting that modification of C373 leads to inactivation of the WT PRORP1. Additional experiments with PRORP1 crystals soaked with juglone for 3 hr revealed a covalent modification by juglone at C346, located next to C345, which coordinates a structural Zinc ion in the central domain. Further work will investigate the significance of C346. Similar structural studies were also done with gambogic acid, but gambogic acid was not found in the crystals.

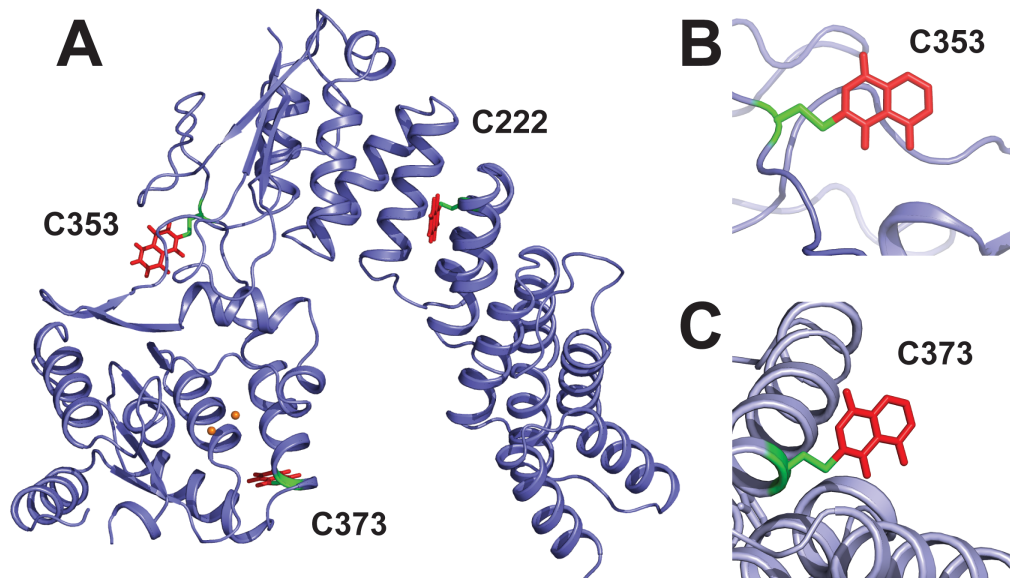


**Figure 3-6 Crystal structure of PRORP1 in complex with juglone after overnight incubation.** (A) PRORP1 makes a covalent interaction with juglone (red) through cysteine thiol side chains (green) at C222, C353, and C373. Active site metals modeled from a previously solved structure of WT PRORP1 with  $Mn^{2+}$  ions (10) shown as orange spheres. Zoomed in view of juglone modification at C353 (B) and C373 (C).

## DISCUSSION

In this study, we demonstrate the robustness of a FP assay and use the assay to identify inhibitors of a new class of enzymes: human and plant mitochondrial PRORPs. There are currently no inhibitors reported to date. Gambogic acid and juglone are potent inhibitors of both protein-only RNase P enzymes in human and plant mitochondria (Figure 3-3), but at least 50-fold less potent against bacterial RNP RNase P in bacteria. These data demonstrate that gambogic acid and juglone recognize specific features of PRORP that are not present in bacterial RNP RNase P. Furthermore, we use gambogic acid and

juglone as tools for understanding the function of PRORP1, which has implications for probing important structural features of PRORPs.

### **Gambogic acid binds to the enzyme-substrate complex**

Our results show that both  $k_{cat}$  and  $K_M$  decrease with increasing gambogic acid concentration, and as a result,  $k_{cat}/K_M$  remains constant, consistent with the behavior of a reversible uncompetitive inhibitor that binds exclusively to the enzyme-substrate (ES) complex. As shown in the model for an uncompetitive inhibition (Figure 3-4B), gambogic acid (shown as I) binds to ES reversibly and pulls the equilibrium such that E and S bind with higher apparent affinity (decrease in  $K_{M,app}$ ) and reduced  $k_{cat,app}$ . Gambogic acid inhibits PRORP1 with a Hill coefficient of 3, indicative of cooperative inhibition. One explanation is that there are multiple binding sites on PRORP1 for gambogic acid. The structure of gambogic acid resembles nucleotide bases and therefore could bind to the RNA-binding PPR domain. Given that gambogic acid is an uncompetitive inhibitor, it likely recognizes an interface that includes both pre-tRNA and PRORP1. Gambogic acid can be useful in structural studies of pre-tRNA and PRORP1 since it decreases the value of  $K_{M,app}$ . There is currently no detailed structural information of PRORP1 in complex with pre-tRNA.

Gambogic acid has many cellular targets ranging from kinases to proteins involved in maintaining the structural integrity of the cell and is thus considered a broad spectrum clinical agent (24). Gambogic acid has anti-inflammatory, anti-cancer, antibacterial, and antioxidant effects due to its ability to modulate many

cell signaling pathway intermediates including epigenetic regulators, protein kinases, transcription factors, inflammatory biomarkers, and growth regulators (25,26). The anti-inflammatory and anticancer effects of gambogic acid are associated with its inhibitory response on Nuclear Factor-Kappa B (NF- $\kappa$ B) induced by TNF- $\alpha$ , LPS, and various agents (27). NF- $\kappa$ B regulates proteins including cyclooxygenase type 2 (COX-2), inducible nitric oxide synthetase (iNOS), involved in inflammation and pain, and immune response, respectively (27,28). Gambogic acid is an antagonist of anti-apoptotic Bcl-2 family proteins and as a result induces apoptosis in cancer cells (29,30). Other targets of gambogic acid include histone acetyltransferase (HAT) and histone deacetylase (HDAC) in lung cancer cells (31).

Gambogic acid does not have sufficient selectivity to serve as an *in vivo* inhibitor of protein-only RNase Ps. Instead, it could serve as a lead compound that is modified to gain selectivity and it is useful for *in vitro* studies of PRORP1 and MRPP1/2/3.

### **Juglone covalently modifies cysteine thiols in PRORP1**

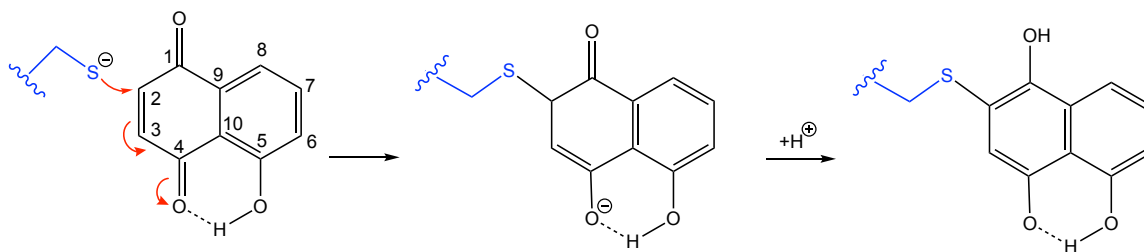
Juglone exhibits the features of a slow binding inhibitor of PRORP1. The data is consistent with a two-step inhibition model where juglone binds to PRORP1 rapidly ( $K_i = 12 \mu\text{M}$ ) to form an inactive enzyme-inhibitor (EI) complex, which then undergoes a slow step to form another inactive EI\* complex described by  $k_{\text{inact}}$  ( $0.014 \pm 0.001 \text{ min}^{-1}$ ). As a time-dependent inhibitor, juglone may form a covalent adduct with PRORP1 or induce a conformation change in

PRORP1, rendering it inactive. We propose a model for inhibition of PRORP1 by juglone, in which the second step is a structural rearrangement and/or covalent modification (Scheme 3-1).

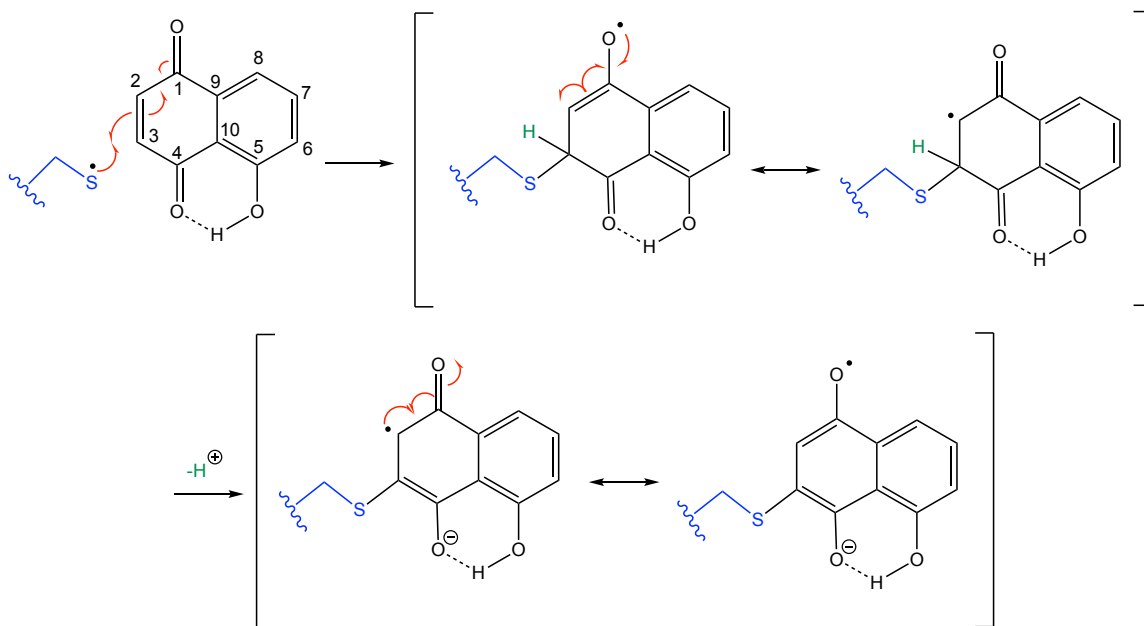


**Scheme 3-1 Proposed model of inactivation by a slow-binding inhibitor**

Juglone (represented by I) inactivates PRORP1 (represented by E) through a rapid first step to form EI described by  $K_I$ , followed by a slow second step to form  $EI^*$  described by  $k_{inact}$ . Both EI and  $EI^*$  are inactive species of the enzyme.



**Scheme 3-2 Michael addition reaction mechanism of cysteine thiol with juglone at C-2**



**Scheme 3-3 Radical addition reaction mechanism of cysteine thiol with juglone at C-2**

Our structural work is the first crystal structure of protein that is covalently modified by juglone. This work suggests that juglone forms a covalent bond with up to four cysteine residues in PRORP1. There is precedence for the covalent modification of cysteine residues by juglone. Juglone inactivates *E. coli* parvulin by covalently modifying two cysteine residues through a Michael addition (32). Quinones such as juglone are potent electrophiles that are readily reactive with thiol groups in proteins. Thus, juglone would not be used as a specific inhibitor of mitochondrial RNase P *in vivo*, but is used to understand potential regions within PRORP1 that are more susceptible to modification and inhibition. We propose two possible mechanisms for the modification of a cysteine thiol in PRORP1 at positions C-2 (Scheme 3-2) and C-3 (Scheme 3-3). From our structural studies, a radical addition mechanism through a semiquinone is proposed (Scheme 3-3), consistent with the modification at C-3 observed. Structural studies are performed under pH 5.5, which is well below the  $pK_a$  for a cysteine thiol, favoring the presence of a sulfur substituent at C-3 (33). Furthermore, a covalent modification at C-2 with juglone is also possible through a radical addition mechanism (Scheme 3-2). A previous study has shown that a radical addition mechanism is more favorable with increasing pH (33). It is possible that under our biochemical assay conditions (pH 7.8), a covalent modification is achieved through a radical addition mechanism at C-2 while a Michael additional mechanism at C-3 is used under conditions for crystallography (pH 5.5).

Further investigation of the importance of individual cysteine residues for inactivation by juglone showed that C353A mutation PRORP1 increased the



value of  $k_{\text{inact}}$  at least 3-fold compared to wild type. Removal of the thiol group results in enhancement of the rate of time-dependent inhibition, which means that juglone modification of C353 is not the site that leads to inhibition of PRORP1. Furthermore, an increase in the value of  $k_{\text{inact}}$  suggests that the removal of a thiol at C353 may affect modification at other sites that are important for time-dependent inhibition. Juglone also modified PRORP1 at C222 located on the PPR domain, which is involved in RNA binding. A double mutation of C222A and C353A resulted in less than 2-fold change in  $k_{\text{inact}}$  between C353A and C222A/C353A. Thus, removal of the thiol group at C222 does not have a significant effect on the time-dependent inhibition (Figure 3-5C), but instead affects the non-covalent binding sites for juglone since there was no inhibition without pre-incubation at the concentrations tested.

C373 is important for the second step in PRORP1 inhibition (Scheme 3-1). A C353A/C373A PRORP1 double mutant decreased  $k_{\text{inact}}$  7-fold compared to C353A PRORP1 suggesting that modification of C373 leads to PRORP1 inactivation (Figure 3-5C). C373 is located in the metallonuclease domain and modification of this site by juglone could affect the positions of active site residues that coordinate catalytic metal ions. Furthermore, C373 is located in a region with secondary structure and modification of this site could destabilize the protein and/or affect substrate binding. These proposals could be further tested by analysis of a C373A single mutant. C373 is located on the back side of the metallonuclease domain containing aspartic acid residues that coordinate active

site metal ions in PRORP1. Modification of C373 by juglone may also affect the binding of metal ions for PRORP1 activity.

## **CONCLUSIONS AND FUTURE DIRECTIONS**

We have demonstrated the use of an FP assay in a high throughput screen that identified compounds that inhibit plant PRORP1 and human MRPP1/2/3 activity. Gambogic acid and juglone are potent inhibitors against PRORP1 that target different steps in RNase P-catalyzed pre-tRNA cleavage. We have shown that gambogic acid is an uncompetitive inhibitor of PRORP1 and recognizes both pre-tRNA and PRORP1. The structure of gambogic acid resembles nucleotide bases and therefore could bind to the PPR domain of PRORP1. Given that gambogic acid has many cellular targets, it would not be a viable inhibitor to study RNA processing *in vivo*. However, gambogic acid can be used to stabilize a PRORP1-pre-tRNA complex for structural studies since it decreases the value of  $K_{M,app}$ . There is currently no detailed structural information of PRORP1 in complex with pre-tRNA.

Our work is the first crystal structure of protein that is covalently modified by juglone. Biochemical studies of three cysteine residues that are modified by juglone suggest that C373 is important for the time-dependent inhibition of PRORP1 by juglone. Furthermore, C222 may affect non-covalent binding sites for juglone. Modification at C353 was present in all crystallization conditions suggesting that it may be more susceptible to modification although it does not lead to inhibition. Our work demonstrates the use of an inhibitor to identify

regions of PRORP1 that are more susceptible to modification and may important for PRORP1 activity. In the future, juglone can be used as a tool to further probe the important structural features of PRORP1 and all other cysteine containing proteins. Our work with juglone identified surface cysteine residues that readily react with juglone in addition to the sites that are important for PRORP1 inhibition. Future work with juglone can provide the details on the effects of juglone on PRORP1 structure and activity. Juglone may affect PRORP1 active site metal ion binding since C373 is located in the metallonuclease domain. Juglone can also serve as a lead compound to be further elaborated to gain selectivity for human MRPP1/2/3 studies *in vivo*.

Further analyses of gambogic acid and juglone will be done to understand their modes of inhibition for PRORP1 and MRPP1/2/3. The mode of inhibition for juglone will be determined in future work by investigating the effects of varying substrate concentrations on PRORP1 activity. Gambogic acid is an uncompetitive inhibitor and could potentially stabilize the enzyme-substrate complex. Future work can be done to obtain a structure of PRORP1 in complex with pre-tRNA and gambogic acid, which will further our understanding of substrate recognition by PRORP1. These inhibitors have the potential to be developed into tools to investigate the tRNA processing pathways in mitochondria *in vitro* and *in vivo*.

## METHODS

### Materials

Buffer components were all purchased through Sigma unless specified. Baker's yeast tRNA<sup>mix</sup> was purchased from Roche. Gambogic acid was purchased from EMD Millipore and juglone (5-hydroxy-1,4-naphthoquinone) was purchased from Sigma at the highest purity. Recombinant His<sub>6</sub>-T7 RNA polymerase was expressed in *E. coli* and purified as previously described (34). Guanosine 5'-monothiophosphate (GMPS) was synthesized from 2',3'-isopropylidene guanosine and thiophosphoryl chloride as previously described (35).

### Protein preparation

Recombinant *A. thaliana* PRORP1 with the deletion of the first 76 residues on the N terminus was used in this study. Wild type and mutant PRORP1 were purified from *E. coli* as previously described (10). The protein component of RNase P from *B. subtilis* was purified from *E. coli* as previously described (36). MRPP 1, 2, and 3 were purified using immobilized nickel metal ion affinity columns as previously described with the following change (6): we used a truncation of MRPP3 lacking the first 45 residues ( $\Delta$ 45MRPP3). The N-terminal His<sub>6</sub>-tag was removed during the purification.

To prepare a plasmid for the co-expression of MRPP1 and MRPP2, DNA with an N-terminal truncation of the MRPP1 gene (*TRMT10C*) corresponding to

residues 40-403 ( $\Delta$ 39MRPP1) with an N-terminal His<sub>6</sub>-tag followed by a TEV protease site and the full-length MRPP2 gene (*SDR5C1*) were cloned into a pCDFDuet-1 (Novagen) co-expression vector (pHisTEVMP1+MP2) (for full details see (37)). Rosetta (DE3) or Rosetta2 (DE3) *E. coli* cells were transformed with the pHisTevMP1+MP2 plasmid and grown to an OD<sub>600</sub> of 0.6-0.8 in terrific broth or auto-induction media (Novagen) containing 50 mg/L streptomycin and 34 mg/L chloramphenicol at 37 °C. Expression was induced by addition of 0.2-0.5 mM isopropyl  $\beta$ -D-1-thiogalactopyranoside (IPTG) and cells were grown at 18 °C for 16 h after induction. Cells were harvested and lysed using a microfluidizer in buffer A (20 mM Tris-HCl pH 7.5 or 50 mM 3-(*N*-morpholino) propanesulfonic acid (MOPS) pH 7.5, 1 mM Tris(2-carboxyethyl)phosphine (TCEP, pH 7.5), 10% glycerol, 1 M NaCl, 15 mM imidazole) and one tablet of Complete EDTA free protease inhibitor cocktail (Roche). Cell lysate was pelleted for 60 min at 30,600  $\times$  g at 4 °C. The soluble fraction was added to a 5 mL Ni-Sepharose fast-flow resin (GE Healthcare Life Sciences) pre-equilibrated with buffer A at room temperature. The column was washed with buffer A containing 150 mM NaCl and bound proteins were eluted by an imidazole gradient (50 mM to 500 mM). Fractions containing His<sub>6</sub>-MRPP1/2 were pooled and dialyzed overnight at 4 °C against buffer A containing 150 mM NaCl and His<sub>6</sub>-tagged TEV protease. The sample was applied to a second Ni-Sepharose fast-flow resin pre-equilibrated with buffer A containing 150 mM NaCl. The flow-through fractions containing MRPP1/2 were pooled and dialyzed overnight into dialysis buffer (50 mM MOPS pH 7.5, 300 mM NaCl, and 1 mM TCEP), and then concentrated using a

centrifugal filter with a 10K MWCO (Amicon). The sample was loaded onto a Sephacryl-200 gel-filtration column (GE Healthcare) that was pre-equilibrated with the dialysis buffer. Protein was eluted at 1 mL/min and the  $A_{280}$  value was monitored. Peak fractions were analyzed by SDS-PAGE and coomassie blue stain. Fractions containing MRPP1/2 were pooled, flash frozen, and stored at -80 °C.

### **Pre-tRNA preparation**

Pre-tRNA was transcribed from a PCR product containing a T7 promoter region and pre-tRNA<sup>Asp</sup> with a 5-nucleotide leader and a discriminator base at the 3' end (pre-tRNA). The PCR product was made using a plasmid encoding *B. subtilis* pre-tRNA<sup>Asp</sup> with a 5-nucleotide leader and GCCA trailer as the template. *In vitro* transcription was done using 3 µg of PCR product as the template in the presence of 4 mM adenosine triphosphate (ATP), 4 mM cytidine triphosphate (CTP), 4 mM uridine triphosphate, 5 mM GMPS, 0.8 mM guanosine triphosphate (GTP), 25 mM MgCl<sub>2</sub>, 1 mM spermidine, 5 mM dithiothreitol (DTT), and 50 mM Tris-HCl, pH 8.0. The transcription reaction was incubated with 5-(iodoacetamido)fluorescein (5-IAF) to fluorescently label the 5' end (38). Unlabeled pre-tRNA was prepared using *in vitro* transcription as described above without the addition of GMPS, and increasing the concentration of GTP from 0.8 nM to 4 mM. Substrates were purified on 12% urea-polyacrylamide gels, crush-soaked to elute, then washed, and concentrated. The concentration of pre-tRNA substrates was calculated by absorbance using an extinction coefficient of

685,000 M<sup>-1</sup>cm<sup>-1</sup> at 260 nm. Labeling efficiency was assessed by fluorescein absorbance at 492 nm using an extinction coefficient of 78,000 M<sup>-1</sup>cm<sup>-1</sup>.

### **Fluorescence polarization (FP) assay**

The activity of *A. thaliana* PRORP1 catalyzed pre-tRNA cleavage was measured using an FP assay. Activity was measured by monitoring the fluorescence anisotropy (FA) signal ( $\lambda_{\text{ex}} = 485$  nm and  $\lambda_{\text{em}} = 535$  nm) over time at 25 °C in buffer conditions optimized for a high-throughput format, 30 mM MOPS pH 7.8, 5 mM MgCl<sub>2</sub>, 100 mM NaCl, 1 mM TCEP, 500 nM (12 µg/mL) yeast tRNA, 5 mM spermidine, 6.65 µg/mL BSA, and 0.01% NP-40. Yeast tRNA<sup>mix</sup> (Roche) was added to the reaction buffer to reduce the number of compound hits that inhibit PRORP1 activity by targeting tRNA. Prior to each experiment, pre-tRNA was unfolded for 3 min at 95 °C and refolded in the reaction buffer at room temperature (25 °C) for 30 min. Reactions were performed in black, 96-well plates (Corning Incorporation, #3686) using a TECAN plate-reader (Infinite F500, G-factor = 1.05) at 25 °C. Reactions were initiated with the addition of substrate to enzyme. Experiments were done in the presence of excess substrate ([E] = 0.3-5 nM, [FI-pre-tRNA] = 40 nM, [pre-tRNA] = 120-4000 nM). The concentration of labeled substrate (FI-pre-tRNA) was held constant in all reactions.

## FP data analysis

To correct for small fluctuations in the FA reading that are inherent in the instrument, a correction factor (CF) was calculated using a negative control well without the addition of enzyme.

$$CF = \frac{r_s}{r_{s,0}} \quad \text{Equation 3-1}$$

$$r = \frac{r_{raw}}{CF} \quad \text{Equation 3-2}$$

$$[P] = \frac{(r-r_0)}{\Delta r[S]} \quad \text{Equation 3-3}$$

[P] = concentration of product

[S] = concentration of substrate

r = corrected FA value in millianisotropy (mA)

r<sub>0</sub> = corrected FA at initial time

r<sub>s</sub> = FA reading of substrate only control

r<sub>s,0</sub> = FA reading of substrate only at initial time

r<sub>raw</sub> = raw FA reading

Δr = total change in FA

## High-throughput screening

To identify potent inhibitors of PRORP1, we screened a small molecule library of compounds from microsources and pharmacologically active compounds (Prestwick, LOPAC, MS2400, BioFocus NCC, ~6,000 compounds) provided by the Center for Chemical Genomics (CCG) at the University of Michigan. In this primary screen, the FA assay was performed using 12.5 μM compound, 1% DMSO, 0.3 nM PRORP1, 800 nM pre-tRNA containing 40 nM FI-



pre-tRNA, at 22°C in 30 mM MOPS pH 7.8, 5 mM MgCl<sub>2</sub>, 100 mM NaCl, 1 mM TCEP, 500 nM (12 µg/mL) yeast tRNA<sup>mix</sup>, 5 mM spermidine, 6.65 µg/mL BSA, and 0.01% NP-40. Enzyme is incubated with 25 µM compound or 1.25% DMSO in 384-well plates (Perkin Elmer Proxiplate 384F Plus #6008269) for 30 min before the addition of equal volumes of substrate to initiate the reaction. The reaction was quenched with 80 mM CaCl<sub>2</sub> after 1 h. The FA value was read on a PHERAstar plate reader. The Z' factor for each plate was calculated using Equation 3-4.

$$Z' = 1 - \frac{(3\sigma_{c+} + 3\sigma_{c-})}{|\mu_{c+} - \mu_{c-}|} \quad \text{Equation 3-4}$$

$\mu_{c+}$  = mean FA value of the positive control

$\mu_{c-}$  = mean FA value of the negative control

$\sigma_{c+}$  = standard deviation of the positive control

$\sigma_{c-}$  = standard deviation of the negative control

### **Gel-based activity assay**

To validate inhibitors identified from the high throughput FP assay, we used an orthogonal gel-based assay to measure RNase P activity. This assay detects the presence of substrate and product by the fluorescence signal from fluorescein-labeled pre-tRNA run on a 20% PAGE gel containing 8 M urea. Compounds that resulted in no observed RNase P activity in the presence of 12.5 µM compound after 1h were then used in a dose response assay. The dose response was measured using the FP assay as described above with varying concentrations of compound.

### Dose-response and determination of mode of inhibition

Compounds were incubated with PRORP1 at twice the reaction concentration for 30 minutes prior to the addition of equal volumes of substrate to initiate the reaction. Experiments were done under multiple turnover conditions (same buffer conditions as the FP assay), and the results were converted to activity (%) using DMSO as a 100% activity control and CaCl<sub>2</sub> or no enzyme as 0% activity controls. PRORP1 activity was determined as a function of inhibitor concentration, and Equation 3-5 was fit to the data to determine the IC<sub>50</sub> value, where n is the Hill coefficient.

$$Activity (\%) = \frac{100}{1 + \left(\frac{[I]}{IC_{50}}\right)^n} \quad \text{Equation 3-5}$$

Equations 3-6, 3-7, and 3-8 were used to obtain a global fit for the analysis of gambogic acid and calculate the value of K<sub>I</sub>.

$$\frac{v_0}{[E]} = \frac{k_{cat,app}[S]}{K_{M,app} + [S]} \quad \text{Equation 3-6}$$

$$k_{cat,app} = \frac{k_{cat}}{1 + \left(\frac{[I]}{K_I}\right)^n} \quad \text{Equation 3-7}$$

$$K_{M,app} = \frac{K_M}{1 + \left(\frac{[I]}{K_I}\right)^n} \quad \text{Equation 3-8}$$

For the analysis of juglone, PRORP1 activity was measured with varying pre-incubation time and juglone concentration. PRORP1 was prepared with a total volume of 35 μL at a concentration of 0.3 nM. Varying concentrations of

juglone (0-8  $\mu\text{M}$ ) were pre-incubated with PRORP1 from 2 min to 2 h. The concentration of DMSO in each reaction was held constant at 1%. Reactions were initiated by addition of 5  $\mu\text{L}$  of substrate for a final working concentration of 250 nM pre-tRNA, 0.3 nM PRORP1 and 0-8  $\mu\text{M}$  juglone in a total volume of 40  $\mu\text{L}$ . The initial velocity of each reaction was converted to activity (%) and plotted against pre-incubation time. The data was fit to a single exponential decay equation (Equation 3-9) to determine  $k_{obs}$  as a function of juglone concentration (represented by [I]). The inhibition constant ( $K_I$ ) of PRORP1 by juglone was determined by measuring the  $IC_{50}$  of juglone with a 2 min pre-incubation (12  $\mu\text{M}$ ). This value was then used with Equation 3-10 to determine the rate constant for isomerization or other conformational change step in enzyme inhibition ( $k_{inact}$ ). Equation 3-10 describes the observed rate constant assuming a 2-step inactivation mechanism (Scheme 3-1).

$$Activity (\%) = Ae^{-k_{obs}t} \quad \text{Equation 3-9}$$

$$k_{obs} = \frac{k_{inact}[I]}{K_I + [I]} \quad \text{Equation 3-10}$$

### Human mitochondrial RNase P (MRPP1/2/3) activity assay

The inhibition of human MRPP1/2/3 by gambogic acid and juglone was evaluated via dose-response using a quenched assay. Human MRPP1/2/3 activity was measured as a function of gambogic acid and juglone concentration using 50 nM MRPP3, 500 nM MRPP1/2, 500 nM pre-tRNA containing 40 nM FI-pre-tRNA in 50 mM MOPS (pH 7.8), 4.5 mM  $\text{MgCl}_2$ , 100 mM NaCl, and 1 mM TCEP (pH 7.5). Proteins were mixed together on ice and incubated at room

temperature for 5 min before addition to pre-folded substrate at 37 °C to initiate the reaction. Substrate was folded as described in the FA assay with PRORP1. Reaction time points were taken and quenched with equal volumes of an EDTA-dye quench solution containing 100 mM EDTA, 0.05% xylene cyanol dye, 0.05% bromophenol blue dye, and 8 M urea. Samples were separated by 20% Urea PAGE (Ultra Pure SequaGel), fluorescence signal was quantified using ImageJ, and the data was analyzed using Prism.

### ***B. subtilis* RNase P activity**

The inhibition of *B. subtilis* RNase P activity by gambogic acid and juglone was measured using a previously developed FP assay in real-time (23). The FA value from the FP assay was read for reactions under MTO conditions using 20 nM RNase P and 500 nM FI-pre-tRNA<sup>Asp</sup> in 50 mM Tris (pH 7.2), 5 mM MgCl<sub>2</sub>, 100 mM KCl, 500 nM (12 µg/mL) yeast tRNA<sup>mix</sup>, 20 mM dithiothreitol (DTT), 10 mM spermidine, and 0.01% NP-40 at 37 °C.

### **Crystallization, Data processing and Refinement**

Δ76-PRORP1 was expressed and purified for crystallization as described above. Crystals were grown in 0.1 M sodium citrate pH 5.5 and 18 % (wt/vol) PEG 3350 at 4 °C by sitting drop method with a 2:1 ratio of protein and reservoir solution (10). Δ76-PRORP1 crystals were soaked in reservoir solution containing a saturating amount of juglone (>10 µM) and incubated for 45 min, 3h, and overnight in the presence or absence of 50 mM MnCl<sub>2</sub> before harvesting.

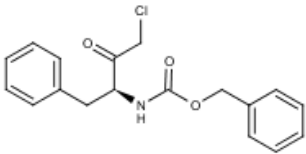
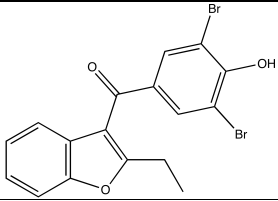
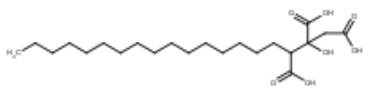
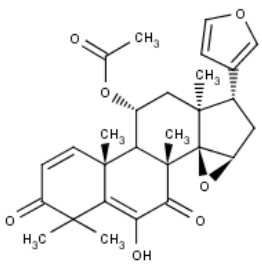
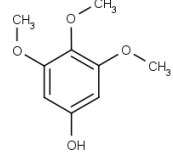
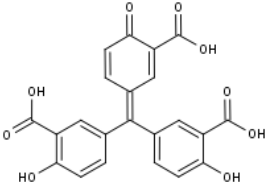
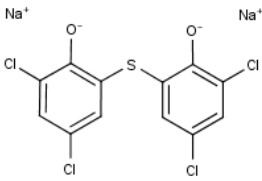
Harvested crystals were cryoprotected by soaking in 14% PEG 3,350, 0.08 M sodium citrate tribasic (pH 5.5), 0.015M SrCl<sub>2</sub> or CaCl<sub>2</sub>, 20% (v/v) glycerol and 10 μM juglone for a few minutes prior to flash cooling in liquid N<sub>2</sub>.

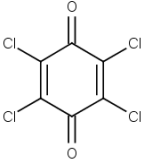
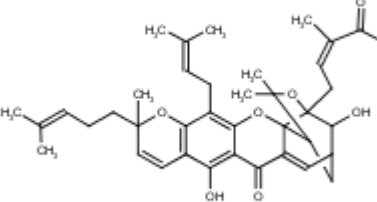
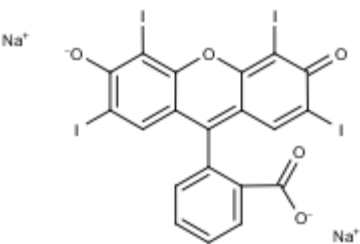
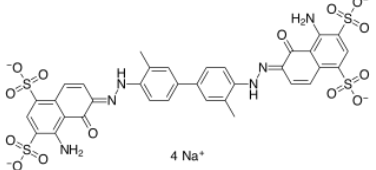
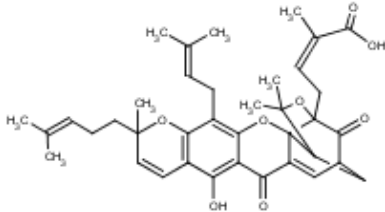
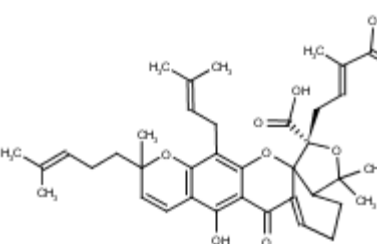
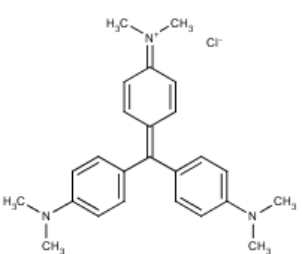
Diffraction data was collected on beamline GM/CA-CAT 23 ID-D and 23 ID-B with Mar 300 CCD and DECTRIS EIGER X 16M detectors respectively at Advanced Photon Source, Argonne National Laboratory (Argonne, IL). The data was processed with XDS and subsequently Phaser MR was used to solve the crystal structures by molecular replacement in the CCP4 software package [28-30]. Energy-minimized coordinates for juglone-cysteine conjugates were obtained by ProDrg webserver (39). Refmac5 in the CCP4i suite was subsequently employed for restrained refinement model building and modification with Coot (40,41). Crystallographic information and refinement statistics are provided in Appendix A, Table A-2. The geometric quality of the model and its agreement with the structure factors were assessed with MolProbity (42). Figures showing crystal structures were generated with PyMOL (43)

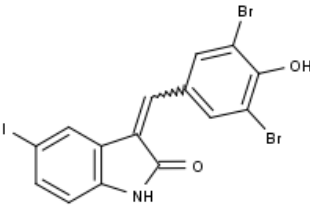
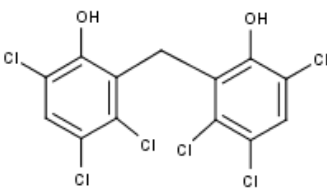
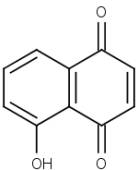
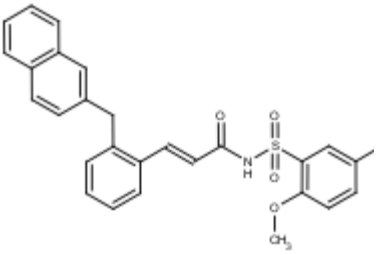
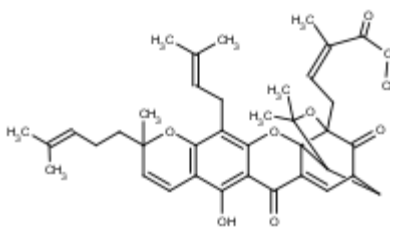
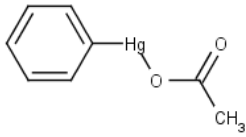
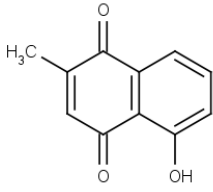
## APPENDIX A

**Table A-1 Compounds identified from a high throughput screen with more than 40% PRORP1 inhibition.**

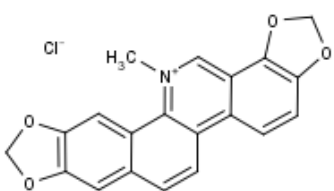
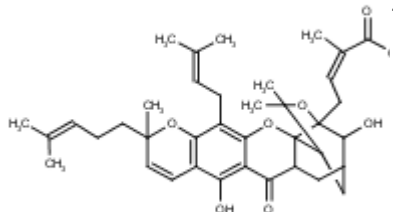
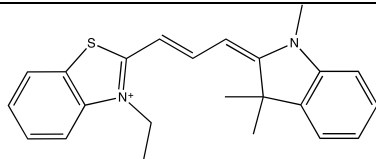
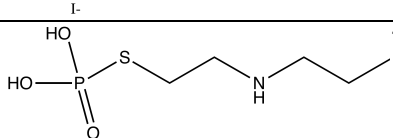
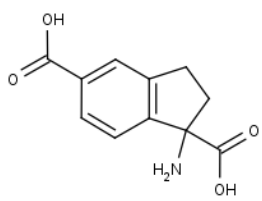
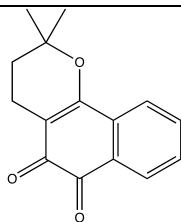
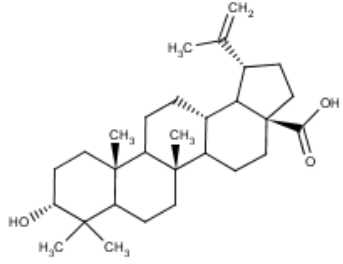
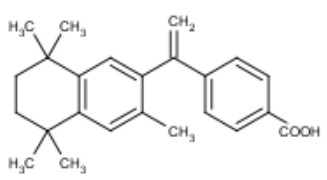
Compounds 1-23 inhibit PRORP1 activity completely at 12.5  $\mu\text{M}$  using a gel-based assay. Percent inhibition is calculated using the reported FA value in comparison to the negative and positive controls from the high throughput screen.

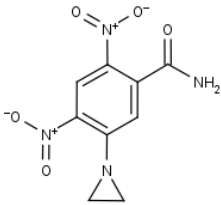
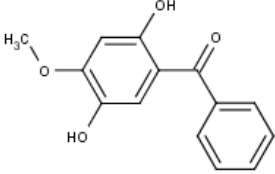
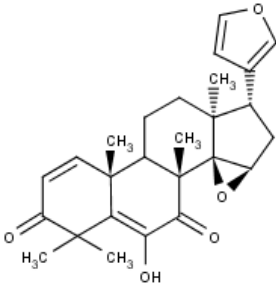
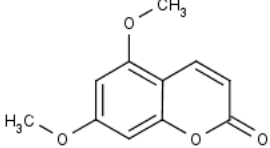
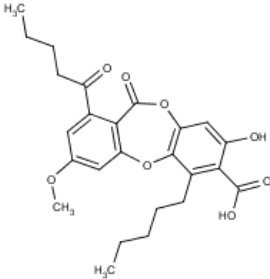
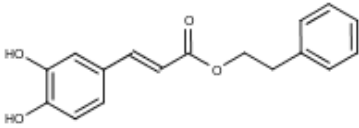
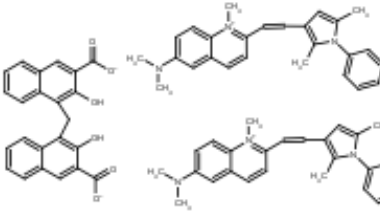
	Compound name	Structure	Pubmed SID	Percent inhibition	$IC_{50}$ ( $\mu\text{M}$ )
1	1-benzyloxycarbonyl aminophenethyl chloromethyl ketone		124637043	98.2	2.4
2	3-[3,5-dibromo-4-hydroxybenzoyl]-2-ethylbenzofuran (Benzbromarone)		124635053	44.8	>6
3	Agaric acid		175611523	93.7	>6
4	Anthothecol		124637615	70.2	~1.7
5	Antiarol		175611538	91.7	>6
6	Aurintricarboxylic acid		124749408	83.7	~6
7	Bithionol		124637544	95.1	>6

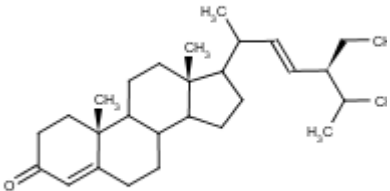
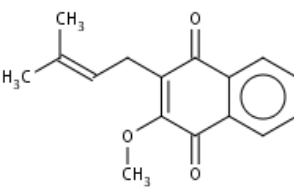
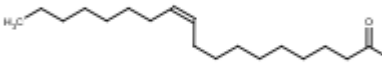
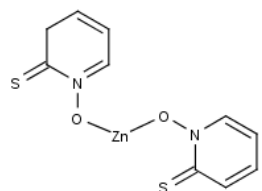
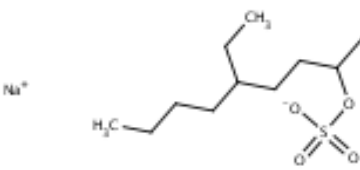
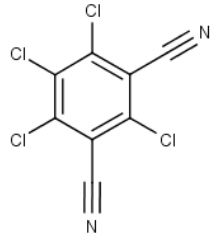
8	Chloranil		124637809	99.1	~5
9	Dihydrogamboic acid		124636393	74.4	>6
10	Erythrosine sodium		175611204	99.4	N/A
11	Evans blue		175611301	98.6	~2
12	Gamboic acid		124636510	110	1
13	Garcinolic acid		124636377	60.3	>6
14	Gentian violet		124637593	63.8	~2

15	GW5074		175612424	65	>6
16	Hexachlorophene		124637598	59.6	>6
17	Juglone		124638073	89.6	<1
18	L-798106		175612334	58.4	>6
19	Methyl gambogate		175611584	97	>2
20	Phenylmercuric acetate		124637581	45.6	3
21	Plumbagin		175607631	46.6	2.5



22	Sanguinarium chloride		175610852	51.7	>6
23	Tetrahydrogambogic acid		124636304	41.6	ND
24	AC-93253 iodide		175612410	174.7	ND
25	Amifostine		124633589	195.3	ND
26	1-Aminoindan-1,5-dicarboxylic acid (AIDA)		124749464	403.9	ND
27	Beta-laphachone (NSC 26326)		124634217	43.2	ND
28	Betulinic acid		124637912	65.2	ND
29	Bexarotene		175612428	66.3	ND

30	CB 1954		124749537	416.3	ND
31	Cearoin		124637309	47.3	ND
32	Cedrelone		124637618	54.2	ND
33	Citropten		124638093	103.2	ND
34	Lobaric acid		124636438	45.2	ND
35	Phenethyl caffeate (CAPE)		124637378	108	ND
36	Pyrvinium pamoate		175612120	41.1	ND

37	Stigmasta-4,22-dien-3-one		124637831	82.5	ND
38	Lapachol methyl ether			43.1	ND
39	Oleic Acid		124750080	51.6	ND
40	Pyrithione Zinc		124636396	94.2	ND
41	Sodium tetradecyl sulfate			79.5	ND
42	Tetrachloroisophthalonitrile		124636919		ND

ND: Not determined

**Table A-2 X-Ray Crystallography Data Collection and Refinement Statistics**

	PRORP1 + Juglone (45 min soaks)	PRORP1 + Juglone (3 hour soaks)	PRORP1 + Juglone (overnight soak)
<b>Data collection</b>			
Beamline	APS, GMCA 23-IDD	APS, GMCA 23-IDD	APS, GMCA 23-IDB
Wavelength (Å)		1.0332	1.0332
Resolution (Å)	50.0-1.79 (1.83-1.79)	50.0-2.20 (2.26-2.20)	50.0-2.10 (2.16-2.10)
Space group	P2 <sub>1</sub> 2 <sub>1</sub> 2 <sub>1</sub>	P2 <sub>1</sub> 2 <sub>1</sub> 2 <sub>1</sub>	P2 <sub>1</sub> 2 <sub>1</sub> 2 <sub>1</sub>
Cell dimensions (Å)	a = 41.6, b = 110.8, c = 140.7	a = 41.7, b = 112.2, c = 139.2	a = 41.8, b = 111.8, c = 139.3
Cell dimensions (°)	$\alpha = \beta = \gamma = 90$	$\alpha = \beta = \gamma = 90$	$\alpha = \beta = \gamma = 90$
R <sub>sym</sub> (%)	3.8 (48.2)	4.0 (69.2)	5.5 (71.7)
<I/σ>	15.5 (2.1)	11.2 (2.1)	17.5 (2.2)
CC(1/2)	1.0 (0.78)	1.0 (0.74)	1.0 (0.75)
Multiplicity	3.7 (3.9)	3.4 (3.3)	6.7 (6.5)
Completeness (%)	99.3 (100)	98.1 (95.8)	100 (99.7)
<b>Refinement</b>			
Resolution range	87.1-1.79	87.3-2.20	87.2-2.10
Number of reflections (work/test set)	57980/3033	31891/1637	37078/1982
R <sub>work</sub> /R <sub>free</sub> (%)	19.1/21.9	20.6/24.3	19.7/24.5
No. of atoms			
Protein	3804	3814	3783
Water	239	105	172
Juglone	13	39	39
Zn/Mn	1/1	1/0	1/0
B-factors (Å <sup>2</sup> )			
Protein	49.3	62.8	63.0
Water	42.2	46.6	50.1
Juglone	65.4	103.5	87.2
Zn/Mn	39.9/32.4	57.0/na	52.0/na
Rmsd deviations			
Bond lengths (Å)	0.014	0.013	0.013
Bond angles (°)	1.52	1.54	1.53
Ramachandran plot			
Favored/allowed/outliers	99.0/1.0/0.0	97.5/1.9.0/0.6	97.7/2.3/0.0
MolProbity Score	0.86 (100 <sup>th</sup> percentile)	1.84 (92 <sup>d</sup> percentile)	1.17 (100 <sup>th</sup> percentile)
PDB			

## REFERENCES

1. Perreault, J. P., and Altman, S. (1993) Pathway of activation by magnesium ions of substrates for the catalytic subunit of RNase P from *Escherichia coli*. *J Mol Biol* **230**, 750-756
2. Beebe, J. A., Kurz, J. C., and Fierke, C. A. (1996) Magnesium ions are required by *Bacillus subtilis* ribonuclease P RNA for both binding and cleaving precursor tRNA<sup>Asp</sup>. *Biochemistry* **35**, 10493-10505
3. Guerrier-Takada, C., Gardiner, K., Marsh, T., Pace, N., and Altman, S. (1983) The RNA moiety of ribonuclease P is the catalytic subunit of the enzyme. *Cell* **35**, 849-857
4. Kikovska, E., Svard, S. G., and Kirsebom, L. A. (2007) Eukaryotic RNase P RNA mediates cleavage in the absence of protein. *Proc Natl Acad Sci U S A* **104**, 2062-2067
5. Walker, S. C., and Engelke, D. R. (2006) Ribonuclease P: the evolution of an ancient RNA enzyme. *Crit Rev Biochem Mol Biol* **41**, 77-102
6. Holzmann, J., Frank, P., Löffler, E., Bennett, K. L., Gerner, C., and Rossmann, W. (2008) RNase P without RNA: Identification and Functional Reconstitution of the Human Mitochondrial tRNA Processing Enzyme. *Cell* **135**, 462-474
7. Cassano, A. G., Anderson, V. E., and Harris, M. E. (2004) Analysis of solvent nucleophile isotope effects: evidence for concerted mechanisms and nucleophilic activation by metal coordination in nonenzymatic and ribozyme-catalyzed phosphodiester hydrolysis. *Biochemistry* **43**, 10547-10559
8. Howard, M. H., Klemm, B. P., and Fierke, C. A. (2015) Mechanistic Studies Reveal Similar Catalytic Strategies for Phosphodiester Bond Hydrolysis by Protein-only and RNA-dependent Ribonuclease P. *Journal of Biological Chemistry* **290**, 13454-13464
9. Gobert, A., Butmann, B., Taschner, A., Gößringer, M., Holzmann, J., Hartmann, R. K., Rossmann, W., and Giegé, P. (2010) A single Arabidopsis organellar protein has RNase P activity. *Nature Structural and Molecular Biology* **17**, 740-744
10. Howard, M. J., Lim, W. H., Fierke, C. A., and Koutmos, M. (2012) Mitochondrial ribonuclease P structure provides insight into the evolution of catalytic strategies for precursor-tRNA 5' processing. *PNAS* **109**, 16149-16154
11. Li, F., Liu, X., Zhou, W., Yang, X., and Shen, Y. (2015) Auto-inhibitory Mechanism of the Human Mitochondrial RNase P Protein Complex. *Scientific reports* **5**, 9878
12. Reinhard, L., Sridhara, S., and Hallberg, B. M. (2015) Structure of the nuclease subunit of human mitochondrial RNase P. *Nucleic acids research*
13. Vilardo, E., Nachbagauer, C., Buzet, A., Taschner, A., Holzmann, J., and Rossmann, W. (2012) A subcomplex of human mitochondrial RNase P is

- a bifunctional methyltransferase-extensive moonlighting in mitochondrial tRNA biogenesis. *Nucleic acids research* **40**, 11583-11593
14. Sen, A., Karasik, A., Shanmuganathan, A., Mirkovic, E., Koutmos, M., and Cox, R. T. (2016) Loss of the mitochondrial protein-only ribonuclease P complex causes aberrant tRNA processing and lethality in *Drosophila*. *Nucleic acids research* **44**, 6409-6422
  15. Lopez Sanchez, M. I. G., Mercer, T. R., Davies, S. M. K., Shearwood, A.-M. J., Nygård, K. K. A., Richman, T. R., Mattick, J. S., Rackham, O., and Filipovska, A. (2011) RNA processing in human mitochondria. *Cell Cycle* **10**, 2904-2916
  16. Deutschmann, A. J., Amberger, A., Zavadil, C., Steinbeisser, H., Mayr, J. A., Feichtinger, R. G., Oerum, S., Yue, W. W., and Zschocke, J. (2014) Mutation or knock-down of 17beta-hydroxysteroid dehydrogenase type 10 cause loss of MRPP1 and impaired processing of mitochondrial heavy strand transcripts. *Human molecular genetics* **23**, 3618-3628
  17. Metodiev, M. D., Thompson, K., Alston, Charlotte L., Morris, Andrew A. M., He, L., Assouline, Z., Rio, M., Bahi-Buisson, N., Pyle, A., Griffin, H., Siira, S., Filipovska, A., Munnich, A., Chinnery, Patrick F., McFarland, R., Rötig, A., and Taylor, Robert W. (2016) Recessive Mutations in TRMT10C Cause Defects in Mitochondrial RNA Processing and Multiple Respiratory Chain Deficiencies. *The American Journal of Human Genetics* **98**, 993-1000
  18. Florentz, C., Sohm, B., Tryoen-Toth, P., Putz, J., and Sissler, M. (2003) Human mitochondrial tRNAs in health and disease. *Cellular and molecular life sciences : CMLS* **60**, 1356-1375
  19. Suzuki, T., Nagao, A., and Suzuki, T. (2011) Human mitochondrial tRNAs: biogenesis, function, structural aspects, and diseases. *Annual review of genetics* **45**, 299-329
  20. Enriquez, J. A., Chomyn, A., and Attardi, G. (1995) MtDNA mutation in MERRF syndrome causes defective aminoacylation of tRNA<sup>Lys</sup> and premature translation termination. *Nat Genet* **10**, 47-55
  21. Yarham, J. W., Elson, J. L., Blakely, E. L., McFarland, R., and Taylor, R. W. (2010) Mitochondrial tRNA mutations and disease. *Wiley Interdisciplinary Reviews - RNA* **1**, 304-324
  22. Helm, M. (2006) Post-transcriptional nucleotide modification and alternative folding of RNA. *Nucleic acids research* **34**, 721-733
  23. Liu, X., Chen, Y., and Fierke, C. A. (2014) A real-time fluorescence polarization activity assay to screen for inhibitors of bacterial ribonuclease P. *Nucleic acids research* **42**, e159
  24. Pandey, M. K., Karelia, D., and Amin, S. G. (2016) Gambogic Acid and Its Role in Chronic Diseases. in *Anti-inflammatory Nutraceuticals and Chronic Diseases* (Gupta, S. C., Prasad, S., and Aggarwal, B. B. eds.), Springer International Publishing, Cham. pp 375-395
  25. Li, X., Liu, S., Huang, H., Liu, N., Zhao, C., Liao, S., Yang, C., Liu, Y., Zhao, C., Li, S., Lu, X., Liu, C., Guan, L., Zhao, K., Shi, X., Song, W., Zhou, P., Dong, X., Guo, H., Wen, G., Zhang, C., Jiang, L., Ma, N., Li, B.,

- Wang, S., Tan, H., Wang, X., Dou, Q. P., and Liu, J. (2013) Gambogic Acid Is a Tissue-Specific Proteasome Inhibitor In Vitro and In Vivo. *Cell Reports* **3**, 211-222
26. Wang, Y., Xiang, W., Wang, M., Huang, T., Xiao, X., Wang, L., Tao, D., Dong, L., Zeng, F., and Jiang, G. (2014) Methyl jasmonate sensitizes human bladder cancer cells to gambogic acid-induced apoptosis through down-regulation of EZH2 expression by miR-101. *British Journal of Pharmacology* **171**, 618-635
  27. Pandey, M. K., Sung, B., Ahn, K. S., Kunnumakkara, A. B., Chaturvedi, M. M., and Aggarwal, B. B. (2007) Gambogic acid, a novel ligand for transferrin receptor, potentiates TNF-induced apoptosis through modulation of the nuclear factor- $\kappa$ B signaling pathway. *Blood* **110**, 3517
  28. Palempalli, Umamaheshwari D., Gandhi, U., Kalantari, P., Vunta, H., Arner, Ryan J., Narayan, V., Ravindran, A., and Prabhu, K. S. (2009) Gambogic acid covalently modifies I $\kappa$ B kinase- $\beta$  subunit to mediate suppression of lipopolysaccharide-induced activation of NF- $\kappa$ B in macrophages. *Biochemical Journal* **419**, 401
  29. Gu, H., Rao, S., Zhao, J., Wang, J., Mu, R., Rong, J., Tao, L., Qi, Q., You, Q., and Guo, Q. (2009) Gambogic acid reduced bcl-2 expression via p53 in human breast MCF-7 cancer cells. *Journal of Cancer Research and Clinical Oncology* **135**, 1777-1782
  30. Zhai, D., Jin, C., Shiau, C.-w., Kitada, S., Satterthwait, A. C., and Reed, J. C. (2008) Gambogic acid is an antagonist of antiapoptotic Bcl-2 family proteins. *Molecular Cancer Therapeutics* **7**, 1639
  31. Qi, Q., Lu, N., Li, C., Zhao, J., Liu, W., You, Q., and Guo, Q. (2015) Involvement of RECK in gambogic acid induced anti-invasive effect in A549 human lung carcinoma cells. *Molecular Carcinogenesis* **54**, E13-E25
  32. Hennig, L., Christner, C., Kipping, M., Schelbert, B., Rücknagel, K. P., Grabley, S., Küllertz, G., and Fischer, G. (1998) Selective Inactivation of Parvulin-Like Peptidyl-Prolyl cis/trans Isomerases by Juglone. *Biochemistry* **37**, 5953-5960
  33. Perlinger, J. A., Kalluri, V. M., Venkatapathy, R., and Angst, W. (2002) Addition of Hydrogen Sulfide to Juglone. *Environmental Science & Technology* **36**, 2663-2669
  34. He, B., Rong, M., Lyakhov, D., Gartenstein, H., Diaz, G., Castagna, R., McAllister, W. T., and Durbin, R. K. (1997) Rapid mutagenesis and purification of phage RNA polymerases. *Protein Expr Purif* **9**, 142-151
  35. Behrman, E. (2000) An improved synthesis of guanosine 5'-monothiophosphate. *J. Chem. Research (S)*, 446-447
  36. Niranjanakumari, S., Kurz, J. C., and Fierke, C. A. (1998) Expression, purification and characterization of the recombinant ribonuclease P protein component from *Bacillus subtilis*. *Nucleic acids research* **26**, 3090-3096
  37. Byrne, R. T., Konevega, A. L., Rodnina, M. V., and Antson, A. A. (2010) The crystal structure of unmodified tRNA Phe from *Escherichia coli*. *Nucleic acids research* **38**, 4154-4162

38. Rueda, D., Hsieh, J., Day-Storms, J. J., Fierke, C. A., and Walter, N. G. (2005) The 5' Leader of Precursor tRNA(Asp) Bound to the *Bacillus subtilis* RNase P Holoenzyme Has an Extended Conformation. *Biochemistry* **44**, 16130-16139
39. Schuttelkopf, A. W., and van Aalten, D. M. F. (2004) PRODRG: a tool for high-throughput crystallography of protein-ligand complexes. *Acta Crystallographica Section D* **60**, 1355-1363
40. Murshudov, G. N., Skubak, P., Lebedev, A. A., Pannu, N. S., Steiner, R. A., Nicholls, R. A., Winn, M. D., Long, F., and Vagin, A. A. (2011) REFMAC5 for the refinement of macromolecular crystal structures. *Acta Crystallographica Section D* **67**, 355-367
41. Emsley, P., Lohkamp, B., Scott, W. G., and Cowtan, K. (2010) Features and development of Coot. *Acta Crystallographica Section D* **66**, 486-501
42. Davis, I. W., Leaver-Fay, A., Chen, V. B., Block, J. N., Kapral, G. J., Wang, X., Murray, L. W., Arendall, I. I. I. W. B., Snoeyink, J., Richardson, J. S., and Richardson, D. C. (2007) MolProbity: all-atom contacts and structure validation for proteins and nucleic acids. *Nucleic acids research* **35**, W375-W383
43. Delano, W. L. (2002) The PyMOL Molecular Graphics System, Version 1.4 (Shrödinger, LLC, Portland, OR).



## CHAPTER 4

### Conclusions and Future Directions

#### OVERVIEW

This work describes the function and inhibition of a new class of endonucleases. We investigated the mechanism of pre-tRNA hydrolysis catalyzed by human mitochondrial RNase P (MRPP1/2/3) and present a kinetic model that highlights the importance of a methyltransferase/dehydrogenase complex (MRPP1/2) for catalysis. Our work also demonstrates that pre-tRNA stabilizes the human mitochondrial RNase P-substrate quaternary complex consisting of MRPP 1, 2, 3, and pre-tRNA. Additionally, I developed a fluorescence polarization (FP) assay and identified potent inhibitors of *A. thaliana* PRORP1 and human MRPP1/2/3 activity. I have characterized the mode of inhibition for these compounds and have identified both time-dependent and rapidly binding inhibitors of PRORP1 with implications for studying RNase P activity *in vivo*. This work has developed a framework for studying the molecular mechanism of human mitochondrial protein-only RNase P.

## CONCLUSIONS

### Kinetic model for RNase P catalysis

The previous model for human mtRNase P catalysis involved the initial formation of the MRPP1/2/3 tertiary complex followed by binding to and hydrolysis of pre-tRNA (1). However, the search for evidence of a MRPP1/2/3 ternary complex has not been fruitful. MRPP1/2 does not form a stable tertiary complex with MRPP3; instead the MRPP1/2/3-pre-tRNA quaternary complex is stabilized by the addition of pre-tRNA (Chapter 2). Three new mechanisms are possible: (i) MRPP3 recognizes the complex or the interface of MRPP1/2-pre-tRNA, (ii) the structure of pre-tRNA changes upon binding to MRPP1/2 to a conformer that binds to MRPP3 with higher affinity, and/or (iii) the structure of MRPP1/2 changes upon binding to pre-tRNA, which then binds MRPP3 with higher affinity.

We have developed a kinetic model to explain the mechanism of catalysis (Chapter 2). There are two likely paths for catalysis. Pre-tRNA binds to MRPP1/2 and then the complex binds to MRPP3 in a step-wise manner of pre-tRNA binds to MRPP3 followed by binding to MRPP1/2. The pathway may vary depending on the concentrations of MRPP1/2 and MRPP3. Considering that there are additional steps in the tRNA maturation pathway including specific base modifications, it is possible that methylation of pre-tRNA catalyzed by MRPP1/2 may occur before cleavage catalyzed by RNase P for some mt-tRNAs. Furthermore, the rate-limiting step in this pathway may not be the cleavage step

catalyzed by RNase P. In the model we propose, pre-tRNA undergoes an additional step, likely a conformational change, upon binding to MRPP1/2 to form an active MRPP1/2-S\* complex. This MRPP1/2-S\* complex is recognized by or binds with higher affinity to MRPP3.

### **The role of MRPP1/2 in human mitochondrial RNase P**

MRPP3 houses the active site for RNase P activity. However, MRPP3 is inactive without MRPP1/2. MRPP1/2 knockdowns via siRNA resulted in a 10-fold greater effect on the build-up of some tRNA precursor transcripts in HeLa cells compared to a similar level of MRPP3 knockdown, indicating that MRPP1/2 has a significant role in pre-tRNA maturation (2). We evaluated the effects of MRPP1/2 on kinetic parameters measured under MTO and STO conditions to elucidate the mechanism of MRPP1/2/3 catalysis (Chapter 2). MRPP1/2 enhances the catalytic efficiency of MRPP3 and increases the affinity of MRPP3 for pre-tRNA.

### **MRPP1/2/3-pre-tRNA complex**

One goal of this work was to understand the stoichiometry requirements for an active MRPP1/2/3-pre-tRNA complex. Prior research suggests a 1:4 or 2:4 MRPP1:2 ratio (1,3). A crystal structure of MRPP2, reveals a homotetramer structure (4). No crystal structure exists for MRPP1, however homologs of MRPP1 behave as dimers (5). A ratio of 2:4 MRPP1-MRPP2 was initially proposed from studies quantifying MRPP1 and MRPP2 complex from a

denaturing PAGE stained with coomassie blue (6). Previous studies using gel filtration resulted in a complex with a molecular weight of 170 kDa, consistent with a 1:4 MRPP1-MRPP2 ratio (159 kDa) (3). However the authors concluded a 2:4 ratio, which has a molecular weight of 202 kDa. In Chapter 2, we used analytical ultracentrifugation to demonstrate that a catalytically active MRPP1/2 complex has a molecular weight of 174 kDa, consistent with a 1:4 MRPP1-MRPP2 ratio (153 kDa).

### **Inhibition of plant PRORP1 and human MRPP1/2/3**

I adapted and optimized a fluorescence polarization (FP) assay that was previously used to identify inhibitors of bacterial RNP RNase P in high throughput (7) (Chapter 3). In this thesis, we identified potent inhibitors of plant PRORP1 and human MRPP1/2/3. Inhibitors of MRPP1/2/3 can be used to probe the *in vivo* function of MRPP1/2/3 in the mitochondria. We demonstrate that we have identified inhibitors that are specific against plant PRORP1 and human MRPP1/2/3 compared to bacterial RNP RNase P. This is important for the development of inhibitors to probe the *in vivo* function of human mitochondrial RNase P because the human nucleus contains an RNP RNase P.

### **Gambogic acid**

Two of the most potent inhibitors of PRORP1 from our high throughput screen, gambogic acid and juglone, were evaluated to determine their mode of inhibition. I demonstrated that gambogic acid is a rapidly binding inhibitor that

decreases both the value of  $k_{\text{cat}}$  and  $K_{\text{M}}$  with no effect on the value of  $k_{\text{cat}}/K_{\text{M}}$ , indicative of an uncompetitive inhibitor. Given that gambogic acid is an uncompetitive inhibitor, it likely recognizes an interface that includes both pre-tRNA and PRORP1. Furthermore, given that gambogic acid inhibits PRORP1 and MRPP3 with similar  $IC_{50}$  values, it may inhibit with similar modes of action.

Gambogic acid has previously been shown to inhibit multiple cellular targets including proteins involved in modulating the nuclear factor- $\kappa$ B signaling pathway and the transferrin receptor involved in triggering apoptosis (8,9). Gambogic acid has anti-inflammatory, anti-cancer, antibacterial, and antioxidant effects due to its ability to modulate many cell signaling pathway intermediates including epigenetic regulators, protein kinases, transcription factors, inflammatory biomarkers, and growth regulators (9-11). Given that gambogic acid has many cellular targets, it would currently not be viable for *in vivo* studies. However, gambogic acid can be useful in structural studies of pre-tRNA and PRORP1 since it decreases the value of  $K_{\text{M,app}}$ . There is currently no detailed structural information of PRORP1 in complex with pre-tRNA.

## **Juglone**

In this work, I demonstrated that juglone is a slow-binding inhibitor that covalently modifies PRORP1. Structural studies with juglone revealed modifications at multiple cysteine thiol groups. Site-directed mutagenesis to silence three individual cysteine residues revealed that C353 reacts with juglone readily yet has little effect on inhibition and that C373 is a time-dependent

inhibitor likely through a covalent modification. C373 is located in the metallonuclease domain and modification of this site by juglone may induce a structural change in PRORP1 or may disrupt metal ion or pre-tRNA binding. Our work with juglone identified surface cysteine residues that readily react with juglone in addition to the sites that were important for the inhibition of PRORP1. Biochemical studies are indicative of a 2-step inhibition mechanism where juglone rapidly binds and inhibits PRORP1 with low potency followed by a slow covalent modification step.

## **FUTURE DIRECTIONS**

This work describes the mechanism and inhibition of protein only RNase P and answers many important questions in the field including the role of MRPP1/2 on catalysis, the subunit stoichiometry of an active MRPP1/2 complex, and insights into the stability of the quaternary MRPP1/2/3/pre-tRNA complex. However, some questions still remain unanswered. First, the mechanism utilized by MRPP1/2/3 is not fully understood. A metal-bound water molecule is the proposed nucleophile for pre-tRNA cleavage, but more work needs to be done to test this hypothesis. Second, the structure of the active quaternary MRPP1/2/3/pre-tRNA complex is unclear. Our data suggest that both protein-protein and protein-RNA interactions are essential for the stability of the active complex. And third, this work was done using a canonical bacterial substrate lacking a 3'-CCA sequence. Investigations using cognate substrates, namely

human mitochondrial pre-tRNAs, to elucidate mechanism will be important for understanding molecular recognition of MRPP1/2/3. Furthermore, a study of MRPP1/2/3 activity *in vivo* with native polycistronic transcripts is needed. This will be especially helpful to better understand the mechanism of tRNA processing in patients with diseases arising from mitochondrial dysfunction.

### **Mechanism of MRPP1/2/3 catalysis**

We present a putative model for the mechanism of pre-tRNA hydrolysis catalyzed by MRPP1/2/3. Our model includes a step following binding of MRPP1/2 and pre-tRNA, likely a conformational change step. This would be tested using stopped flow experiments to study the transient kinetics for binding and conformational change using fluorescein-labeled pre-tRNA. The work in this thesis was done using a canonical bacterial pre-tRNA substrate from *B. subtilis*. Future work will be done to elucidate the kinetic mechanism with cognate human mitochondrial substrates, most of which deviate from the canonical type 0 tRNA found in bacteria and thus may have a unique mechanism for catalysis. Additional studies may be needed to evaluate the turnover of cognate polycistronic transcripts since the human mitochondrial is transcribed into three long precursor transcripts that are processed by RNase P.

There are still many questions to be answered about the catalytic mechanism of phosphodiester bond hydrolysis catalyzed by MRPP1/2/3. A metal-bound water molecule is proposed to act as a nucleophile. However, there is not strong structural and biochemical evidence for human mitochondrial RNase

P. Structures of MRPP3 and biochemical studies on PRORP1 provide some insights on its mechanism. MRPP3 likely coordinates active site metal ions through conserved aspartate residues, similar to PRORP1. In the future, a crystal structure of MRPP3 with bound metal ions would provide insight into the active site and orient key residues involved in catalysis. MRPP3 is inactive without MRPP1/2, but there may be a subset of substrates that can be processed by MRPP3 alone. Thus, a study to determine the reactivity of MRPP3 with all the predicted substrates in the mitochondrial genome would enhance our understanding of the role of MRPP1/2 and possible requirements for processing different human mitochondrial pre-tRNA substrates.

### **Structure of PRORP1-pre-tRNA and MRPP1/2/3/pre-tRNA complexes**

We are currently working in collaboration with the Koutmos lab at Uniformed Services University of the Health Sciences to solve a crystal structure of PRORP1 in complex with pre-tRNA or tRNA. To contribute to these efforts, gambogic acid, an uncompetitive inhibitor of PRORP1, is being used to try to stabilize the PRORP1-pre-tRNA complex for structural studies. We and others predict that the canonical secondary and tertiary structure of tRNAs include the D and T domains, and the variable loop, which are important for making contacts with PRORP1 (12).

Our mechanistic work demonstrates that a stable quaternary complex is formed between MRPP1/2/3/pre-tRNA indicative of protein-protein and RNA-protein interactions that are synergistic. We have also improved our methods for



the expression and purification of MRPP1/2. A structure of the quaternary complex obtained using electron microscopy and/or x-ray crystallography will inform on important features for substrate recognition and valuable information on the catalytic mechanism.

### **Inhibition of PRORP1 with gambogic acid and juglone**

Structural studies of PRORP1 in complex with juglone revealed covalent modifications of cysteine residues. Our work suggests that modification of C373 is an important for juglone inhibition. Future work will be done to evaluate the effect of a single C373A mutation on the time-dependent PRORP1 inhibition with juglone. Activity assays in the absence of juglone will be done to test if the removal of the cysteine affects PRORP1 activity. C373 is located in the metallonuclease domain and modification of this site by juglone may induce a structural change in PRORP1 or disrupt the positioning of catalytic aspartic acid residues that are important for coordinating active site metal ions. Thus, future work will include evaluating the metal ion dependence of PRORP1 activity in the presence of juglone.

Additionally, preliminary structural studies reveal a covalent modification with juglone at C346, which is close to C344 and C347 that coordinate a structural  $Zn^{2+}$  in the central domain. The importance of C346 on juglone inhibition will be determined using a PRORP1 C346A mutant to evaluate the effect that removal of the thiol side chain has on protein structure, inhibition with juglone, and zinc coordination.

### **Function of MRPP1/2/3 *in vivo***

One question that remains in the field is whether all mitochondrial tRNAs are processed by MRPP1/2/3 *in vitro* and *in vivo*. Mitochondrial tRNAs are transcribed as polycistronic transcripts and some pre-tRNAs such as tRNA<sup>Ser</sup><sub>(AGY)</sub> and pre-tRNA<sup>Leu</sup><sub>(CUN)</sub>, are transcribed immediately adjacent to one another. Therefore, the 3'-end maturation of one tRNA catalyzed by RNase Z may as a result liberate an adjacent tRNA without a need for RNase P activity. Using inhibitors specific for MRPP1/2/3, we could evaluate the buildup of unprocessed transcripts, indicative of impaired RNA processing. These sites can be mapped to the transcriptome to identify the tRNAs that may be substrates of MRPP1/2/3. This work could also identify potential novel non-tRNA substrates.

We have identified inhibitors that are potent against PRORP1 and MRPP1/2/3. However, gambogic acid has been previously shown to inhibit multiple cellular targets including proteins involved in modulating the nuclear factor- $\kappa$ B signaling pathway and the transferrin receptor involved in triggering apoptosis (8,9). This indicates that gambogic acid does not have sufficient selectivity for to serve as an *in vivo* inhibitor of protein-only RNase P. Juglone reacts readily with thiols to form a covalent modification and inhibits other enzymes (13,14). Therefore, additional screening or chemical modifications of the current inhibitors are necessary before the inhibitors can be used *in vivo*.

### **tRNA methylation**

The first step in tRNA maturation is proposed to be RNase P-catalyzed cleavage and thus, additional tRNA modifications are not essential for our work. Many human mitochondrial tRNAs have an A or G at position 9 that is methylated (15) but it is unclear if MRPP1 catalyzes the methylation of all of these sites. Furthermore, the canonical structure of the mitochondrial pre-tRNA<sup>Lys</sup> is stabilized by methylation at A9 (16,17), which then presumably is a substrate for cleavage catalyzed by MRPP1/2/3. Therefore, it is possible that the pathway for maturation of some mitochondrial tRNAs requires methylation preceding 5' end cleavage. Current work done in collaboration with the Koutmos lab at Uniformed Services University of the Health Sciences, is focused on studying the effect of pre-tRNA methylation on MRPP1/2/3 activity. Our lab is focused on the development of a primer extension assay using fluorescein labeled DNA oligomers to detect methylation at the Watson crick face and a radioactivity assay to detect the methylation of pre-tRNA in the presence of <sup>14</sup>C-labeled S-adenosylmethionine. These experiments can provide insight into the role of methylation in the pre-tRNA maturation pathway.

## REFERENCES

1. Holzmann, J., Frank, P., Löffler, E., Bennett, K. L., Gerner, C., and Rossmann, W. (2008) RNase P without RNA: Identification and Functional Reconstitution of the Human Mitochondrial tRNA Processing Enzyme. *Cell* **135**, 462-474
2. Lopez Sanchez, M. I. G., Mercer, T. R., Davies, S. M. K., Shearwood, A.-M. J., Nygård, K. K. A., Richman, T. R., Mattick, J. S., Rackham, O., and Filipovska, A. (2011) RNA processing in human mitochondria. *Cell Cycle* **10**, 2904-2916
3. Falk, M. J., Gai, X., Shigematsu, M., Vilaro, E., and Takase, R. (2016) A novel HSD17B10 mutation impairing the activities of the mitochondrial RNase P complex causes X-linked intractable epilepsy and neurodevelopmental regression. *RNA Biology* **13**, 477-485
4. Kissinger, C. R., Rejto, P. A., Pelletier, L. A., Thomson, J. A., Showalter, R. E., Abreo, M. A., Agree, C. S., Margosiak, S., Meng, J. J., Aust, R. M., Vanderpool, D., Li, B., Tempczyk-Russell, A., and Villafranca, J. E. (2004) Crystal Structure of Human ABAD/HSD10 with a Bound Inhibitor: Implications for Design of Alzheimer's Disease Therapeutics. *Journal of Molecular Biology* **342**, 943-952
5. Van Laer, B., Roovers, M., Wauters, L., Kasprzak, J. M., Dyzma, M., Deyaert, E., Kumar Singh, R., Feller, A., Bujnicki, J. M., Droogmans, L., and Versées, W. (2016) Structural and functional insights into tRNA binding and adenosine N1-methylation by an archaeal Trm10 homologue. *Nucleic acids research* **44**, 940-953
6. Vilaro, E., Nachbagauer, C., Buzet, A., Taschner, A., Holzmann, J., and Rossmann, W. (2012) A subcomplex of human mitochondrial RNase P is a bifunctional methyltransferase-extensive moonlighting in mitochondrial tRNA biogenesis. *Nucleic acids research* **40**, 11583-11593
7. Liu, X., Chen, Y., and Fierke, C. A. (2014) A real-time fluorescence polarization activity assay to screen for inhibitors of bacterial ribonuclease P. *Nucleic acids research* **42**, e159
8. Kasibhatla, S., Jessen, K. A., Maliartchouk, S., Wang, J. Y., English, N. M., Drewe, J., Qiu, L., Archer, S. P., Ponce, A. E., Sirisoma, N., Jiang, S., Zhang, H.-Z., Gehlsen, K. R., Cai, S. X., Green, D. R., and Tseng, B. (2005) A role for transferrin receptor in triggering apoptosis when targeted with gambogic acid. *Proceedings of the National Academy of Sciences of the United States of America* **102**, 12095-12100
9. Pandey, M. K., Karelia, D., and Amin, S. G. (2016) Gambogic Acid and Its Role in Chronic Diseases. in *Anti-inflammatory Nutraceuticals and Chronic Diseases* (Gupta, S. C., Prasad, S., and Aggarwal, B. B. eds.), Springer International Publishing, Cham. pp 375-395
10. Li, X., Liu, S., Huang, H., Liu, N., Zhao, C., Liao, S., Yang, C., Liu, Y., Zhao, C., Li, S., Lu, X., Liu, C., Guan, L., Zhao, K., Shi, X., Song, W., Zhou, P., Dong, X., Guo, H., Wen, G., Zhang, C., Jiang, L., Ma, N., Li, B.,

- Wang, S., Tan, H., Wang, X., Dou, Q. P., and Liu, J. (2013) Gambogic Acid Is a Tissue-Specific Proteasome Inhibitor In Vitro and In Vivo. *Cell Reports* **3**, 211-222
11. Wang, Y., Xiang, W., Wang, M., Huang, T., Xiao, X., Wang, L., Tao, D., Dong, L., Zeng, F., and Jiang, G. (2014) Methyl jasmonate sensitizes human bladder cancer cells to gambogic acid-induced apoptosis through down-regulation of EZH2 expression by miR-101. *British Journal of Pharmacology* **171**, 618-635
  12. Gobert, A., Pinker, F., Fuchsbauer, O., Gutmann, B., Boutin, R., Roblin, P., Sauter, C., and Giegé, P. (2013) Structural insights into protein-only RNase P complexed with tRNA. *Nature Communications* **4**, 1-8
  13. Hennig, L., Christner, C., Kipping, M., Schelbert, B., Rücknagel, K. P., Grabley, S., Küllertz, G., and Fischer, G. (1998) Selective Inactivation of Parvulin-Like Peptidyl-Prolyl cis/trans Isomerases by Juglone. *Biochemistry* **37**, 5953-5960
  14. Kong, Y.-h., Zhang, L., Yang, Z.-y., Han, C., Hu, L.-h., Jiang, H.-l., and Shen, X. (2008) Natural product juglone targets three key enzymes from *Helicobacter pylori*: inhibition assay with crystal structure characterization. *Acta Pharmacol Sin* **29**, 870-876
  15. Clark, W. C., Evans, M. E., Dominissini, D., Zheng, G., and Pan, T. (2016) tRNA base methylation identification and quantification via high-throughput sequencing. *Rna* **22**, 1771-1784
  16. Helm, M., Brulé, H., Degoul, F., Capanec, C., Leroux, J.-P., Giegé, R., and Florentz, C. (1998) The presence of modified nucleotides is required for cloverleaf folding of a human mitochondrial tRNA. *Nucleic acids research* **26**, 1636-1643
  17. Helm, M., Giegé, R., and Florentz, C. (1999) A Watson-Crick Base-Pair-Disrupting Methyl Group (m1A9) Is Sufficient for Cloverleaf Folding of Human Mitochondrial tRNA<sup>Lys</sup> *Biochemistry* **38**, 13338-13346